

# PolyWEC

polymeric wave energy converter

“New mechanisms and concepts for exploiting electroactive  
Polymers for Wave Energy Conversion”

FP7-ENERGY-2012-1-2STAGE  
FUTURE EMERGING TECHNOLOGIES

Grant Agreement N. 309139

<b>Material property database of existing EEs</b>				
Deliverable No.		<b>2.1</b>		
WP No.	<b>2</b>	WP Title	<b>New materials and transducers</b>	
Task	<b>T1.1</b>	Task Title	<b>Analysis and test of existing materials</b>	
Nature (R: Report, P: Prototype, O: Other)		<b>R</b>		
Dissemination level (PU, PP, RE, CO)		<b>PU</b>		
Lead beneficiary:		<b>2-PPIMC</b>		
Authors List:		<b>Marco Fontana (SSSA)</b> <b>Rocco Vertechy (SSSA)</b> <b>Maria Cazacu (PPIMC)</b> <b>Carmen Racles (PPIMC)</b> <b>George Stiubianu (PPIMC)</b> <b>Adrian Bele (PPIMC)</b> <b>Francesco Damiani (SSSA)</b>		
Status (F: final; D: draft; RD: revised draft):		<b>F</b>		
File Name:		<b>D2.1 Material property database.pdf</b>		
Due Delivery Date:		<b>M12</b>		
Actual Delivery Date:		<b>13 November 2013</b>		

### Version History table

Version no.	Dates and comments
1	29 Sept 2013 First draft
2	31 October 2013 Contribute gathered from all partners
3	13 November 2013 Final version

## Table of Contents

Table of Contents .....	3
Executive Summary .....	5
Section 1: Introduction .....	7
1.1 Electroactive Elastomers for Wave Energy Conversion (SSSA) .....	7
1.2 Relevant properties (SSSA).....	10
Section 2 Existing type of materials .....	15
2.1 Introduction .....	15
2.2 Natural Rubbers.....	15
2.2.1. General description.....	15
2.2.2. Chemistry.....	16
2.2.3. General characteristics .....	18
2.3 Silicones.....	18
2.3.1. General description.....	18
2.3.2. Chemistry.....	19
2.3.3. General characteristics .....	20
2.4 Acrylic .....	22
2.4.1. General description.....	22
2.4.2. Chemistry.....	22
2.4.3. General characteristics .....	23
2.5 Polyurethanes .....	23
2.5.1. General description.....	23
2.5.2. Chemistry.....	24
2.2.3. General characteristics .....	26
Section 3: Measurement procedures.....	29
3.1 Introduction .....	29
3.2 Dielectric constant.....	29
3.2.1 Measurement equipment.....	29
3.2.2 Experimental procedure .....	30
3.3 Electrical Breakdown (SSSA) .....	30
3.3.1 Measurement equipment.....	30
3.3.2 Experimental procedure .....	31
3.4 Mechanical properties .....	31
3.4.1 Measurement equipment.....	31
3.4.2 Experimental procedure .....	32
3.5 Water adsorption .....	36
3.5.1 Measurement equipment.....	36
3.5.2 Experimental procedure .....	36
3.6 Conductivity Properties .....	37
3.6.1 Measurement equipment.....	37
3.6.2 Experimental procedure .....	38
3.7.1 Measurement equipment.....	39
3.5.2 Experimental procedure .....	40
Section 4: Preliminary novel electroactive elastomers materials .....	41
4.1.Composites based on PDMS and ceramic materials .....	41
4.1.1. Composites with TiO <sub>2</sub> .....	41
4.1.1.1. Composites and film formation.....	41
4.1.1.2. Mechanical tests.....	41
4.1.1.3. Dynamic mechanical analysis.....	43
4.1.1.4. Dielectric thermal analysis .....	44
4.1.1.5. Vapor sorption capacity.....	47
4.1.1.6. Actuation and energy harvesting measurements.....	48

4.1.2. Composites with barium titanate .....	51
4.1.2.1. Preparation of barium titanate and its characterization (XRD, TEM, SEM).....	51
4.1.2.2. Composites and film formation.....	53
4.1.2.3. The effect of the barium titanate morphology on some properties of silicone composites....	54
4.1.2.3.1. Mechanical tests.....	54
4.1.2.3.4. Dielectric spectroscopy .....	55
4.1.2.3.3. Vapor sorption capacity.....	55
4.1.2.4. The effect of the molecular mass of the polymeric matrix on some properties of silicone composites thereof .....	56
4.1.2.4.1. Mechanical tests.....	56
4.1.2.4.2. Dielectric spectroscopy .....	57
4.1.2.4.3. Vapor sorption capacity.....	57
4.1.2.5. Polydimethylsiloxane-barium titanate composites as improved electroactive materials .....	58
4.1.3. Composites with lead zirconate .....	64
4.1.3.1. Preparation of lead zirconate and its characterization (XRF, XRD, TEM, SEM) .....	64
4.1.3.2. Composites and film formation.....	65
4.1.3.3. Mechanical tests.....	66
4.1.3.4. Dielectric spectroscopy .....	67
4.1.3.5. Thermal analysis .....	68
4.1.3.6. Vapor sorption capacity.....	69
Section 5: Conclusions .....	70
5.1 Discussion.....	70
5.2 Conclusion.....	71
5.3 Future Works .....	72
References.....	73
ANNEX I .....	77

## Executive Summary

For the purpose of building wave energy converters (WEC) using dielectric elastomers as transducers of mechanical to electrical energy, it is necessary to have elastomer materials which possess a set of desired properties. These properties refer mainly to mechanical and electrical behaviour, which must be well characterized by numerical values that are in a required range.

A large number of materials are already available on the market, with properties of dielectric elastomers. Such materials are used in most of the fields of technology, either as main components or small secondary parts in various devices. Having dielectric elastomers which possess a set of properties with defined values is a prerequisite for the construction of WEC with optimal capability for electricity production. Thus it comes natural that one of the first steps in such a project consists of thorough characterization of existing elastomers available on the free market.

This characterization was **the first target** of the first year in our project. As a result and **deliverable**, a database was built concerning the properties of interest of commercially available materials.

Also during the first year of the project PolyWEC the team in PPIMC (which is responsible for the task of production of new elastomer materials that possess the desired properties for use in WEC) created new composite materials based on silicone elastomers using the expertise in the field of polymers. These new materials were also characterized by specific measurements.

The preparation and characterization of some new materials for WEC was the **second objective** for the first year of the project, in the responsibility of PPIMC.

The scope of this document is to bring together in a clear, concise and easy to read manner all the data characterizing the properties of both the commercial and the newly synthesized materials. For this scope, all the materials were characterized in an identical manner, using the same type of scientific apparatus, thus giving the possibility for obtaining a standardized set of values which can be compared for all materials. Therefore, the data for the properties of the materials can be regarded as an open access database, which offers the possibility for scientists to have access to a unitary set of data, with reduced variability due to difference in the atmospheric conditions of testing and equipment or characterization method.

The document is composed of the following sections. Section 1 starts with an introduction in the field of the electroactive elastomers for wave energy conversion and presents the relevant properties of elastomers that are optimal for wave energy conversion.

In Section 2 the existing types of commercial elastomer materials are described, starting with a short introduction showing the general characteristics of possible materials to be employed. Then, in four subsections are presented various classes of the most important existing polymers tested in laboratories for use as dielectric elastomers in actuators and for renewable energy harvesting: natural rubbers, silicones, acrylic rubber and polyurethanes. For each class of materials there is a general description of the material, followed by the chemistry and characteristics of that material.

In Section 3 are presented the detailed conditions used for the characterization of the materials and the data obtained. It starts with a general description of the contents in the Introduction, followed by specific subsections for: dielectric constant, electrical breakdown, mechanical properties, water adsorption, and conductivity properties. Each subsection contains a detailed description of the measurement equipment for the specific property, the experimental procedure and sample plots of the results.

The Section 4 of this document presents preliminary novel electroactive elastomers materials. It contains three subsections with detailed presentation of the obtained new materials, namely composites based on PDMS and different fillers: commercial titanium dioxide, barium titanate - both commercial and home-prepared -, home-prepared lead zirconate. These fillers were used alone or together with commercial silica home-treated on surface. The obtained materials were studied by dielectric spectroscopy, mechanical tests, thermal analysis, scanning electron microscopy (SEM), dynamic vapour sorption (DVS) and the influence of various parameters on the properties of interest was determined.

Section 5 is composed of three subsections: the first contains a discussion where the data for the tested elastomer materials is compared with the data from literature. Another subsection is for conclusions with regard to the properties of the tested materials and one subsection is dedicated to future paths for research in light of the findings for existing materials and for the newly synthesized materials.

Data tables for material properties are included as annex to this document and they are public available on the Project website at the address: <http://polywec.org/materialdatabase>.

## Section 1: Introduction

### 1.1 Dielectric Elastomers Generators

Dielectric Elastomers (DEs) are incompressible solids which exhibit non-linear elastic finite deformations and linear strain-independent dielectric properties. DEs can deform in response to an applied electric field, and can alter the electric field and/or potential in response to an undergone deformation. Thanks to this Electro-Mechanical (EM) coupling, DEs are currently being investigated as transduction materials for solid-state actuators, sensors and generators.

As stated before, a DEG can be considered as a deformable capacitor (the capacitance of which varies with the deformation) that is operated cyclically. The working principle of DEGs is briefly schematized in Figure 1.

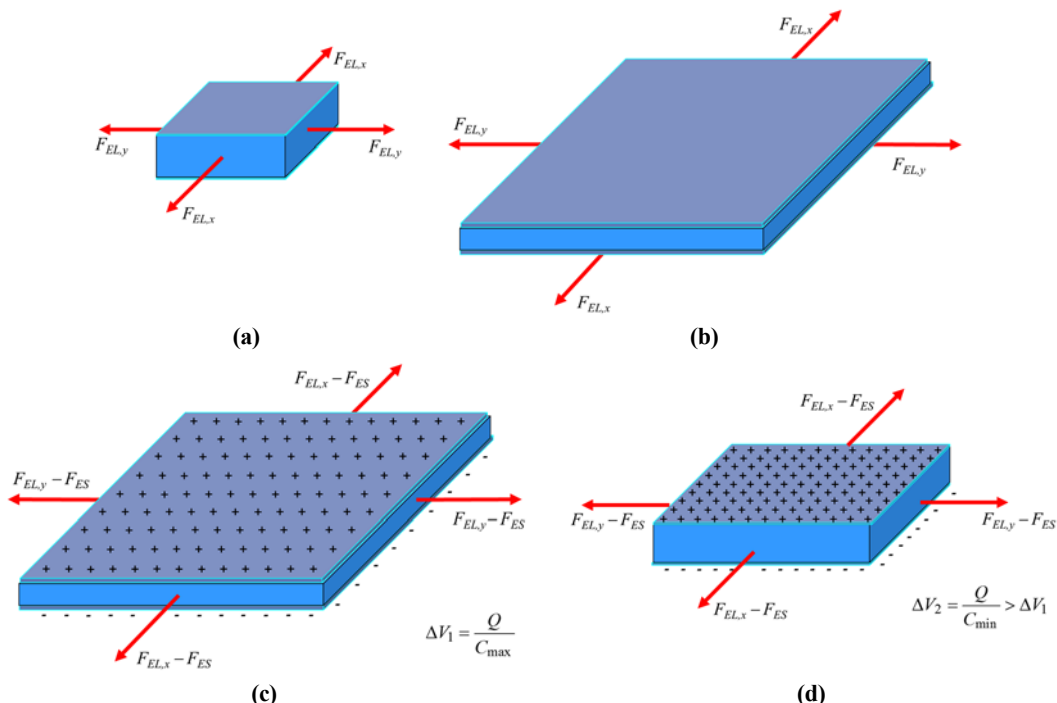


**Figure 1 - DEG working principle**

Starting from an undeformed configuration (Figure 1.a), the DEG is first subjected to an external mechanical load so that its area expands to a maximum value (see Figure 1.b). Since the material is nearly incompressible, while the area of the DE membrane (and thus of the electrodes) increases, its thickness decreases, and the capacitance of the resulting condenser is maximum (being the electrodes surface maximum and the membrane thickness minimum). In this configuration, opposite charges ( $+Q$ ,  $-Q$ ) are deposited on the electrodes (Figure 1.c). Once fully charged, the membrane is brought back to its original configuration (Figure 1.d). This reduces DEG capacitance, thereby producing (in presence of a constant charge  $Q$ ) an increase in the electric energy stored in the DEG. Clearly, part of the mechanical energy conferred to the membrane during the deformation phase has been converted into electrical energy.

The conversion mechanism can be alternatively explained by noticing that the electrostatic attraction of the charges residing on the opposite electrodes yields a decrease in the force that is required to maintain the DE membrane in the stretched state. For this reason, as represented in Figure 1, the tractive force ( $F_{el} - F_{es}$ ) during membrane contraction is lower than the tractive force ( $F_{el}$ ) during membrane expansion. As a consequence, the mechanical work returned by the DEG during the contraction phase is lower than the mechanical work absorbed during the expansion phase (the difference between these works representing the amount of energy that is converted into electricity).

The working principle described above is only ideal. In the reality, some energy dissipation occurs due to both mechanical and electrical dissipative phenomena. The most important causes for these energy losses are: internal material visco-elasticity; power dissipation due to the resistivity of the electrodes; leakage currents through the DE membrane thickness.

With regard to energy conversion performances, a significant parameter that is employed to evaluate and compare different DEG architectures is the energy per unit weight of elastomer that the generator is able to convert. This parameter plays a significant role in the determination of the amount of material that is required in a given application and, thus, in the determination of the level of compactness that the resulting DEG can achieve.

A summary of the major achievements in DEG technology is provided below.

A pioneer experimental study on DEGs was carried out by Pelrine et al. [1] who measured energy densities of 0.4 J/g and estimated possible densities up to 1.5 J/g.

Koh et al. [2],[3] performed a theoretical study on a square DEG that is subjected to an equi-biaxial state of deformation (namely, as depicted in Figure 2, the membrane is stretched uniformly along the two sides). For this configuration, a maximum energy density of 3.2 J/g was estimated.

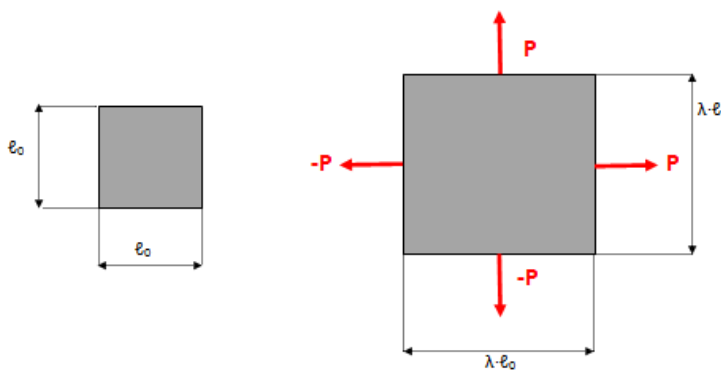


**Figure 2 - Equi-biaxial state of deformation**

For a similar configuration, Jean-Mistral [4] measured a maximum energy density of 1.7 J/g.

Similar to piezoelectric ceramics, DEGs generally work at high voltages, typically in the range 1-10 kV. This requires proper driving circuits and electrical/electronic components. To date, the availability of transistors that could be used for this specific application is very limited.

## 1.2 Dielectric Elastomer Wave Energy Converters

The present paragraph introduces the use of DEGs in Wave Energy Converters (WECs).

A traditional WEC comprises several rigid components, which are made of stiff, heavy, shock-sensitive, corrosion-sensitive and costly metallic materials, and include wave-interacting bodies, mechanical/hydraulic transmissions, electromagnetic generators, step-up transformers and eventually frequency changers or rectifiers.

In a first simple approach, the employment of DEGs may be confined only to the replacement of the traditional (electric or hydraulic) PTO system of existing WEC architectures.

In a more ambitious perspective, DEGs could integrate all the components of a WEC (including wave-interacting bodies, mechanical transmissions and power electronics) into a single soft electroactive elastomeric body, which undergoes liquid-like deformations under the action of sea waves.

The interesting aspects concerning the application of DEGs to wave energy conversion can be summarized in the following points:

- DE materials are soft, resilient and lightweight. Thanks to their high deformability, they are suited to be directly coupled with moving oscillating WECs that undergo large displacements without the necessity of any intermediate mechanical transmission.

- Polymeric materials are corrosion-resistant. Thus, they are particularly suited for applications in aggressive environments (like sea water).
- Many common polymeric materials are already widely spread and largely used. Thus, they are available at relatively low price.
- Traditional electrical and mechanical generators are not suited to operate within the sea environment, since they are made by a number of sensitive moving parts that have to be kept isolated from the water. DEGs application would significantly reduce the amount of moving mechanical parts. Moreover, due to the simplicity of their mechanical layout (that essentially includes an articulated frame and a deformable membrane), they allow a drastic reduction in the number of parts that can potentially meet mechanical failure.
- As already mentioned, a large variety of DEGs can be designed, each exploiting a particular motion condition (angular pitch oscillation, linear reciprocating motion, movements with multiple degrees of freedom). Therefore, for a particular design of a WEC device, a proper architecture for the corresponding polymeric PTO can be investigated and identified.
- DEGs convert the energy from the waves into high-voltage direct-current electricity, that is immediately ready to be delivered to the coast via long underwater transmission lines. Therefore, their application would allow to solve the troublesome problem of using frequency changers to interface a natural low frequency system (the WEC moving within the waves) and a system that requires high frequency (the traditional electric apparatus, since traditional electric machines usually have a high nominal frequency of operation).

As a counterpart, some possible criticalities are listed below:

- DE materials may be subjected to aging and performance losses during their lifecycle.
- DE materials present both mechanical (hysteretic) and electrical losses. A proper analysis of the limitations to the amount of convertible energy has to be carried out, and a targeted choice of the materials has to be done.
- In order to avoid the rupture of the polymeric material, DEGs must be subjected to limited displacements (in order to keep the strain on the elastomeric membranes below the rupture value). WECs operating in real sea are subjected to storms and gales that provoke very large oscillation amplitudes of the moving part of the converter. DEGs for WECs should be designed in a way that the material is kept below the stretch safety value in a certain range of conditions; when the sea conditions exceed the safety limit, the oscillating body must be halted or, anyway, the DEG must be disconnected from the moving body. In order to achieve this result, proper safety devices (like controlled clutches, brakes etc.) must be designed.
- DEGs are a relatively new concept. In fact, their study and application is limited to experimental laboratory-scale applications. Many of the weak points of this technology have not been identified yet, mainly because of the lack of sufficient trials in a real operating environment.

Based on the different mode of interaction between the DEG Unit (DEGU) and the fluid, two types of Polymeric WECs can be identified: first-generation devices and second-generation devices. The characteristics and peculiarities of each kind of Polymeric WEC are described in the following sections.

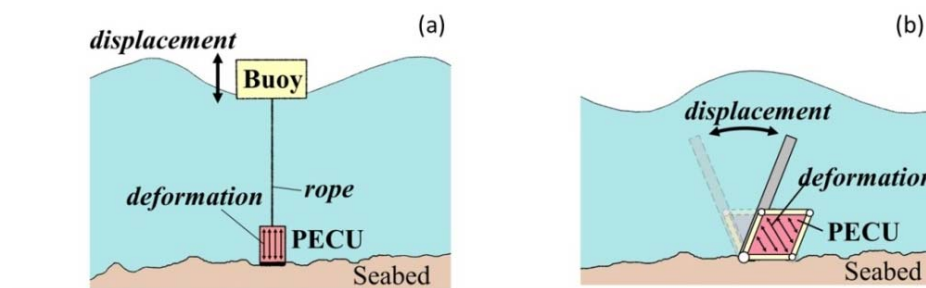


**Figure 3 - Examples of first-generations DE-WECs**

### 1.2.1 First-Generation Devices

These devices are characterized by the indirect interaction between DEGU and fluid. In this case, DE deformations are not directly generated by fluid pressures, but by a mechanical interface (see Figure 3.a and Figure 3.b). Thus, in this case, two distinct bodies are identified: a WEC, that is the body mechanically excited by the waves; a DEG PTO that converts kinetic and potential energy of the WEC to electrical energy.

Examples of first generation DE-WECs are heaving or pitching bodies (buoys, flaps etc) that activate a deformable DEG provided with a rigid frame that is partially built within the WEC.

Due to the absence of direct fluid-DEGU interaction, the modeling, design and control of first-generation DE-WECs is simplified.

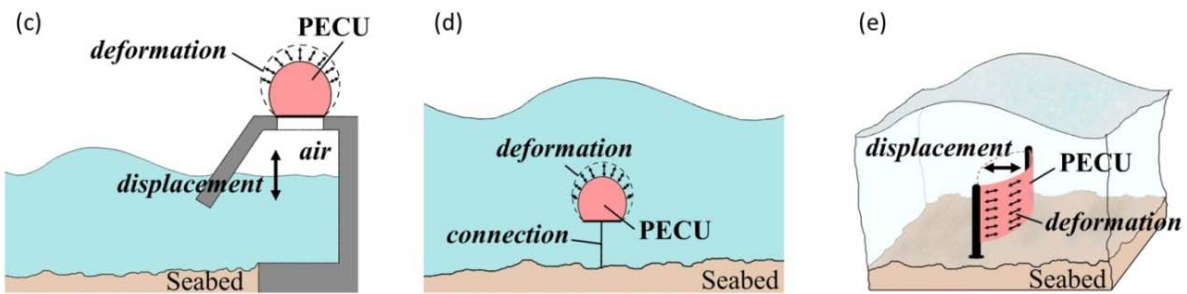


**Figure 4 - Examples of second-generation DE-WECs**

### 1.3.2 Second-Generation Devices

These devices are characterized by direct interaction between DEGU and fluid, which occurs over wide contact surfaces.

In this case, fluid-DEGU interaction is not mediated by any mechanical means, and DE membrane deformation is directly generated by wave-induced fluid pressures (see Figure 4).

As a result, second-generation devices are highly-integrated WECs that feature the minimal number of mechanical and electrical components beside the DEGU. Moreover, thanks to their intrinsic and tunable compliance, such devices make it possible to optimize and control their radiation impedance in order to achieve maximal wave-energy extraction.

Examples of second generation converters are close-chamber oscillating water-columns exploiting a deformable membrane instead of an air turbine and inflatable bodies.

With respect to first-generation devices, this second type of DE-WECs is much more difficult to model, design and control.

### 1.3 Relevant material properties

In order to define the relevant material properties that can guarantee optimal generation efficiency of DE, a in depth analysis of electro-elastic model have been conducted and reported in Section 2 of Deliverable 1.1 of PolyWEC project. This mathematical analysis considers how each material property weights on the amount of energy that can be produced by a unit volume of elastomer.

In this section, we report the outcome of that analysis describing briefly each of the relevant identified material property that are:

- Dielectric constant;
- Electrical Breakdown;
- Ultimate stretch;
- Constitutive mechanical parameters;
- Water Adsorption;

- Conductivity.

Common materials that are employed as dielectric: acrylics, silicones, natural rubber and polyurethanes. Such three classes of material are considered and tests are reported in the following sections.

A more detailed description on the relation between material properties and performances of the energy converter can be found in Deliverable 1.1: "Architectures and material specifications".

### 1.3.1 Dielectric Constant and conductivity

The working principle of DEGs (based on the concept of variable capacitance condenser) requires the elastomeric membrane (housed between the compliant electrodes) to be non-conductive (since it constitutes the dielectric mean between the armatures, with the aim of electrically decoupling the opposite faces of the capacitor).

The dielectric constant for a generic medium is expressed by

$$\varepsilon = \varepsilon_r \varepsilon_0 \quad (1)$$

where  $\varepsilon_0$  is the permittivity of the vacuum, that amounts to  $8.85 \cdot 10^{-12} F \cdot m^{-1}$ , and  $\varepsilon_r$  is the relative dielectric constant of the material.

In general, high values of  $\varepsilon_r$  are desirable for DEG since the effective amount of converted energy is directly proportional to the value of  $\varepsilon$ .

Typical values of the dielectric constant for common DE materials are reported in Table 1.

Elastomer	$\varepsilon_r$
Natural Rubber	2.7
Silicone	3-7
Acrylic	3-4.5

Table 1 - Relative dielectric constant for some classes of DEs

Another property of the dielectric elastomer layer which is very relevant to the purpose of energy conversion is the electrical conductivity of the elastomer membrane. Dielectric elastomer can be considered as insulating materials but of course they show very low conductivity. Excess in conductivity can lead to important losses, especially if the period of the cyclical deformation of DEG is slow. For an optimal design of PolyWECs it is important to ensure that conductivity is lower than specific thresholds in order to avoid unwanted losses in the dielectric.

### 1.3.2 Electrical Break-down field

As already mentioned, the break-down limitation determines an upper admitted value,  $E_{BD}$ , for the electric field within the polymeric capacitor.

Generally,  $E_{BD}$  is considered as a constant intrinsic parameter of the material. However, some dependence of this parameter on the deformation may exist.

For instance acrylic elastomers undergoing equi-biaxial deformation exhibit a strain-dependent break-down field that varies according to the relationship

$$E_{BD}(\lambda) = \bar{E}_{BD} \lambda^R \quad (2)$$

In general, high values for the break-down field are desirable. In fact, as shown in Figure 5, larger values of  $E_{BD}$  lead to larger amounts of converted energy (the amount of converted energy is proportional to the area that is included within the various limit-curves).

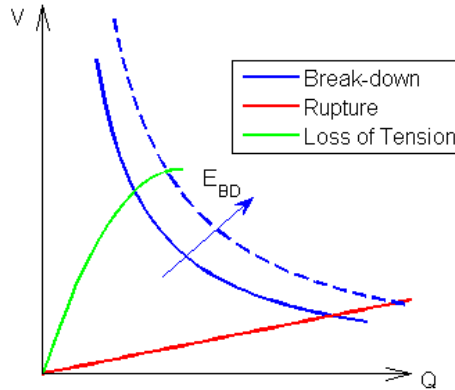


Figure 5 - Effect of an increase in EBD on ECCs

Typical values of break-down field for common DE materials are reported in Table 2.

Elastomer	$E_{BD}$ [MV/m]
Natural Rubber	30-200
Silicone	30-100
Acrylic	30-200

Table 2 - Break-down field for some classes of DEs

Another aspect that is highly relevant for DEG employed as wave energy converters is the possible variation of electrical breakdown in wet environments. Electrical breakdown of elastomers can be strongly influenced by their **water adsorption** when exposed to wet or submerged environments.

### 1.3.3 Rupture stretch

The condition of mechanical rupture of the polymeric material can be expressed as a limitation on the maximum allowed value,  $\lambda_u$ , of the stretch within the material.

As already mentioned, DE materials exhibit large values of limiting stretches (over 500%). A large value of  $\lambda_u$  is obviously desired in order to obtain a large amount of convertible energy.

As shown in Figure 6, large values of  $\lambda_u$  produce a rupture curve with low slope, and, consequently larger area that represents more energy that can be converted.

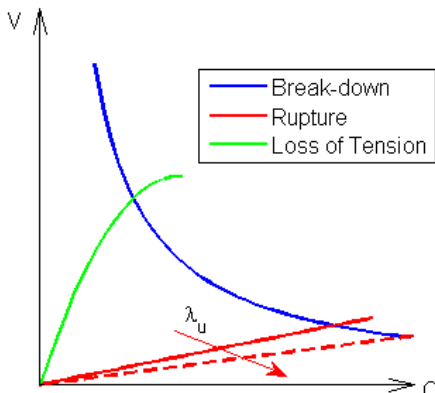


Figure 6 - Effect of an increase in  $\lambda_u$  on the ECC

Typical values of rupture stretch for common DE materials are reported in Table 3.

Elastomer	$\lambda_u$
Natural Rubber	5-7
Silicone	3
Acrylic	4-8

Table 3 - Rupture stretch for some classes of DEs

### 1.3.4 Hyperelastic parameters

DE materials are non-linear elastic solids. Their mechanical behavior is usually described by a proper hyperelastic model. The constitutive equations plays a role in the determination of the loss of tension curve in the V-Q plane.

An increase in the value of elastomer stiffness ( $\mu$ ) produces an increase in the slope of the limit curve corresponding to the loss of tension condition.

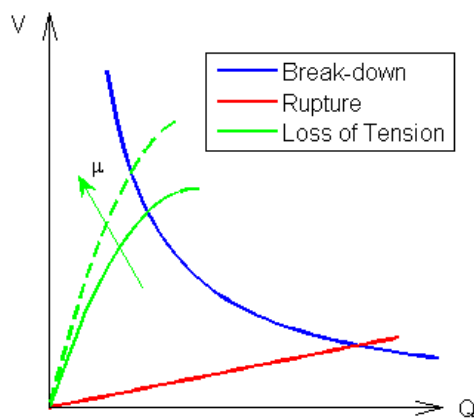


Figure 7 - Effect of an increase in  $\mu$  on the ECC

Thus the effect of using a stiffer material is an increase in the energy that can be converted by the DEG.

### 1.3.5 Effect of Material Properties on DE-WEC Response

Up to this point, it has been assumed that the DEG undergoes a conversion cycle bounded by the transformations identified by the failure conditions discussed above. Beside appropriate power electronics and controller, this hypothesis requires the availability of an external source of mechanical work that is capable of exerting on the generator the required forces and displacements exhibited by the DEG in the Force-Displacement plane.

This is not generally the case when the DEG needs to absorb a significant amount of energy from a mechanical system, such as a wave interacting body, having an intrinsic impedance (namely a specific dynamic response). In this circumstance, maximization of the energy that can be harvested by a DEG may require the appropriate matching of the impedance of the DEG to that of the source of the mechanical energy. From the point of view of material property specifications, this could modify the requirements described in the preceding sections for both mechanical and electrical parameters.

Referring to wave energy harvesting and according to linear waves theory the amount of energy that can be extracted is maximized when the system composed by WEC and PTO has a natural frequency that equals that of the incident wave (in the hypothesis of monochromatic waves). In this context, the major effect of using DEGs as PTO corresponds to a modification of the overall stiffness response of the WEC.

In particular, this stiffness modification depends on the following electro-mechanical properties and design parameters of the DEG:

- The shear modulus ( $\mu$ ) of the DE material;
- The dielectric constant multiplied by the square of the maximum electric field employed during the ECC (namely,  $\epsilon \cdot E^2$ );

- The level of pre-stretch of the DE membrane.

The overall effects of DE material electro-mechanical parameters on wave energy harvesting via DEGs can be summarized as follows:

- *Mechanical material parameters*: in an ideal context, rigid materials allow larger energy conversion capabilities; in a practical context, they may increase to much the stiffness response of the WEC, which could make it unsuitable for the operation in specific wave climates. Depending on the specific converter, location of installation and reference sea states, a trade off for the material shear modulus needs to be found.
- *Electrical material parameters*: in an ideal context, maximum values for the product  $\varepsilon \cdot E^2$  allow larger energy conversion capabilities; in a practical context, they may modify excessively the stiffness response of the WEC (either increasing or decreasing it depending on the specific DEG architecture), which could make it unsuitable for the operation in specific wave climates. Depending on the specific converter, location of installation and reference sea states, a trade off for the product  $\varepsilon \cdot E^2$  needs to be found.
- *Material pre-stretch*: since DEs are non-linear materials, irrespective of their electro-mechanical properties, the practical stiffness of a DEG with specific architecture can be tuned by properly pre-tensioning the DE membrane. Thus, in a practical context, appropriate values of DE membrane pre-stretches need to chosen depending on the specific converter, location of installation and reference sea states.

### **1.3.6 Considerations on electrodes**

A further fundamental aspect that concerns the materials employed for DEG manufacturing is the electrode component. Electrodes are highly deformable and conductive layers which are sandwiched between dielectric membranes. Rosset and Shea [5] provide an extensive review of different manufacturing processes for electrodes of dielectric elastomer transducer. In the case of DE employed as actuators, the problem of manufacturing process of electrodes is well investigated. For DE generators, the electrode problem is mainly connected with to extremely high stretch values that are required to enable fast response and guarantee maximum efficiency. The realization of fully working laboratory prototypes is always enabled by the use of conductive grease or powders. However, such process requires a lot of manual work and the duration/reliability of the obtained electrodes is not compatible with a real full-scale applications.

The study of an industrial process for the manufacturing of electrodes is a key element for the deployment of full scale WECs based on dielectric elastomers. In this report, we are not tackling the problem of electrodes. However, materials and manufacturing issues of effective electrodes will be considered in the forthcoming activities of the project.

## Section 2 Existing type of materials

### 2.1 Introduction

The mechanical energy contained in water flows has been used for millennia, hydro power plants being the first large scale power plants built for electricity production starting in the late 19<sup>th</sup> century [6]. Until today the wave energy in seas and oceans was converted into electrical energy with the aid of mechanical devices like buoys and connected tubes [7],[8].

Dielectric electroactive polymers (DEAP) are made of thin films composed of elastomeric material and compliant electrodes coated on the elastomer surface. This setup allows a deformation with large percentage relative to the initial size of the membrane and can be used either as an actuator or in the inverse operation mode as generators, when it converts mechanical strain energy into electrical energy using the polymer's capacitive behaviour [9]. In the case of dielectric elastomer generators (DEG), the operating principle is based on changes in geometry of the elastomer capacitor and an initial charge, similar with the principle of electrostatic energy conversion [10].

There is a set of characteristics that make a dielectric elastomer suitable for use in wave energy generators. In comparison with classic transduction systems such as electric motors, the dielectric elastomer generation units (DEGU) feature several advantages [11] such as: low mass density ( $\sim 1000 \text{ kg/m}^3$ ); large deformability (deformations up to 700 %) with a value for Young's modulus of 0.01-20 MPa; high energy density (in the range 0.1-3.5 kJ/kg); large break-down strength (20-400 MV/m); moderate (relative) dielectric permittivity (in the range 1.8-7); good electro-mechanical conversion efficiency (60-90%); moderate or low cost (100€/kg for small batches and less than 10€/kg for large batches); solid-state monolithic embodiment with no sliding parts and very low internal friction; easy manufacturability, assembling and recyclability; good chemical resistance to corrosive environments; silent operation and no need of lubrication. Thus a polymeric wave energy conversion unit with purchase cost of 100 €/kg for small batches built using polyacrylate elastomer in the form of a two-centimeter-thick stack of twenty identical polyacrylate elastomer layers separated by compliant electrodes, at deformation cycles with 100 % maximum strain has the capability to harvest energy with 200 J/kg per single cycle and will reach the theoretical generation limit of 1.7 kJ/kg per cycle when using optimal DEGU design [3]. Thus such a device can generate 4 kJ/m<sup>2</sup> per single cycle and the harvested electrical energy can be delivered as High-Voltage Direct-Current at nearly 100 kV, eliminating the need for the presence of transformer and inverter electronics [12]. While the cost of materials is important for commercial application, the preliminary experiments on new materials presented in Section 4 are focused on achieving the expected values for the mechanical and electrical properties.

### 2.2 Natural Rubbers

#### 2.2.1. General description

Rubber is an elastomer type polymer and possesses the property of returning to its original shape after being stretched or deformed. The polymer molecular chains are coiled in the resting state. The elastic properties are due to the capability to stretch the chains apart and to return fast to the original position when the tension is released.

Natural rubber, also called India rubber or *caoutchouc*, is harvested as milky white fluid called latex from the tropical rubber tree. The latex must be refined into rubber suitable for commercial processing. Natural rubber is used in various applications, either alone or in combination with other materials, due to its properties of large stretch ratio, high resilience, and excellent waterproofing [13].

The number one commercial source of natural rubber latex is the Pará rubber (*Hevea brasiliensis*), from the spurge family, Euphorbiaceae. This species is used because it grows well in tropical climate and the tree produces more latex when the wounding in the bark is made. Different forms of latex rich in isoprene polymers are produced by many plants but are not as easily usable as the one from the Pará rubber tree, as those plants are being difficult to tap and require more elaborate processing to produce the usable rubber.

Some plants that are commercially exploited, or show promise as sources of rubber include the rubber fig (*Ficus elastica*), Panama rubber tree (*Castilla elastica*), lettuce (*Lactuca* species), spurge (*Euphorbia* spp.), *Scorzonera tau-saghyz*, guayule (*Parthenium argentatum*) and some of the *Taraxacum* species including common dandelion (*Taraxacum officinale*) and Russian dandelion (*Taraxacum kok-saghyz*). The tree-obtained version of natural rubber is named gum rubber in order to distinguish it from the synthetic version [9].

The field of research for electroactive polymers was started in 1880 with the publication of a paper by Roentgen [14]. In his experiments, a film made of natural rubber was made to change in shape when a large electric field was applied across it. This paper presents the first observation of dielectric elastomer material used for actuation. However for the construction of polymeric energy conversion units, the natural rubber elastomers are too stiff and this has lead researchers to study acrylic and silicone rubbers for this purpose.

### 2.2.2. Chemistry

Natural rubber is an addition polymer of the monomer isoprene (2-methyl-1,3-butadiene) which possesses two double bonds, and the polymer chain retains one of them. Natural rubber has the cis configuration for the methyl groups and it is cis-1,4-polyisoprene, with molecular mass of 100,000 to 1,000,000 daltons. Up to 5% of the dry rubber mass consists of other materials, namely proteins, fatty acids, resins, inorganic salts. Polyisoprene can be created synthetically, but the synthetic and the natural routes are completely different [13].

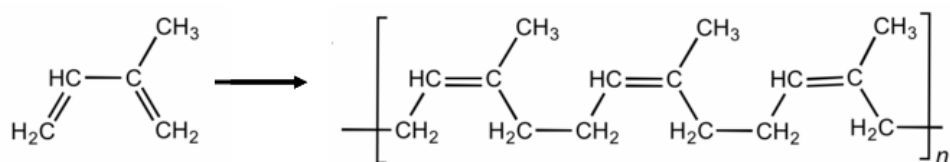


**Figure 8 - Chemical structure of cis-polyisoprene, the main constituent of natural rubber**

The main solvents used for rubber are turpentine and naphtha (petroleum). The use of turpentine as solvent for rubber was discovered in 1764 by François Fresnau, while Giovanni Fabbroni discovered naphtha as a rubber solvent in 1779. However since rubber does not dissolve easily, prior to its immersion in solvent the material must be divided by shredding in fine pieces. During transportation from the collection site the coagulation of raw latex is prevented by using an ammonia solution.

Other natural rubber sources, such as gutta-percha, are composed of trans-1,4-polyisoprene. The properties of this structural isomer are similar, but not identical.

Natural rubber is both an elastomer and a thermoplastic material. Using the process of vulcanization, the rubber is turned into a thermoset. Most rubber for commercial use is vulcanized to a point where it shares properties of both thermoplastic and thermosets: if it is heated and cooled, it degrades but it is not destroyed.

Vulcanization or vulcanisation is the chemical process when rubber or related polymers are converted into more durable materials via the addition of sulfur [13] or other equivalent "curing agents" or "accelerators". The addition of such additives leads to formation of crosslinks (bridges) between individual polymer chains [15] and vulcanized rubber is less sticky and has superior mechanical properties. The process is named after Vulcan, the Roman god of fire.

There are several methods for vulcanization but the economically most important method (for vulcanization of tires) uses high pressure and temperature. A passenger tire is treated for 10 minutes at 170 °C by compression molding when the rubber article is intended to adopt the shape of the mold. In order to make other parts such as door profiles for cars, other methods are used: hot air vulcanization or microwave heated vulcanization, which are continuous processes).

Charles Goodyear discovered by accident that a mix of sulfur and rubber leads to rubber materials with improved properties: it is tougher, resistant to heat and cold, and has increased elasticity. In the process of vulcanization the shorter chains cross link through the sulfur and form longer chains. Vulcanization of rubber creates disulfide bonds between chains, so it limits the degrees of freedom. The polymer chains tighten more

quickly for a given strain, and thus increase the elastic force constant and make rubber harder and less extensible.

Due to the use of most natural rubber for the production of car tyres, the most common vulcanizing methods depend on sulfur. Sulfur is a slow vulcanizing agent and does not vulcanize synthetic polyolefins. Even with natural rubber it is necessary to use large amounts of sulfur and high temperatures and long heating time, but the crosslinking efficiency, strength and aging properties are still unsatisfactory. In order to obtain quality corresponding to today's level of technology it is necessary to use vulcanization accelerators. Various vulcanization effects are achieved with a large number of diverse additives, comprising the combined cure package.

This consists of sulfur together with compounds that modify the kinetics of crosslinking and stabilize the final product. Among the additives used are accelerators, activators like zinc oxide and stearic acid and antidegradants. The accelerators and activators are catalysts. For a better control of reaction, retarding agents are used to inhibit vulcanization until some optimal time or temperature.

The vulcanization of rubber is a complex chemical process involving several chemical species (Figure 9). The reaction starts with the formation of an accelerator-activator complex. It then proceeds to pick-up sulfur (which naturally occurs as an  $S_8$  ring) and forms the activated sulfurating species ( $A_x$ ). The sulfurating species are polysulfidic -  $x$  can vary from 1 to more than 20.

In the next step the activated sulfurating species undergoes decomposition and reacts with the allylic carbon in the rubber to form  $B_x$  - another polysulfidic species terminated with rubber on one end and one benzothiazole group on the other.

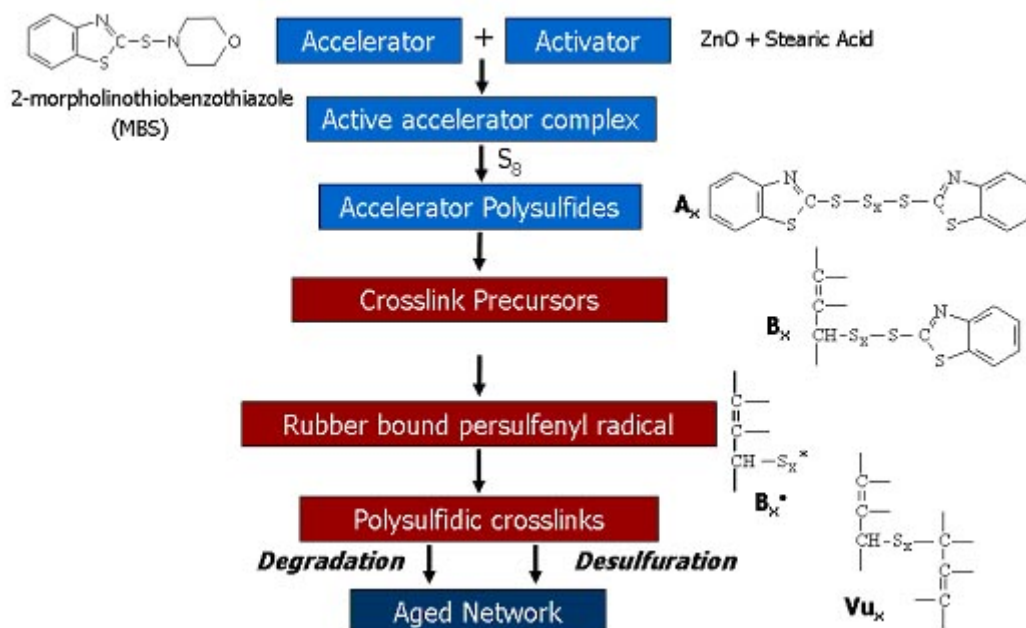


Figure 9 - Basic mechanism of accelerated sulphur vulcanization [16].

The species  $B_x$  undergoes decomposition to form the radical species  $B_x^*$ .

The radical species then reacts with an allylic carbon from a second rubber chain to form the crosslink  $Vu_x$ .

The polysulfidic crosslinks  $Vu_x$  undergoes additional reactions that shorten the crosslinks (reduce  $x$ ) or form additional crosslinks or degrade completely [16].

The final properties of a crosslinked rubber depend not just on the polymer, but also on modifiers and fillers, such as carbon black, and various treatments that can be applied after the crosslinking reaction. Antidegradants are used to prevent degradation of the vulcanized product by heat, oxygen and ozone [17].

### 2.2.3. General characteristics

Uncured natural rubber is sticky, deforms easily at warm temperature and is brittle when cold. Therefore it is a poor material when a high level of elasticity is required. The inelastic deformation of un-vulcanized rubber is the result of its chemical structure, since rubber is composed of long polymer chains that can move independently relative to each other, so the material changes shape. Crosslinking bridges introduced by vulcanization prevent the polymer chains from moving independently. The result of crosslinking is that when stress is applied the vulcanized rubber deforms, but upon release of the stress, the article reverts to its original shape.

Rubber exhibits specific physical and chemical properties. Thus the stress-strain behaviour of rubber exhibits the Mullins effect and the Payne effect, and is modelled as hyperelastic. Rubber presents strain crystallization.

Natural rubber is susceptible to vulcanisation and sensitive to ozone cracking due to the existence of a double bond in each repeat unit.

The elastic behaviour is caused by bond distortions in most elastic materials, such as metals used in springs. When force is applied, bond lengths deviate from the minimum energy equilibrium. The strain energy is stored electrostatically. In the case of rubber, unlike in metals, strain energy is stored thermally.

In its relaxed state, rubber consists of long, coiled-up chains. When rubber is stretched, the chains are taut. Their kinetic energy is released as heat. The entropy and temperature increases during elongation but decreases during relaxation. This change in entropy is related to the changes in degrees of freedom [13]. Relaxation of a stretched rubber band is thus driven by a decrease in entropy and temperature, and the force experienced is a result of the cooling of the material being converted to potential energy. Rubber relaxation is endothermic, and for this reason the force exerted by a stretched piece of rubber increases with temperature. The material undergoes adiabatic cooling during contraction. Stretching of a rubber band is in some ways opposite to compression (although both undergo higher levels of thermal energy of an ideal gas), and relaxation is opposed to gas expansion (rubber bands last longer in the cold) [13].

Vulcanized rubber is used for making various different products, such as tires, shoe soles, hoses, conveyor belts and hockey pucks. Vulcanized rubber with high degree of crosslinking is sold under the brand names ebonite or vulcanite, and can be found in the composition of hard articles such as bowling balls and saxophone mouth pieces.

At very low temperatures rubber is brittle. This is happening because when rubber is cooled below the glass transition temperature, the quasifluid chain segments "freeze" into fixed geometries and the rubber abruptly loses its elastic properties, although the process is reversible. This property is shared by most elastomers.

## 2.3 Silicones

### 2.3.1. General description

Polysiloxanes are heterocatenar polymers consisting of alternate silicon and oxygen atoms with organic substituents attached to silicon atoms (Figure 10). This is why polyorganosiloxane elastomers are considered "organic-inorganic" compared with pure organic elastomers. The type of the organic group attached to the silicon atom significantly influences the physical, chemical and mechanical properties of polysiloxanes.

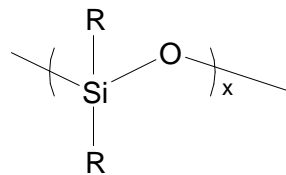


**Figure 10 - The structure of siloxanes (R = organic group)**

What distinguishes siloxane polymers from their organic counterparts is the very flexible chain composed of alternating atoms of silicon and oxygen. This structure allows exceptional mobility and orientation capability. Many of the properties are derived from the flexibility of the siloxanes siloxane bond.

For dielectric elastomers, at sufficiently high driving voltages, the quadratic curve and elastic stress curve can intersect, inducing the pull-in effect and possible eventual dielectric breakdown [11]. When the film is prestrained, the origin of the actuation stress/strain curve shifts to O' and the curve is less likely to intersect the elastic stress/strain curve, making the process of actuation more stable (Figure 11). Prestrain is effective for silicone and acrylic films and also for other elastomers, but the effect varies from material to material.

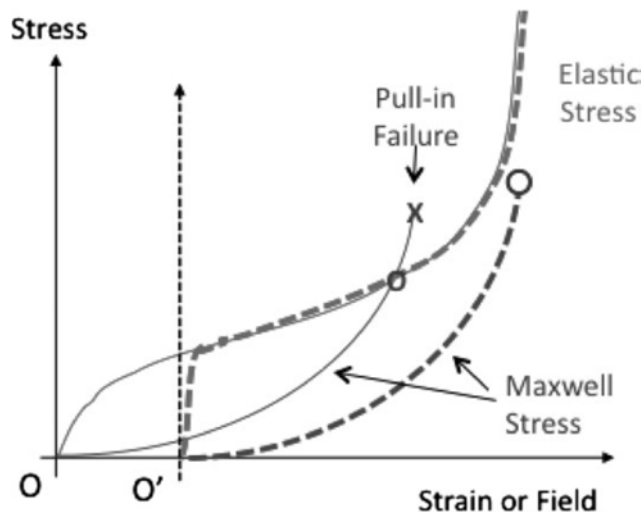


Figure 11 - Characteristic stress of a dielectric elastomer film as a function of mechanical strain or electric field (constant voltage condition). The charts with origin at O are for a non-prestrained film and at O' for the prestrained film. Small o and large O

A disadvantage for a device built with dielectric elastomers is that it requires the use of a large operating voltage, either as actuator or as energy harvesting device. There are two methods that can be used for achieving reduced value for the operating voltage: 1) reducing the thickness of elastomer films so that the required field for functioning of the device occurs at lower voltages; 2) increasing the dielectric constant of the elastomer films to reduce the required electric field intensity. A number of approaches have been explored for the second option, most researchers using the addition of high dielectric constant filler materials to an elastomer host. Silicone rubbers are very interesting for this type of approach as they possess good actuation properties, are readily available in gel form and have a low dielectric constant. These characteristics made this category of elastomers attractive for use in devices based on dielectric elastomers.

### 2.3.2. Chemistry

The most widely used member of the silicone family, polydimethylsiloxane- $\alpha,\omega$ -diol, is usually synthesized either by heterogeneous cationic ring-opening polymerization of octamethylcyclotetrasiloxane, according to procedure described in ref. [18] (Figure 12) or by homogeneous ionic ring-opening polymerization of octamethylcyclotetrasiloxane in the presence of strong acid or base catalysts.

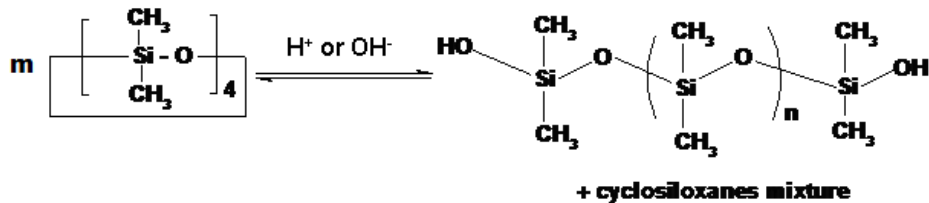


Figure 12 - Ionic ring-opening polymerization of octamethylcyclotetrasiloxane (D4)

The well-developed chemistry of silicones enables the replacement of the methyl groups with a wide variety of functional groups, either random, statistic or block along the polysiloxane chain.

The temperatures where polydimethylsiloxane is typically used ranges from -40 °C to 150 °C for a variety of products and it is influenced by the nature of the chemical side groups at the silicon atom and by their interactions [19].

A severe limitation of silicone rubbers for various applications is represented by the poor mechanical properties, especially the low breaking and tear resistance [20] [21]. In order to overcome these drawbacks, siloxanes cross-linking is used and for this purpose. One of the most important classes of reactions used for crosslinking siloxanes in commercial applications is based on the condensation of silanol groups to form siloxane bonds. A typical system contains PDMS with end silanol groups, a crosslinking agent and a catalyst. Trifunctional and tetrafunctional cross-linking agents, such as tri- and tetraalkoxysilanes, allow curing in the presence of moisture in the atmosphere. The alkoxy function is hydrolyzed to form silanol, and the corresponding alcohol. The silanol can condense with -SiOH end groups of the PDMS, leading to a cross-linked structure. Suitable catalysts for these systems are in general organometallic such as tin carboxylates.

Depending on the desired applications fillers can be added, together with other additives for building domain-specific applications. After curing these systems generate silicone films with low degree of cross-linking that have the ability to dissipate normal and shear loads at high temperature (in applications such as protective coatings that can be detached from the substrate) and also to flexible and strong silicone elastomers, that maintain their elastic properties in a wide range of temperatures [22].

In order to reinforce silicone elastomers, they are often combined with other compounds that have better mechanical properties. These combinations should be stable over time and may be designed as blends, copolymers or polymer interpenetrated network (IPN). In most cases, however, chemical crosslinking is not enough, and it is necessary to add finely divided silica with large specific surface area to obtain interesting properties. Recently, the use of physical cross-linking (formation of hydrogen bonds between two complementary groups attached to the siloxane chain) allowed the synthesis of PDMS rubbers that have exceptional properties without the addition of silica [23]-[25].

Another method of obtaining the silicone rubber without silica filler consists in the preparation of copolymers in which the elastomeric segments (low  $T_g$  polymers - PDMS) are combined with the thermoplastic segments (higher  $T_g$ ) to generate the thermoplastic elastomer (TPE) with improved mechanical properties [26] [27]. By this method were synthesized copolymers of siloxanes with epoxy [28], imide [29] acrylate [30], polycarbonate and eugenol [31]. Furthermore, amphiphilic copolymers can be obtained by combination of PDMS with a hydrophilic polymer [32]. The incorporation of a polysiloxane unit in another polymer is used to modify the properties of other polymers, so that their surface becomes hydrophobic, and the gas permeability of these materials changes and an improvement in the flexibility of the material is also acquired.

### **2.3.3. General characteristics**

Polyorganosiloxanes (Figure 13) show exceptional properties as a result of the polymer chain constitutive unit made of Si-O-Si. The Si-O bond length is equal to 1.64 Å, substantially less than the length of Si-O bond calculated by addition of atomic radii (1.83 Å). This is due, on the one hand, to the double bond character of the Si-O bond, and on the other hand, to the partly ionic character (40-50%) of the Si-O bond (electronegativity of Si is 1.8 and for O it is 3.5) [33]. The main disadvantage arising from the polarity of the Si-O bond is that polysiloxanes are sensitive to hydrolysis under acidic or basic conditions.

The high value of Si-O-Si bond angle (140°) and the flexibility of the Si-O bond are the reasons for the exceptionally low glassy transition temperature observed for polyorganosiloxanes. For example, polydimethylsiloxane  $\alpha,\omega$ -diol (PDMS) has a glass transition temperature of -123 °C due to the movement of twisting along the chain. It has been shown [33], [34] that polydiorganosiloxanes have low value for the intermolecular forces, this leading to higher molar volume ( $75.5 \text{ cm}^3 \text{ mol}^{-1}$ ) and a low density of cohesion energy.

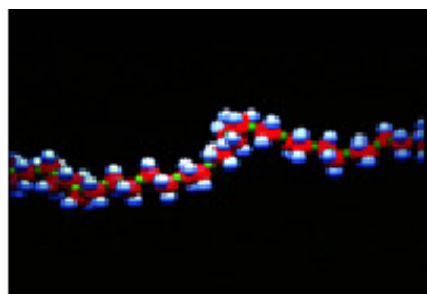
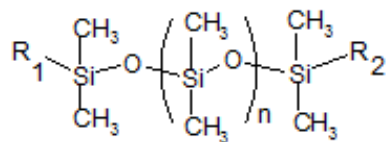


**Figure 13 - The structure of PDMS: R1, R2 are end-chain groups and can be the same or different: OH, H, -CH=CH2**

Other specific properties of siloxanes such as low values for surface tension, surface energy, solubility parameter and dielectric constant observed for PDMS can also be attributed to low intermolecular forces between PDMS chains. The presence of nonpolar methyl groups around the Si-O-Si chain explains their high lipophilic and hydrophobic character. The value of breaking energy of Si-O bond ( $110 \text{ kcal mol}^{-1}$ ) is large when compared with that of the C-O bond ( $85.5 \text{ kcal mol}^{-1}$ ), C-C ( $82.6 \text{ kcal mol}^{-1}$ ) and Si-C ( $76 \text{ kcal mol}^{-1}$ ), and this explains the excellent thermal stability of polyorganosiloxanes. In addition, PDMS shows good gas permeability and is transparent to visible and UV light (methyl groups do not absorb radiation with  $\lambda > 300 \text{ nm}$ ) [34], [35].

Changes in the length of siloxane chain, the type of organic side groups and the cross-linking degree of the chains lead to a broad range of silicones with different composition and properties. The desired properties can be obtained by judicious choice of substituent side groups for the desired application. Thus, the values of melting and boiling temperatures of the siloxanes depend on the side substituents: those with lower aliphatic groups (even polymers with very high molecular weights) are liquid at room temperature, while siloxanes with aromatic substituents (starting with the first term of the series - hexaphenyl-disiloxane) are solid at room temperature.

Siloxanes with mixt substituted groups possess intermediate properties between these extreme types. However, electrophile substituents such as halogen atoms (Br, Cl) or hydroxyl and phenyl groups have the effect of strengthening the Si-O-Si bond and weakening of the Si-R bond (R = substituent on the silicon atom). Nucleophile substituents have an opposite effect on the strength of these connections [36].

By increasing the molecular weight of linear polymer PDMS, viscosity at room temperature can be varied from about  $0.65 \text{ cP}$  to over 100 million cP. At low molecular weight, these materials behave essentially as Newtonian fluids (their viscosity is a function of shear rate) up to shear rates of  $1000 \text{ s}^{-1}$  [19].

The low  $T_g$  value together with almost temperature-independent viscosity and high thermal stability are factors that determine the use of siloxanes in applications where it is required to operate over a wide temperature range [37]-[41].

Despite their unique properties, PDMS rubbers require extremely high molecular weights to develop useful mechanical properties. To better exploit the properties of siloxanes, the polymer chains can be cross-linked. One of the most important reactions for crosslinking siloxanes used in commercial applications are based on the condensation of silanol groups to form siloxane bonds.

When there is a spill or an electrical device such as a transformer brakes, the released silicone polymers degrade relatively rapidly and completely in normal environmental conditions [42]. Such degradation can occur in water, air, and especially in the soil. This is because the polymers come into contact with one or more reactive species which can cause degradation. One of these is the nitrate ion present in nature in streams. This ion is a source of atomic oxygen and of hydroxyl radicals which initiate the degradation process.

UV light itself has very little effect on the structure of siloxanes. Only the shorter wavelengths present in sunlight have some influence and can generate methyl radicals from methyl side groups. Polysiloxanes are resistant to all types of radiation, in particular when they contain aromatic groups, such as phenyl groups in polymethylphenylsiloxane.

## 2.4 Acrylic

### 2.4.1. General description

Acrylic rubber, known by the chemical name alkyl acrylate copolymer (ACM) (or sometimes the tradename Hytemp), is a specialty synthetic rubber used when resistance to petroleum fuel, oil, oxygen, ozone and heat are required. It has outstanding resistance to hot oil and oxidation. ACM is polar and doesn't contain unsaturation. It is resistant to ozone and has low permeability to gases [43]. It is generally resistant to extreme pressure, lubricants, hot oils, petroleum solvents, animal and vegetable fats. It is generally attacked by moisture, water, alcohols, acids, glycols, alkali, esters, aromatic hydrocarbons, halogenated hydrocarbons and phenol. The most industrially produced acrylic rubbers are based on ethyl-, butyl- and metoxy ethyl acrylate and monomers containing chlorine or carboxyl groups. Their suitable combination usually compromise between ACM oil resistance, appropriate properties under low temperatures, heat resistance and acceptable curing rate.

Conventional acrylic films, such as the VHB 4910 series of elastomers from 3M, possess several advantages that make them useful for building polymer transducers: very good actuation strain, energy density, and coupling efficiency. However the acrylic elastomers-based films must be pre-strained in order to achieve these high performance values [11].

### 2.4.2. Chemistry

From chemical point of view, the acrylic rubbers are copolymers or terpolymers of different types of either different acrylic monomers or of acrylic monomers and other monomers containing functional groups suitable for curing (Figure 14). The most frequently used are the vinyl monomers with reactive atoms of chlorine, epoxy or carboxylic groups. The content of these monomers is low (1-3 % wt.) and has no significant influence on their properties [44].

ACM are produced by emulsion (exceptionally by suspension) radical polymerization. For its initiation peroxides, azo-compounds or oxidation-reduction initiation systems are used. Since acrylic monomers have ester groups in their molecules the pH of reaction medium must be > 7, in order to avoid their hydrolysis. Fillers or other additives of acidic character may have the same negative influence in these compounds [45].

ACM properties under low temperatures are influenced mainly by the structure of the alkyl substituents in their ester groups: they are improved with increasing the carbon number in alkyl groups (brittle temperature of poly-n-alkylacrylate is reduced for substituents with carbon number C = 1-8 from +3 °C down to -65°C). Simultaneously, their polarity is decreasing, and thus their non-polar oil and ageing resistance is decreasing.

ACM based on polyethyl acrylate are high-polar and very well resistant to oils and increased temperatures, but they have relatively high  $T_g$  (approximately -15°C) and their vulcanizates are less flexible under low temperatures. Replacement of ethyl groups by butyl ones determine a decrease of  $T_g$  to -50°C and the vulcanizates are significantly more flexible under low temperatures, but their swelling resistance in non-polar oils is lower. Polyoctyl acrylate is practically not resistant against non-polar oils. The properties of ACM under low temperatures may be modified by copolymerization of acryl monomers (ethyl acrylate, butyl acrylate, eventually octyl acrylate or acryl monomer with alkoxy groups) and they can be partially modified also by adding of suitable, less volatile softeners; the best one is of ester type.

For cross-linking of ACM rubbers mainly functional groups of non-acrylate monomers are used, despite the fact that under presence of metallic oxides of alkaline character one cannot exclude even self-curing of polyacrylate chains caused by reactions of their ester groups and active hydrogen in  $\alpha$ -position against them (Claisen's condensation) [45]. The first types of ACM were cured mostly by diamines or polyamines, at present the ACM rubbers are cured also by combination of polyamines, higher fatty acids or their esters and sulfur, eventually by sulfur donor. Their efficiency is increased by addition of very fast or ultra accelerators. The most often used systems for curing of ACM with epoxy and carboxyl groups is based on quaternary ammonium salts.

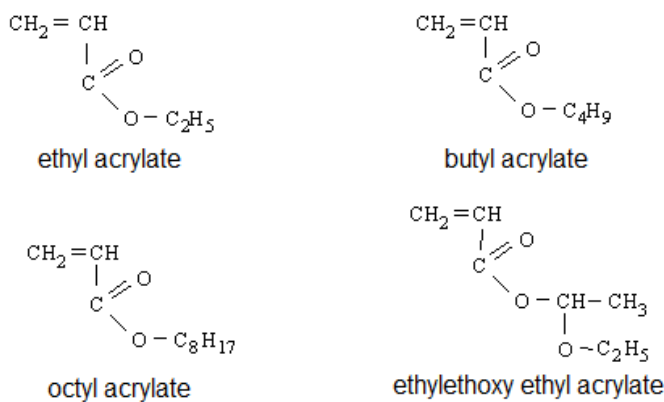


Figure 14 - Examples of the acrylic monomers used during production of ACM

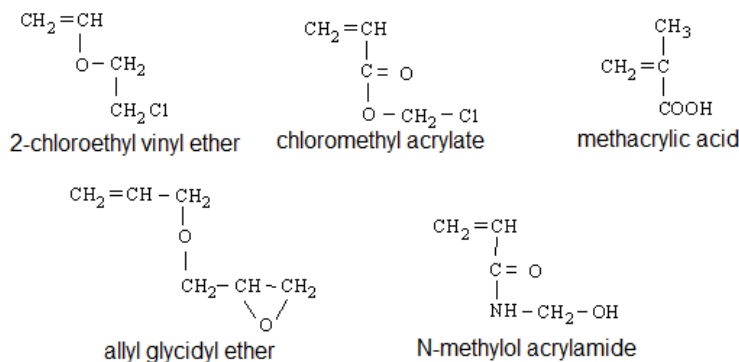


Figure 15 - Examples of functional co-monomers used during production of ACM

#### 2.4.3. General characteristics

ACM is commonly used in automotive transmissions and hoses [45]. It is also used in shaft seals, adhesives, beltings, gaskets and O-rings [46] [47], in vibration damping mounts due to the damping properties.

Acrylic rubber has specific gravity between 1.09 - 1.11, tensile strength values between 2.7 MPa for pure gum and 12 MPa for reinforced rubber [48] [49]. Acrylic rubbers are used mainly for production of materials resistant to oils applicable in automotive motors and other mechanical equipments, in form of latexes for impregnation of textile and paper and in form of solutions as adhesive agents and coating compositions. ACM has a continuous working temperature of 150 °C and an intermittent limit of 180 °C (nu stiu la ce se refeera). It should not be used in temperatures below -10 °C.

### 2.5 Polyurethanes

#### 2.5.1. General description

A polyurethane (PUR or PU) is a polymer composed of a chain of organic units joined by carbamate (urethane) links. While most polyurethanes are thermosetting polymers that do not melt when heated, thermoplastic polyurethanes are also available.

Polyurethane polymers are formed by reacting an isocyanate with a polyol. Both the isocyanates and polyols used to make polyurethanes contain on average two or more functional groups per molecule.

Polyurethane products often are simply called “urethanes”, but should not be confused with ethyl carbamate, which is also called urethane. Polyurethanes neither contain nor are produced from ethyl carbamate.

Polyurethanes are used in the manufacture of flexible, high-resilience foam seating, rigid foam insulation panels, microcellular foam seals and gaskets, durable elastomeric wheels and tires (such as roller coaster and escalator wheels), automotive suspension bushings, electrical potting compounds, high performance adhesives, surface coatings and surface sealants, synthetic fibers (Spandex, carpet underlay, hard-plastic parts (e.g., for electronic instruments), hoses and skateboard wheels).

The electromechanical response of PU is due to both Maxwell pressure and electrostriction. The Maxwell pressure has a significant contribution to the strain response of PU films above the glass transition temperature [50]. While PU films in the 20<sup>th</sup> century proved promising for use as dielectric elastomers, their use was limited due to the dramatic improvements in the actuation properties of silicone and acrylic films with prestrain. The research for use as dielectric elastomers since then has focused on PU-based composites.

### 2.5.2. Chemistry

Polyurethanes are in the class of compounds called reaction polymers, which include epoxies, unsaturated polyesters, and phenolics [51] [52]. Polyurethanes are produced by reacting an isocyanate containing two or more isocyanate groups per molecule ( $R-(N=C=O)_{n \geq 2}$ ) with a polyol containing on average two or more hydroxy groups per molecule ( $R'-(OH)_{n \geq 2}$ ), in the presence of a catalyst. Thus, the reaction for obtaining polyurethane rubbers (U) is polyaddition of diisocyanates and diols. Possible usage of different types of monomers and also combination of diisocyanate monomers and pre-polymer diols, their mutual ratio content and selection of reaction conditions allow creating polyurethanes with different chemical structure and various properties. As a consequence of the nature of starting reagents used in the synthesis, the polyurethane polymers may be conventional or thermoplastic rubbers, hard and tough thermoplasts, reactive solutions or foams. Common functional group of polyurethanes are urethane structural units (Figure 16).

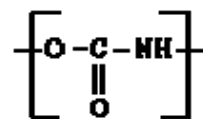


**Figure 16 - The urethane structural unit**

Polyurethane elastomers are prepared using an excess of diols. These are polyurethane-polyester (AU) or polyurethane-polyether (EU) copolymers. The AU rubbers are vulcanized by diisocyanates (toluene diisocyanate or its combination with hydroquinonedioxyethyl ether) or peroxydes in combination with co-catalysts (triallyl cyanurate).

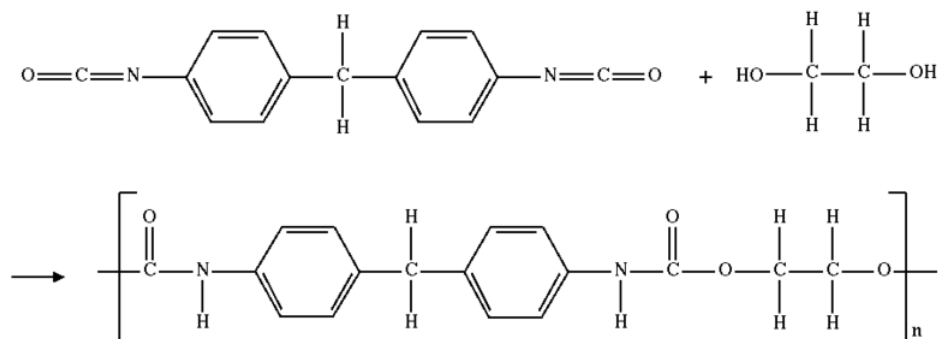


**Figure 17 - Polyurethane synthesis**

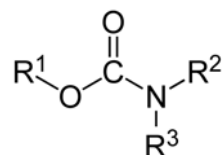


Figure 18 - Chemical structure of carbamates

Isocyanates are very reactive materials. This makes them useful in making polymers but also requires special care in handling and use. The aromatic isocyanates, diphenylmethane diisocyanate (MDI) or toluene diisocyanate (TDI) are more reactive than aliphatic isocyanates, such as hexamethylene diisocyanate (HDI) or isophorone diisocyanate (IPDI). Most of the isocyanates are difunctional that is they have exactly two isocyanate groups per molecule. An important exception to this is polymeric diphenylmethane diisocyanate (MDI), which is a mixture of molecules with two, three, and four or more isocyanate groups. In cases like this, the material has an average functionality greater than two, commonly 2.7. Isocyanates with functionality greater than two act as crosslinking sites.

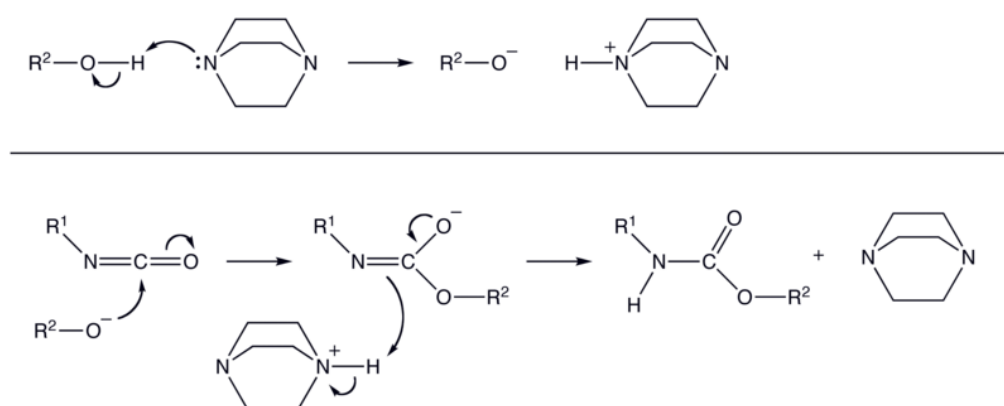


Figure 19 - PU reaction mechanism catalysed by a tertiary amine

Polyols are polymers in their own right and have on average two or more hydroxyl groups per molecule. Polyether polyols are mostly made by polymerizing ethylene oxide and propylene oxide. Polyester polyols are made similarly to polyester polymers. The polyols used to make polyurethanes are not "pure" compounds since they are often mixtures of similar molecules with different molecular weights and mixtures of molecules that contain different numbers of hydroxyl groups, which is why the "average functionality" is often mentioned. Despite them being complex mixtures, industrial grade polyols have their composition sufficiently well controlled to produce polyurethanes having consistent properties. As mentioned earlier, it is the length of the polyol chain and the functionality that contribute much to the properties of the final polymer. Polyols used to make rigid polyurethanes have molecular weights in the hundreds, while those used to make flexible polyurethanes have molecular weights up to ten thousand or more.

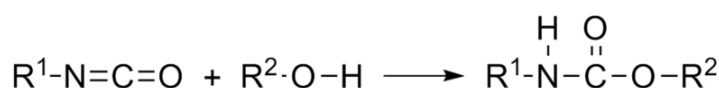


Figure 20 - The general urethane reaction

The polymerization reaction makes a polymer containing the urethane linkage,  $-\text{RNHCOOR}'-$  and is catalysed by tertiary amines, such as 1,4-diazabicyclo[2.2.2]octane (DABCO or TEDA), and metallic compounds, such as dibutyltin dilaurate or bismuth octanoate. This is often referred to as the gellation reaction or simply gelling.

If water is present in the reaction mixture (it is added intentionally for making foams), the isocyanate reacts with water to form a urea linkage and carbon dioxide gas and the resulting polymer contains both

urethane and urea linkages. This reaction is referred to as the blowing reaction and is catalyzed by tertiary amines like bis-(2-dimethylaminoethyl)ether.

A third reaction, important in making insulating rigid foams is the isocyanate trimerization reaction, which is catalyzed by potassium octoate, for example.

One of the most desirable attributes of polyurethanes is their ability to be turned into foam. Making a foam requires the formation of a gas at the same time as the urethane polymerization (gellation) is occurring. The gas can be carbon dioxide, either generated by reacting isocyanate with water, or added as a gas or produced by boiling volatile liquids. In the latter case heat generated by the polymerization causes the liquids to vaporize. The liquids used are HFC-245fa (1,1,1,3,3-pentafluoropropane) and HFC-134a (1,1,1,2-tetrafluoroethane), and hydrocarbons such as n-pentane.

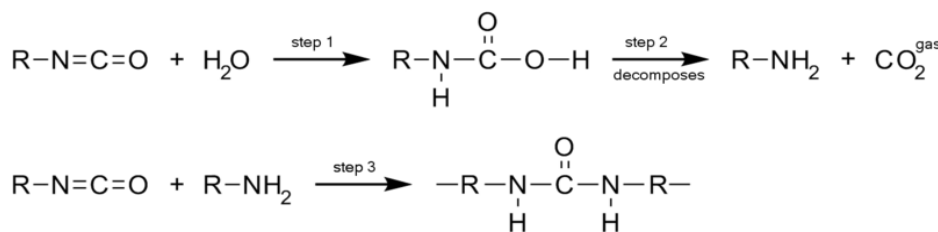


**Figure 21 - Formation of carbon dioxide gas by reacting water and isocyanate**

The balance between gellation and blowing is sensitive to operating parameters including the concentrations of water and catalyst. The reaction to generate carbon dioxide involves water reacting with an isocyanate first forming an unstable carbamic acid, which then decomposes into carbon dioxide and an amine. The amine reacts with more isocyanate to give a substituted urea. Water has a very low molecular weight, so even though the weight percent of water may be small, the molar proportion of water may be high and considerable amounts of urea produced. The urea is not very soluble in the reaction mixture and tends to form separate "hard segment" phases consisting mostly of polyurea. The concentration and organization of these polyurea phases can have a significant impact on the properties of the polyurethane foam [53].

### 2.2.3. General characteristics

Polyurethanes are produced by mixing two or more liquid streams. The polyol stream contains catalysts, surfactants, blowing agents and so on. The two components are referred to as a polyurethane system, or simply a system. The isocyanate is commonly referred to in North America as the 'A-side' or just the 'iso'. The blend of polyols and other additives is commonly referred to as the 'B-side' or as the 'poly'. This mixture might also be called a 'resin' or 'resin blend'. In Europe the meanings for 'A-side' and 'B-side' are reversed. Resin blend additives may include chain extenders, crosslinkers, surfactants, flame retardants, blowing agents, pigments, and fillers. Polyurethane can be made in a variety of densities and hardnesses by varying the isocyanate, polyol or additives.

The properties of a certain polyurethane are greatly influenced by the types of isocyanates and polyols used to make it. Long, flexible segments, contributed by the polyol, give soft, elastic polymer. High amounts of crosslinking give tough or rigid polymers. Long chains and low crosslinking give a polymer that is very stretchy, short chains with lots of crosslinks produce a hard polymer while long chains and intermediate crosslinking give a polymer useful for making foam. The crosslinking present in polyurethanes means that the polymer consists of a three-dimensional network and molecular weight is very high. In some respects, a piece of polyurethane can be regarded as one giant molecule. One consequence of this is that typical polyurethanes do not soften or melt when they are heated; they are thermosetting polymers. The choices available for the isocyanates and polyols, in addition to other additives and processing conditions allow polyurethanes to have the very wide range of properties that make them such widely used polymers.

High-density microcellular foams can be formed without the addition of blowing agents by mechanically frothing or nucleating the polyol component prior to use.

Surfactants are used in polyurethane foams to emulsify the liquid components, regulate cell size, and stabilize the cell structure to prevent collapse and surface defects. Rigid foam surfactants are designed to

produce very fine cells and very high closed cell content. Flexible foam surfactants are designed to stabilize the reaction mass while at the same time maximizing open cell content to prevent the foam from shrinking.

Foam with even higher degree of rigidity can be made with the use of specialty trimerization catalysts which create cyclic structures within the foam matrix, giving a harder, more thermally stable structure, designated as polyisocyanurate foams. Such properties are desired in rigid foam products used in the construction sector.

Careful control of viscoelastic properties — by modifying the catalysts and polyols used —can lead to memory foam, which is much softer at skin temperature than at room temperature.

Foams can be either "closed cell", where most of the original bubbles or cells remain intact, or "open cell", where the bubbles have broken but the edges of the bubbles are stiff enough to retain their shape. Open cell foams feel soft and allow air to flow through so they are comfortable when used in seat cushions or mattresses. Closed cell rigid foams are used as thermal insulation, for example in refrigerators. Microcellular foams are tough elastomeric materials used in coverings of car steering wheels or shoe soles.

The characteristic properties of the polyurethane-polyester copolymers (AU) and their vulcanizates are high strength, ageing resistance (practically they do not react with oxygen not even with ozone), heat resistance, excellent abrasion resistance and relatively good elastic properties at any hardness, small permeability for gases and vapors and also relatively good swelling resistance in non-polar oils. Their disadvantage is in possible hydrolysis, mainly in medium of hot water, steam, acids and alkalis, and finally also under influence of lubricants, heat and long-term influence of tropical climatic conditions. Thus effective hydrolysis inhibitors are added into their compounds, such as polycarbon diimides. In urethane rubbers the association may appear as consequence of physical attractive forces among their macromolecules (polar forces, hydrogen bridges), which affect the particles of the reinforcing fillers. From this reason AU rubbers are normally processed without fillers and hardness of the vulcanizates is regulated by content of curing agent. But usage of reinforcement and also non-reinforcement fillers is not excluded; the problem is usually with mixing temperature that must be adapted to their volatility during application of isocyanates as curing agents.

The polyurethane rubbers are used mainly for products in automotive industry and machine engineering, as different elements of dampers, flexible connections, and electric lines and also in such cases, when simultaneous high abrasion resistance of the product is required. Over three quarters of the global consumption of polyurethane products is in the form of foams, with flexible and rigid types being roughly equal in market size. In both cases, the foam is usually behind other materials: flexible foams are behind upholstery fabrics in commercial and domestic furniture; rigid foams are inside the metal and plastic walls of most refrigerators and freezers, or behind paper, metals and other surface materials in the case of thermal insulation panels in the construction sector. Its use in garments is well-known in lining the cups of brassieres. Polyurethane is also used for moldings which include door frames, columns, balusters, window headers, pediments, medallions and rosettes.

Polyurethane formulations cover an extremely wide range of stiffness, hardness, and densities. These materials include:

- low-density flexible foam used in upholstery, bedding, and automotive and truck seating;
- low-density rigid foam used for thermal insulation and RTM cores;
- soft solid elastomers used for gel pads and print rollers;
- low density elastomers used in footwear;
- hard solid plastics used as electronic instrument bezels and structural parts;
- flexible plastics used as straps and bands.

Polyurethane foam is widely used in high resiliency flexible foam seating, rigid foam insulation panels, microcellular foam seals and gaskets, durable elastomeric wheels and tires, automotive suspension bushings, electrical potting compounds, seals, gaskets, carpet underlay, and hard plastic parts (such as for electronic instruments).

Fully reacted polyurethane polymer is chemically inert [54]. No exposure limits have been established in the U.S. by OSHA (Occupational Safety and Health Administration) or ACGIH (American Conference of Governmental Industrial Hygienists). It is not regulated by OSHA for carcinogenicity. Polyurethane polymer is a combustible solid and can be ignited if exposed to an open flame [55]. Decomposition from fire can produce mainly carbon monoxide, and trace nitrogen oxides and hydrogen cyanide.

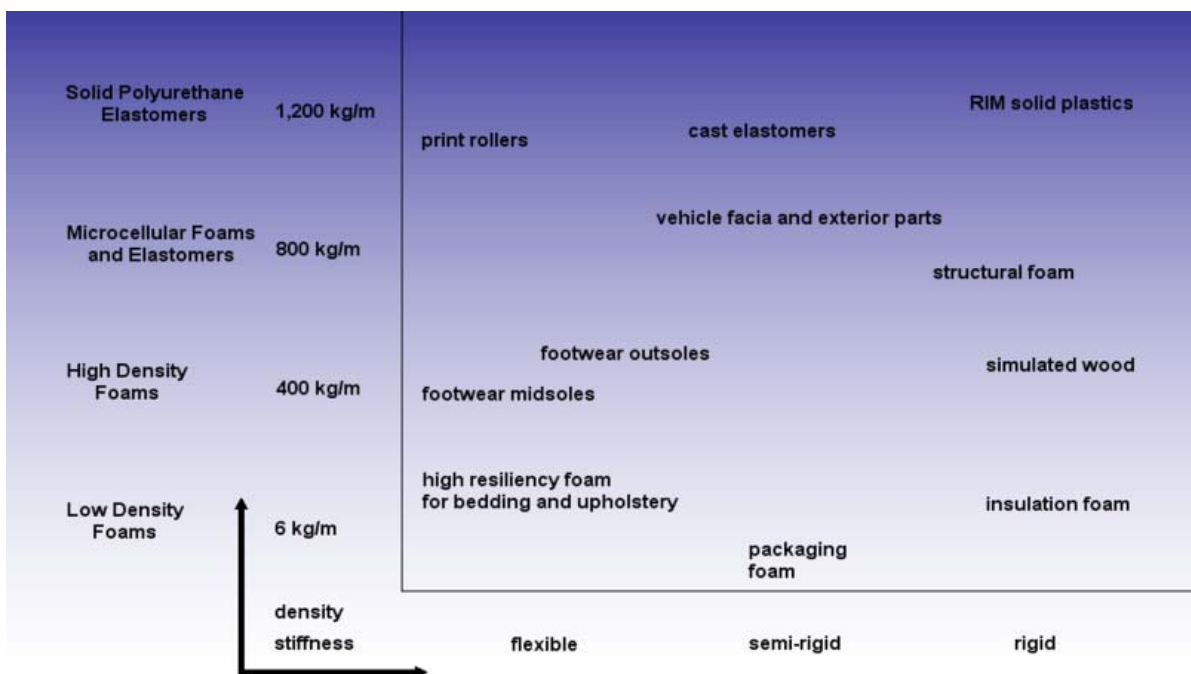


Figure 22 - Characteristics of polyurethane materials [56]

Liquid resin blends and isocyanates may contain hazardous or regulated components. Isocyanates are known skin and respiratory sensitizers. Additionally, amines, glycols, and phosphate present in spray polyurethane foams present risks.

In the United States, additional health and safety information can be found through organizations such as the Polyurethane Manufacturers Association (PMA) and the Center for the Polyurethanes Industry (CPI), as well as from polyurethane system and raw material manufacturers. Regulatory information can be found in the Code of Federal Regulations Title 21 (Food and Drugs) and Title 40 (Protection of the Environment). In Europe, health and safety information is available from ISOPA [54], the European Diisocyanate and Polyol Producers Association.

Polyurethanes, especially those made using aromatic isocyanates, contain chromophores which interact with light. This is of particular interest in the area of polyurethane coatings, where light stability is a critical factor and is the main reason that aliphatic isocyanates are used in making polyurethane coatings. When PU foam, which is made using aromatic isocyanates, is exposed to visible light it discolours, turning from off-white to yellow to reddish brown. It has been generally accepted that apart from yellowing, visible light has little effect on foam properties [57]. This is especially the case if the yellowing happens on the outer portions of a large foam, as the deterioration of properties in the outer portion has little effect on the overall bulk properties of the foam itself. The exposure to visible light can affect the variability of some physical property test results [58]. Higher-energy UV radiation promotes chemical reactions in foam, some of which are detrimental to the foam structure [59].

When chlorine gas reacts with water, HCl and HOCl form and HCl causes the decomposition of the inner part of the polyurethane tubing into amine salts and the polyol [60]. Tropical fungus has been reported to degrade polyurethanes [61]. This fact was reported from a trip to the Ecuadorian Amazon and the fungus is called *Pestalotiopsis microspora*.

## Section 3: Measurement procedures

### 3.1 Introduction

When constructing a device that uses dielectric elastomers for energy harvesting or for actuation it is important to have the data about the properties that are important for these elastomers presented in a single clear document. For this purpose available commercial materials were characterized through a similar procedure with the same type of scientific apparatus. This lead to a set of values having the advantage of comparing all materials in a unitary set of data. It is intended that these data form an open access database that would offer access to information regarding the dielectric elastomers without the variability due to atmospheric conditions of testing and also to differences in equipment and method.

In this section are presented the equipments and parameters for the characterization of the materials and the data obtained. The section is divided in subsections, each presenting a parameter important for dielectric elastomer: dielectric constant – the values for dielectric constant and dielectric loss were recorded, electrical breakdown, mechanical properties – the data for pure breaking strength tests on dumb bell samples and the data for stress-strain curves on large sheets of elastomers, and water adsorption - dynamic vapour sorption isotherms and kinetics. Each subsection contains a detailed description of the measurement equipment for the specific property, the experimental procedure and sample plots of the results.

### 3.2 Dielectric constant

#### 3.2.1 Measurement equipment

Dielectric spectroscopy was performed using the Novocontrol “Concept 40” broadband dielectric spectrometer (Hundsangen, Germany). The samples were mounted between gold platens and positioned in the Novocontrol Quattro Cryosystem. The dielectric experiment was carried out keeping the temperature fixed but sweeping the frequency. The temperature was 25 °C and six decades (log scale) of frequency, i.e. 1–100000 Hz, were scanned, with the dielectric constant ( $\epsilon'$ ) and loss ( $\epsilon''$ ) were recorded in the frequency domain 1 Hz–1 MHz.

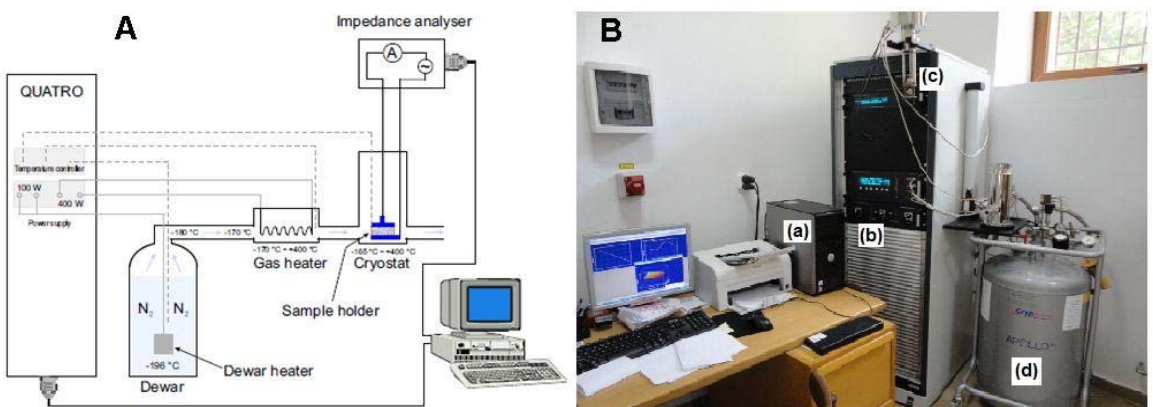


Figure 23 - Dielectric spectrometer: A) the working principle; B) the equipment used in the laboratory: (a) the computer system, (b) power electronics; c) the recess (nu stiu cuvantul; poate sample holder e mai bine) in which the sample is inserted, d) dewar flas

The principle of measurements is shown in Figure 24. The sample material is mounted in sample cell between two electrodes forming a sample capacitor. A voltage  $U_0$  with a fixed frequency  $\omega/2\pi$  is applied to the sample capacitor, which causes a current  $I_0$  at the same frequency in the sample. In addition, there is a phase shift  $\varphi$  between current and voltage. By an Alpha Frequency Response Analyzer, a Fourier correlation analysis is performed and from measured  $U_0$ ,  $I_0$  and  $\varphi$ , values of dielectric permittivity  $\epsilon'$ , dielectric loss  $\epsilon''$ , or loss tangent  $\tan(\delta) = \epsilon'/\epsilon''$  are calculated.

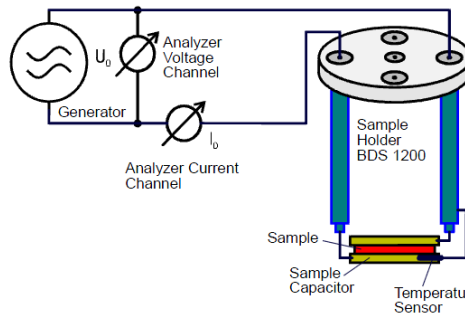


Figure 24 - Principle of dielectric properties measurements

The technical parameters of the setup (measurement ranges) are as follows:

- Frequency  $3 \mu\text{H} \dots 20 \text{ MHz}$
- Impedance  $0.01 \dots 10^{14} \Omega$
- Capacity  $10^{-15} \dots 1 \text{ F}$
- Loss factor  $\tan(\delta) 10^{-5} \dots 10^{-4}$
- A.C. voltage  $100 \mu \dots 3 \text{ Vrms}$

Accuracy: Relative impedance or capacity, absolute loss factor  $\tan(\delta) < 3 \times 10^{-5}$ , absolute phase angle  $< 2 \text{ m}^\circ$ .

Resolution: loss factor  $\tan(\delta)$ , impedance, capacity  $< 10^{-5}$ , phase angle  $< 0.6 \text{ m}^\circ$ .

### 3.2.2 Experimental procedure

For measurement, samples having uniform thickness in the 0.7-1 mm range were placed between gold plated round electrodes, the upper electrode having a 20 mm diameter and a good ohmic contact was ensured.

The dielectric experiment was carried at constant temperature, by sweeping the frequency from 1 Hz to  $10^6 \text{ Hz}$ . Temperature was controlled using a nitrogen gas cryostat and the temperature stability of the sample was better than  $0.1 \text{ }^\circ\text{C}$ . The temperature was  $25 \text{ }^\circ\text{C}$  and the dielectric constant ( $\epsilon'$ ) and loss ( $\epsilon''$ ) were recorded in the frequency domain 1 Hz – 1 MHz.

No.	Sample	Dielectric constant ( $\epsilon'$ )			Dielectric loss ( $\epsilon''$ )		
		1Hz	1kHz	1MHz	1Hz	1kHz	1MHz
1.	0050 SBR	1262.9	511.7	342.2	1.2175E6	1235.1	113.8

Table 3 - Example of dielectric values determined for a commercial elastomer sample

### 3.3 Electrical Breakdown

#### 3.3.1 Measurement equipment

The equipment for measuring the breakdown electrical field has been realized in compliance with the CEI EN 60243 norm (Electric strength of insulating materials). Especially the electrodes shown in Figure 25 are made from brass and the dimensions are 75 mm diameter (ground plate) and 25 mm diameter (HV electrode). The material under test is placed between the electrodes. The electrodes are embedded into a Delrin shield to avoid current flowing through the air and to prevent test operators from electric shock. The electrodes are connected with a high voltage amplifier Trek 10/10B-HS which provides electric field for the test. The amplifier is equipped with voltage and current readout analog signals. The signals are acquired with an oscilloscope and saved on flash memory. As soon as the electrical breakdown event occurs the current readout gives indication of discharge. Reading the breakdown voltage from the oscilloscope and measuring the material thickness the electrical breakdown field is calculated. The thickness of material is measured by Keyence LK-G152 laser. The maximum voltage applicable with such equipment is 10kV. If the material

under test resists to voltage higher then 10kV the material is stretched to get thinner layer. The test is repeated until the breakdown event occurs.

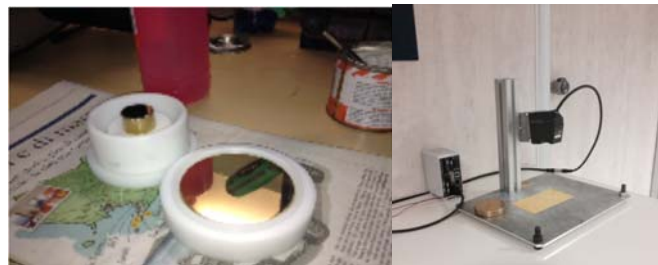


**Figure 25- Apparatus for Dielectric Strenght measurement (left) and laser system for the measurement of membrane thickness**

### 3.3.2 Experimental procedure

Electrical break-down tests are accomplished in two stages. Firstly the thickness of material is measured by laser. Secondly the material is placed between the electrodes and voltage is increased from 0V to 10KV within 5s. As the electrical breakdown occurs the voltage is turned off. Measured breakdown voltage divided by thickness gives breakdown electric field which indicates the capacity of the material to resist to electric fields.

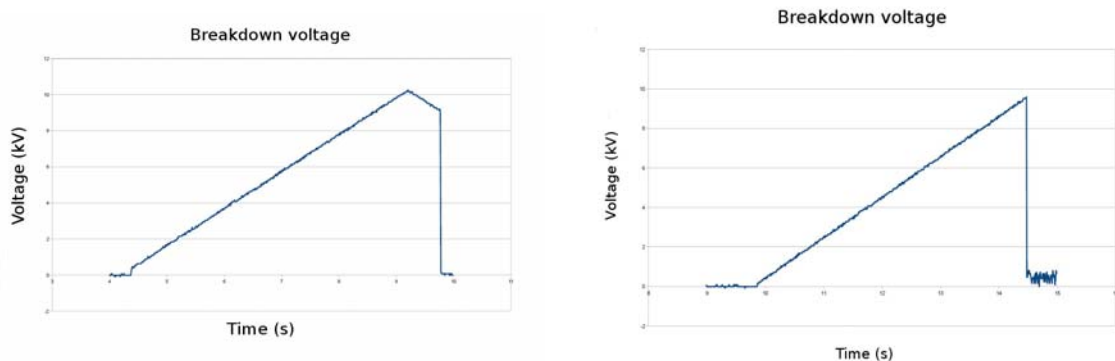


**Figure 26 - Natural rubber electric breakdown test result (left) and Latex free rubber electric breakdown test result (right).**

## 3.4 Mechanical properties

### 3.4.1 Measurement equipment

Stress-strain measurements were performed on TIRA test 2161 apparatus, Maschinenbau GmbH Ravenstein, Germany on dumbbell-shaped cut samples with dimensions of 50x8.5x4 mm. Measurements were run at an extension rate of 20 mm/min, at room temperature (24-25 °C). All samples were measured three times and the averages of the obtained values were taken into consideration.

Cyclic tensile stress tests were performed on the similar samples between 2 and 100% strain. The maximum force applied was tensile stress value as determined by previous test. Five stretch-recovery cycles were registered. The stationary time at minimum and maximum applied stress was 5 s.



**Figure 27 - Equipment used for finding the properties of mechanical strength of the elastomer samples**

The dumbbell shaped samples used were cut from the elastomer sheets using a Ray-Ran Hand Operated Cutting Press, which is designed to cut shapes for test samples from relatively flexible materials, such as plastics, fabrics, boards and paper. The thickness of the material that can be cut depend on the strength of the material and also on the lateral flexibility of the material to allow the cutter to penetrate down into, and pass through the material. The press generates on average up to 600 kg (6 KN) of cutting force, depending on strength of operator. The cutting press is equipped with fine height adjustment of cutter, cutting mat, Arbour locking tool, hexagon key.

The test apparatus for mechanical testing used at Scuola Supriore Sant'Anna is a self assembled stress-strain equipment. The machine is composed of a Linear motor, force sensors and a control unit. The motor is a Linmot PS01-37x120F which provides 100N force. The motor is controlled by a motor driver Linmot B1100. The motor is mounted in vertical direction to exploit the slider weight. An additional weight can be hanged from the slider to increase the maximum force. A force sensor QS Europe 535 QD A1 is mounted on top of the motor slider. The slider position is detected by the internal encoder of the motor. Maximum stroke of the machine is 280mm. The system is controlled by ServoToGo target machine. The model of control has been programmed with Simulink. The control strategy is based on PID controller.



**Figure 28 - (a) Test equipment for mechanical characterization of DE membranes (b) test clamps designed for thin membranes.**

### 3.4.2 Experimental procedure

First dumbbell-shaped samples were cut from the elastomer sheets using the Ray-Ran test equipment (Figure 29). Then the dumbbell-shaped cut samples were clamped at each end with two manual clamps made of metal and the measurements was started with the sample being subjected to an extension rate of 20 mm/min, at room temperature (25 °C). The extension continues until the sample breaks and then the machine automatically brings the clamps in the initial position. In order to have an accurate image of the properties of the samples, they were all measured three times and the averages of the obtained values were taken into consideration.

For cyclic stress-strain tests were used samples with the same dumbbell-shaped cut and after these were clamped, the apparatus was programmed to perform the stretching of the sample between 2 and 100% strain. The maximum force applied was tensile stress value as determined by stress-strain test previously performed with the samples. Five stretch-recovery cycles were registered.

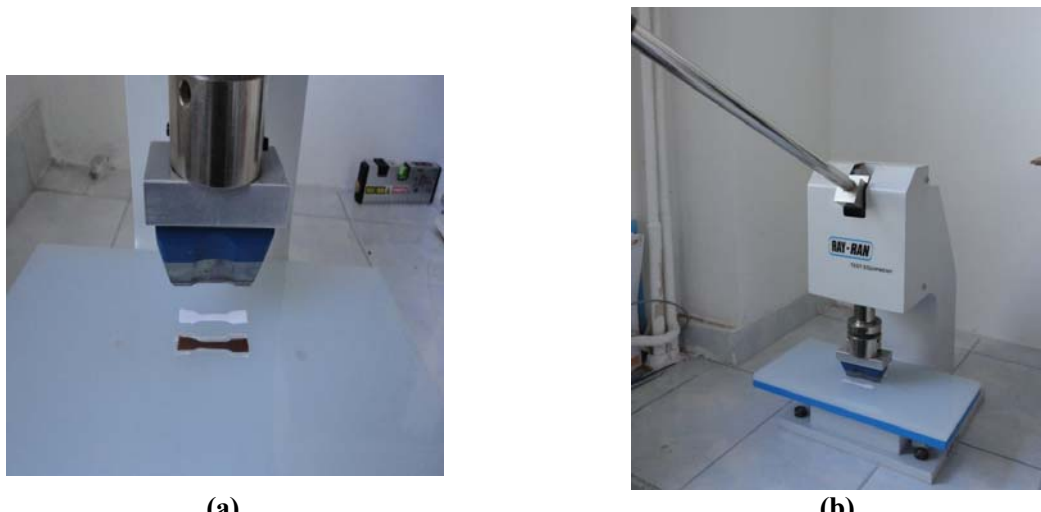
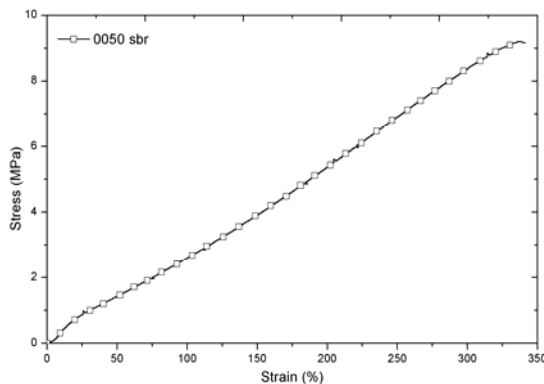
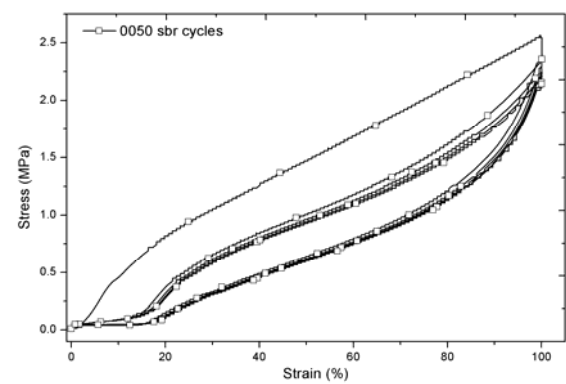


**Figure 29 - Ray-Ran test equipment used for cutting samples for mechanical tests: (a) detail of the cutting head; (b) overall view of the equipment**

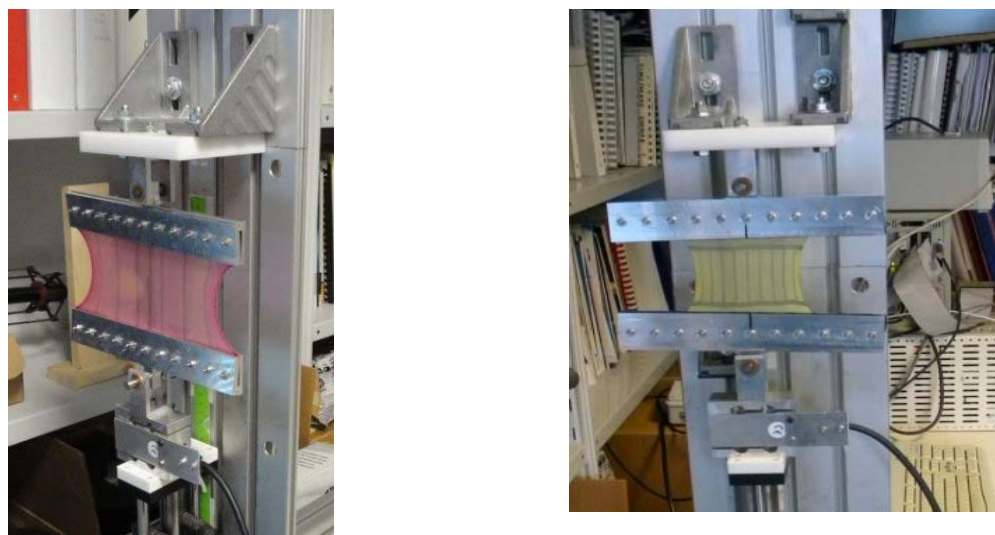


**(a)**



**(b)**

**Figure 30 - (a) Stress-strain curve; (b) Cyclic stress-strain results, for sample 0050 SBR**



**(a)**

**(b)**

**Figure 31 - (a) Properly clamped sample (b) Improperly clamped sample;**

Tests are performed on samples of material cut into rectangular shape pieces. A pattern is drawn on the sample by a pencil. The pattern is useful to understand if the sample is deforming uniformly during the test. Then the sample is secured in the clamps which are placed into the testing machine. Stress-strain test is performed at different speeds. The machine is able to perform repeated cycles and rupture test.

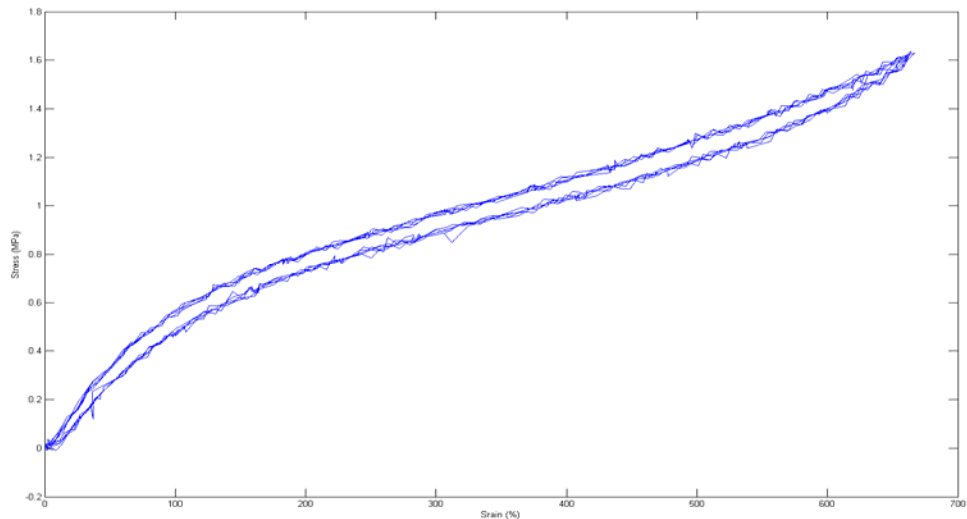


**Figure 32 - Natural rubber stress-strain curve 10mm/s**

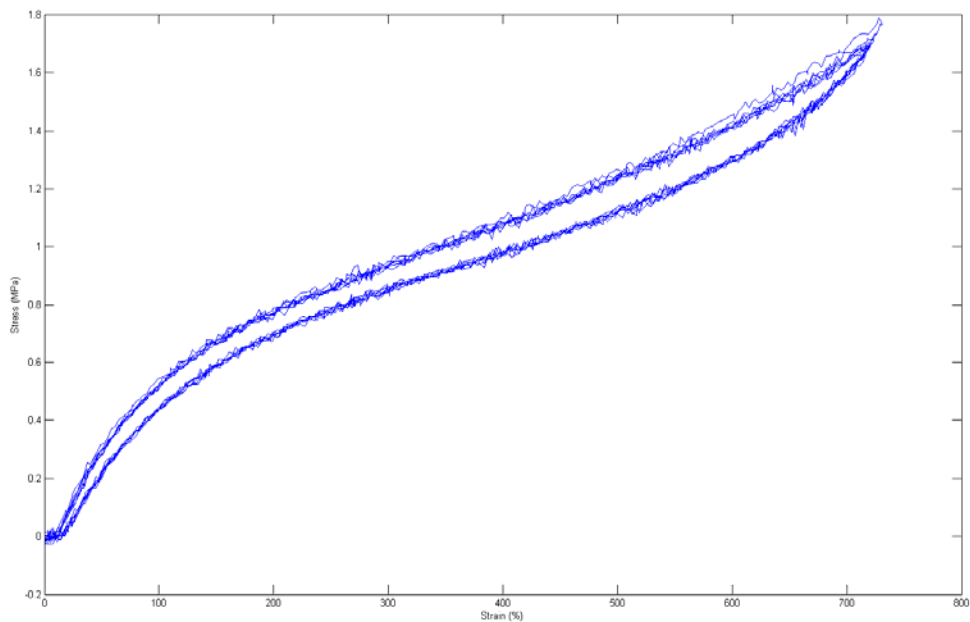


**Figure 33 - Natural rubber stress-strain curve 5mm/s;**

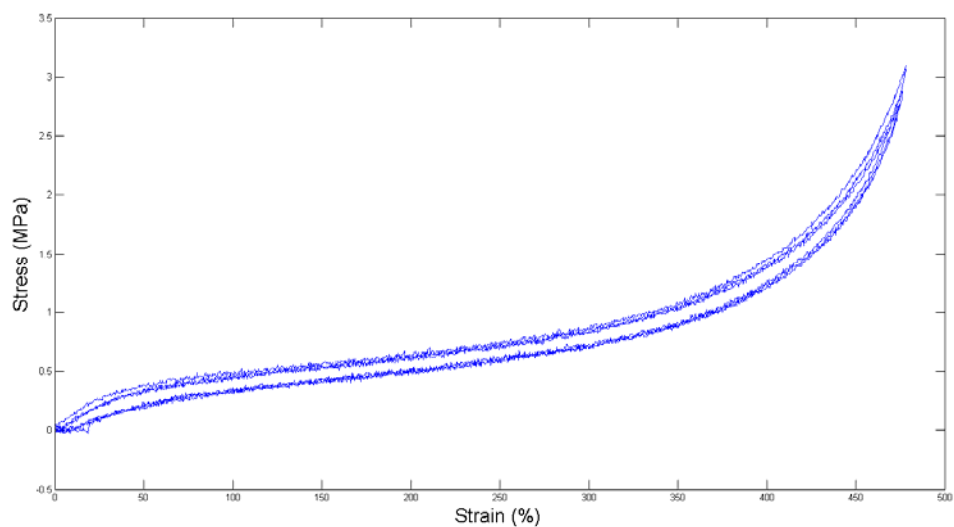


**Figure 34 - Latex free rubber stress-strain curve 1mm/s;**

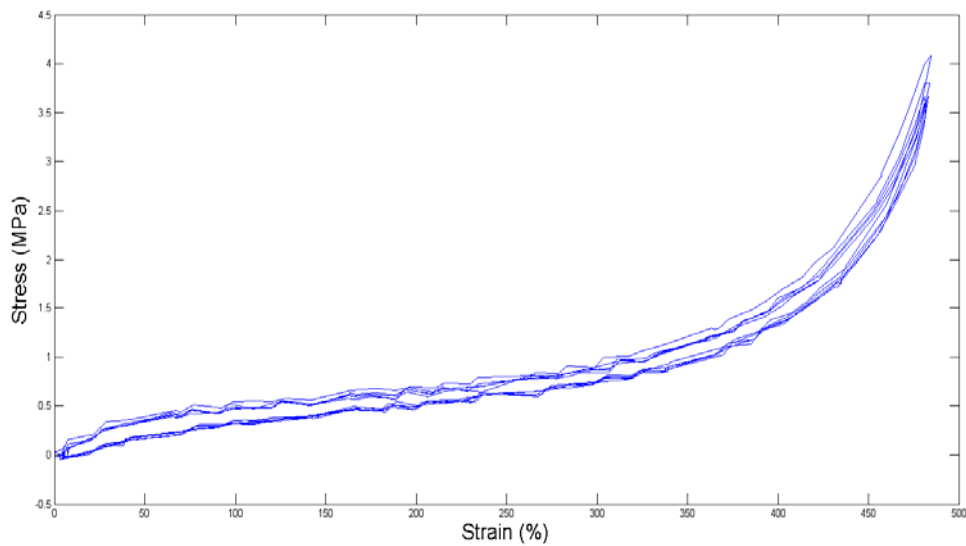


Figure 35 - Latex free rubber stress-strain curve 20mm/s;

### 3.5 Water adsorption

#### 3.5.1 Measurement equipment

The measurements for dynamic vapour sorption and sorption hysteresis were performed with an IGAsorp Dynamic Vapour Sorption apparatus with the following characteristics: minimum gas pressure, 2 bar; resolution of 0.1 µg for 100 mg and sample containers made out of stainless steel micron size mesh.

Before sorption measurements, the samples were dried at 25 °C in a flow of dry nitrogen (250 mL/min) until the weight of the sample was in equilibrium at a relative humidity (RH) less than 1%.

The measurements were performed with programs involving step increase of 10% for the relative humidity of the flow of nitrogen with a cut out time of 60 minutes for each step and recording the mass change for each step.

#### 3.5.2 Experimental procedure

The principle of functioning for this apparatus is based on recording the gravimetric changes of the sample in presence of nitrogen atmosphere with controlled humidity. The samples to be tested can be either liquid or solid. The liquid samples are inserted in a Pyrex glass sphere with a special opening for insertion of liquids. The solid samples can be loaded in a sample containers made out of stainless steel micron size mesh.

The container with the sample is introduced in the sample chamber (Figure 36a). The parameters for the experiment are set using the dedicated software. The sample is first dried with a current of dry nitrogen, and then the relative humidity in the sample chamber is increased in 10% steps. For each step a cut off time of 60 minutes is set, in order to allow the sample to reach a plateau of mass equilibrium due to vapour sorption at a certain humidity value. After reaching the maximum 90% relative humidity, in the following steps there is decreasing value of relative humidity of the atmosphere in 10% steps, going back to 0% humidity. At each step the cut-off time allows stabilization of the sample mass at the respective humidity.



Figure 36 - DVS IGASorp equipment used for recording the water vapour sorption in the samples: (a) sample chamber with sensitive scale; (b) reservoir for the dry gas (nitrogen) that is used to create an atmosphere with controlled humidity in the sample chamber; (c) distilled water reserve where the dry gas is passed through in order to have the desired humidity; (d) computer for control of the equipment; (e) thermostat for the equipment

No.	Sample	Max. Weight (% dry basis)
1.	0050SBR	0.12

Table 4 - Data for maximum sorption capacity of the tested materials

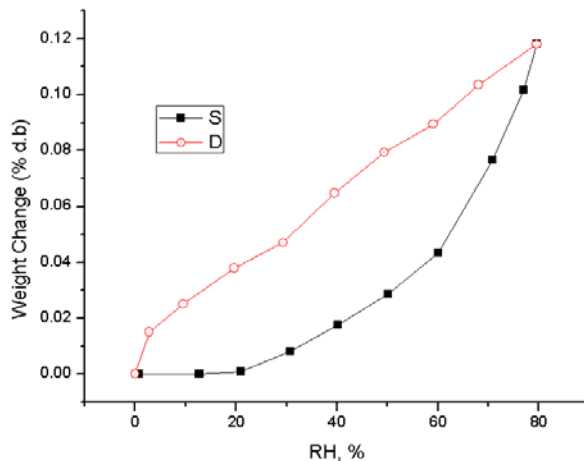


Figure 37- Sorption-desorption isotherm for sample 0050 SBR

### 3.6 Conductivity Properties

#### 3.6.1 Measurement equipment

The test equipment is the same as 3.3.1.

### 3.6.2 Experimental procedure

The test is similar to 3.3.2. the voltage is increased from 0V to 10kV in 5s. The relationship between current and voltage signals from the amplifier readout are recorded on the oscilloscope. The resistivity of polymer should decrease on higher electric fields.

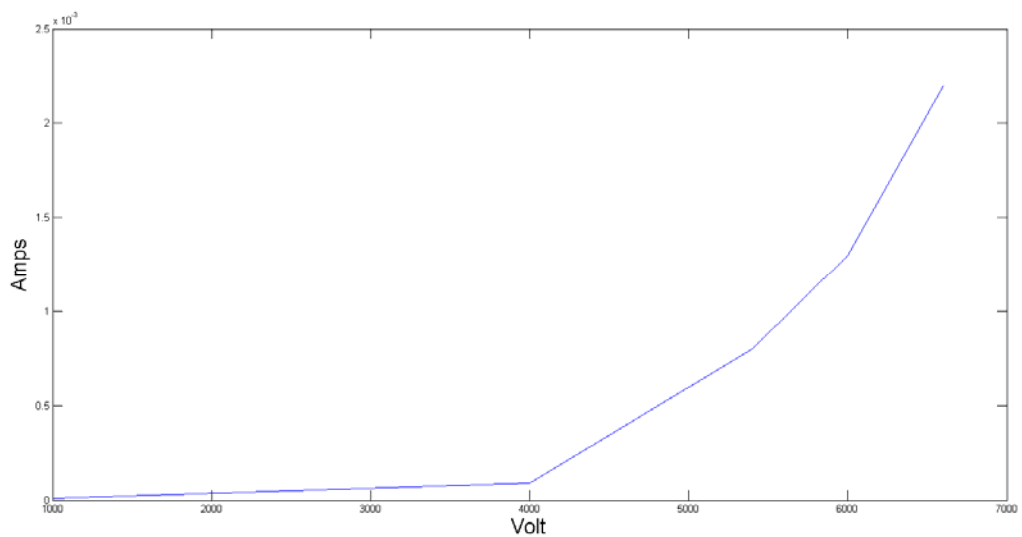


**Figure 38 - Rubber volt vs amps**

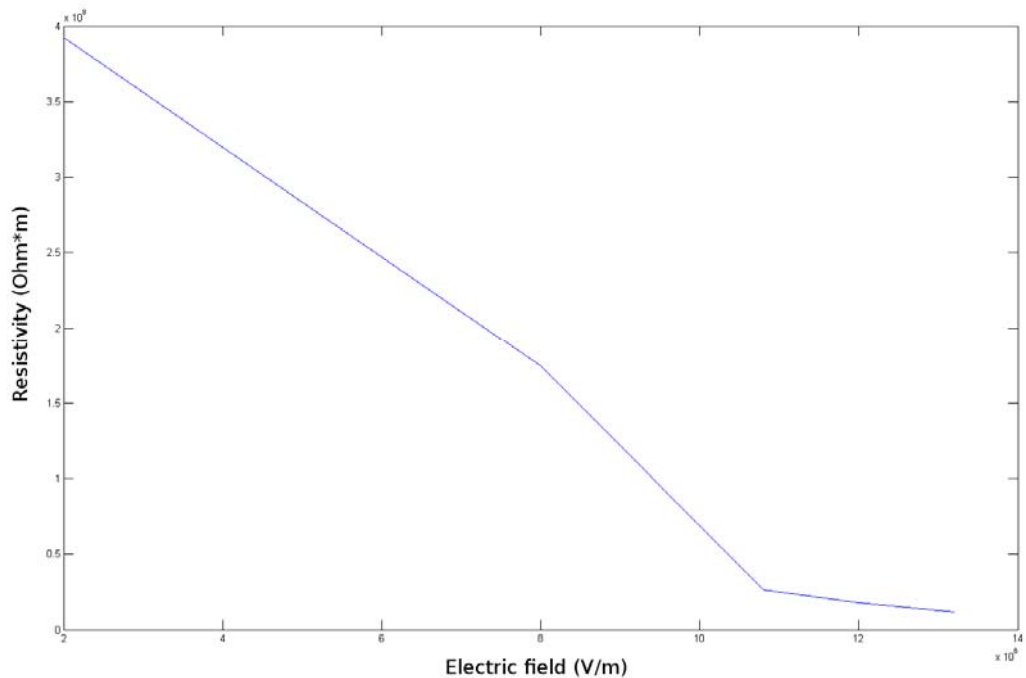


**Figure 39 - Rubber resistivity vs electric field**

### 3.7. Thermal analysis

#### 3.7.1 Measurement equipment

DSC measurements were conducted with DSC 200 F3 Maia equipment (Netzsch, Germany).

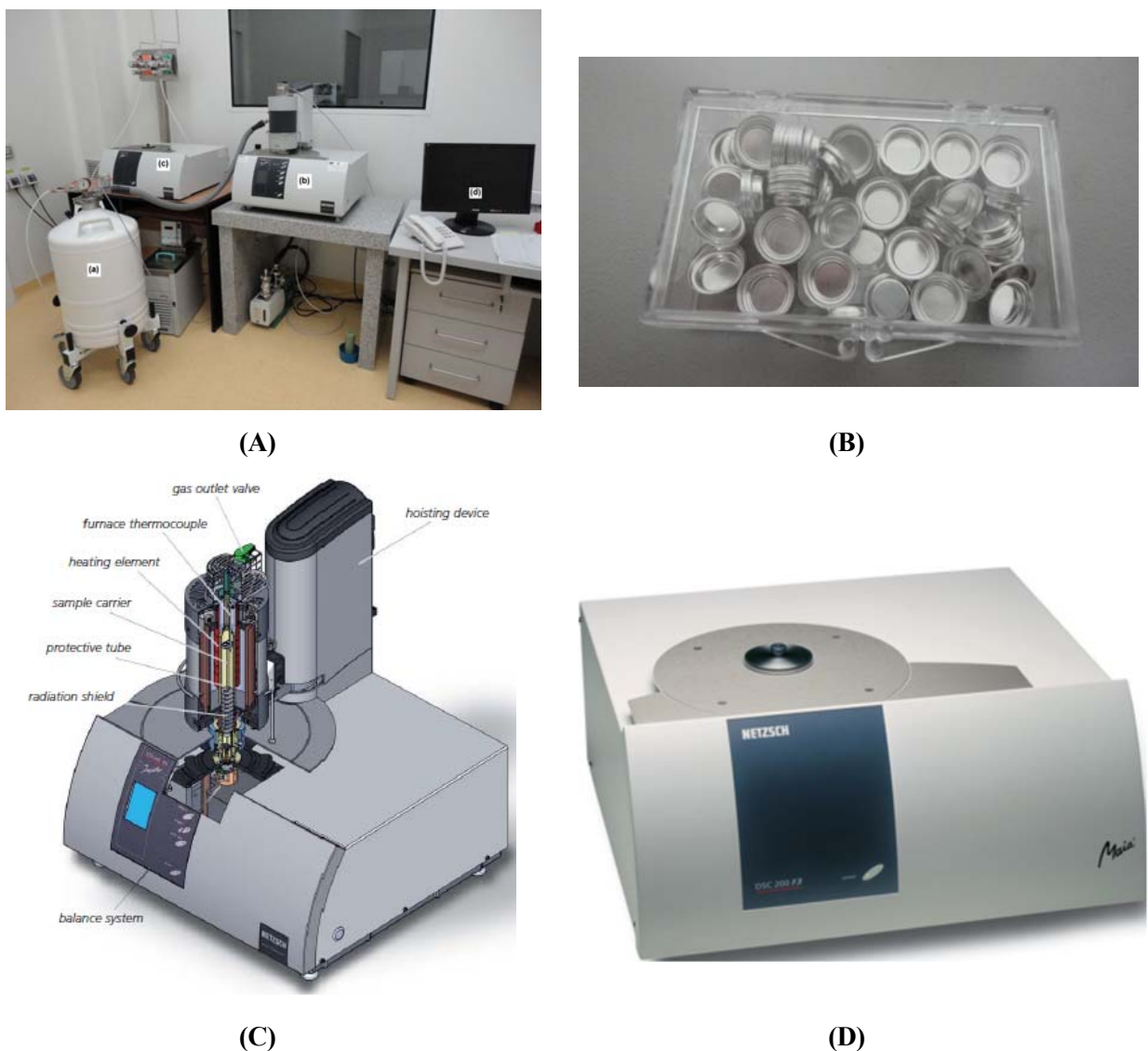


**Figure 40 - The equipment used for DSC analysis:** (A) (a) Dewar flask with liquid nitrogen; (b) Simultaneous Thermal Analyzer STA 449 F1 Jupiter; (c) DSC apparatus DSC 200 F3 Maia where the crucible with the sample is inserted; (d) the display for computer control of the DSC apparatus; (B) set of punched aluminium crucibles used for testing samples; (C) the component parts of the STA 449 F1 Jupiter® with Automatic Sample Changer (ASC); (D) DSC 200 F3 Maia.

Simultaneous Thermal Analysis generally refers to the simultaneous application of Thermogravimetry (TG) and Differential Scanning Calorimetry (DSC) to the same sample in one instrument. There are several advantages for this procedure: the test conditions are perfectly identical for the TG and DSC signals (same atmosphere, gas flow rate, vapor pressure on the sample, heating rate, thermal contact to the sample crucible and sensor, radiation effect). Furthermore, it improves sample throughput as more information is gathered from each test run.

The thermal analysis system includes a STA system combines the DSC and TG methods and accomplishes the measurement of heat flow and mass change under completely identical conditions (Figure 40.A-c and 23.C). The application fields of the STA 449 F1 Jupiter® include plastics, rubbers, resins, fibers,

coatings, oils, ceramics, glass, cements, refractories, metals, fuels, drugs, foods, and so on. The characteristics for this device are as follows:

- Temperature range: -150°C to 2400°C
- Sample weight: up to 5000 mg
- Weighing range: 5000 mg
- TGA resolution: 0.025 µg
- Vacuum: <10<sup>-4</sup> mbar
- Atmosphere: static and dynamic, inert, reducing, oxidizing
- High precision of Cp measurements
- Perfect coupling with FTIR, MS or GC-MS

The furnace of this apparatus is made of steel, has a temperature range of -150 ... 1000°C and a cooling system with liquid nitrogen. With the TG analysis several processes can be recorded, such as:

- Mass changes
- Temperature stability
- Oxidation/reduction behavior
- Decomposition
- Corrosion studies
- Compositional analysis
- Thermokinetics

The DSC 200 F3 Maia® is the tool for differential scanning calorimetry in this system and has the following characteristics:

- Failure Analysis
- Temperature range: -170°C to 600°C
- Automatic gas switching
- Cooling with liquid N<sub>2</sub>
- Automatic sample changer (ASC) for up to 20 samples and references

The DSC apparatus offers the possibility to study the following transformations of the materials:

- Melting/crystallization behavior
- Solid-solid transitions
- Polymorphism
- Degree of crystallinity
- Glass transitions
- Cross-linking reactions
- Oxidative stability
- Purity determination
- Specific heat
- Thermokinetics

### **3.5.2 Experimental procedure**

About 10 mg of sample was heated in pressed and punched aluminium crucibles at a heating rate of 10 °C·min<sup>-1</sup>. Nitrogen was used as inert atmosphere at a flow rate of 100 mL min<sup>-1</sup>. For each sample there was recorded the heating curve, followed by cooling to -150 °C and then a second heating. This treatment of the sample allows the researcher to determine the transformations of the materials mentioned above. The curves were recorded for samples of commercial elastomers (Annex I, 3.5.).

## Section 4: Preliminary novel electroactive elastomers materials

### 4.1. Composites based on PDMS and ceramic materials

#### 4.1.1. Composites with TiO<sub>2</sub>

Although possess low dielectric constant, silicones are between the most used polymer in actuation due to their appropriate mechanical properties (low modulus and high elongation). These can be easily tuned by the preparation strategy: proper choice of the molecular mass and microstructure of the polymer matrix; adding or not of more or less active fillers; whether these are incorporated in the polymeric matrix (*ex situ*) or generated *in situ*; crosslinking mode (through the side or ending functional groups) or mechanism (condensation, radicalic or by hydrosilylation). A relatively low cost and easy scalable procedure was used in this paper to prepare silicone composites based on high molecular weight polydiorganosiloxane copolymer and hydrophobized silica and titania nanoparticles. The matrix polymer was synthesized by bulk ring opening copolymerization of different substituted cyclosiloxanes and characterized by FTIR, <sup>1</sup>H NMR and GPC. The composites prepared by the mechanical incorporation of the fillers were crosslinked by radicalic mechanism and investigated by dielectrical spectroscopy, mechanical tests, dynamo-mechanical analysis (DMA), dynamic vapors sorption (DVS). The actuation and energy harvesting measurements were also performed.

##### 4.1.1.1. Composites and film formation

The composites were prepared according to procedure described in ref. [62] by mixing the siloxane polymer with fillers, in a Yanke - Kunkel laboratory mixer equipped with palettes in Dublex system and cooling mantle. The fillers, first silica followed by titania in different percents (Table 3), were added to the polysiloxane under mixing in small portions until the whole amounts were incorporated. Finally the crosslinking catalyst (1.5 wt% 2, 4-dichlorobenzoyl peroxide) was also added.

Sample	M(0,0)	M(28,0)	M(0,10)	M(28,2)	M(28,6)	M(28,10)	M(28,20)	M(28,30)	M(28,50)
PDMS, pph	100	100	100	100	100	100	100	100	100
SiO <sub>2</sub> , pph	0	28	-	28	28	28	28	28	28
TiO <sub>2</sub> , pph	0	0	10	2	6	10	20	30	50

Table 5 - The prepared samples

A certain composite amount (usually about 25 g) having incorporated catalyst was pressed in an iron mold 1x100x100 mm without special surface preparation. This ensemble was kept 1 h at 100 °C in normal atmosphere when the catalyst determines the crosslinking. Then, the film easily peeled off from the hot substrate was maintained another 3 h at 150 °C in air stream to complete the crosslinking and for devolatilization.

##### 4.1.1.2. Mechanical tests

Stress-strain curves are presented in Figure 41, while the main parameters determined on their basis are summarized in Table 6.

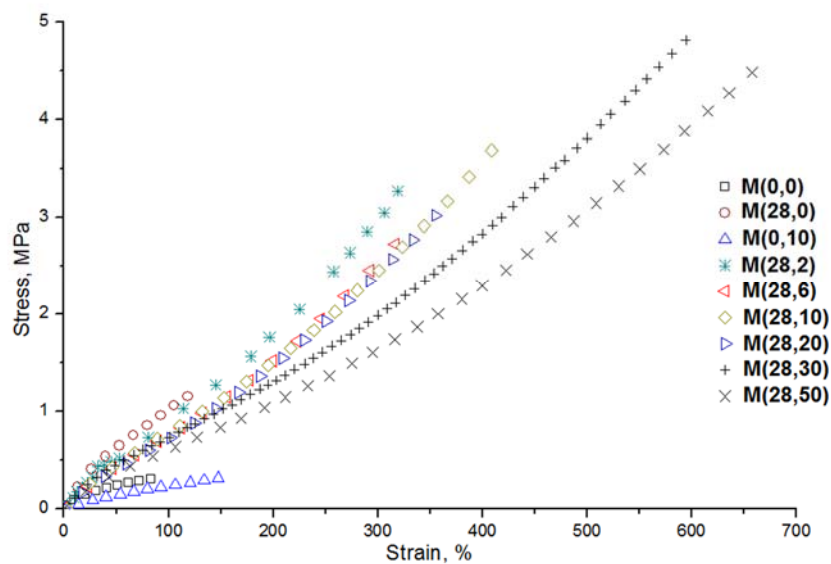


Figure 41 - Stress-strain curves for the prepared samples

Sample	Young's modulus, MPa	Tensile strength, MPa	Elongation at break, %	Hardness, °ShA
M(0,0)	0.63	0.31	90	62.0
M(28,0)	1.97	1.24	128	83.0
M(0,10)	0.23	0.32	160	46.5
M(28,2)	1.42	3.22	312	72.6
M(28,6)	1.13	2.79	313	74.4
M(28,10)	1.37	3.91	406	77.7
M(28,20)	0.97	3.16	363	81.4
M(28,30)	1.32	4.89	589	84.0
M(28,50)	1.02	4.53	635	86.0

Table 6 - The main parameters of the mechanical tests

<sup>a</sup> Young's modulus was calculated as a ratio between the stress and strain when the last has 10% from total elongation. Linear stress-strain dependence is considered on this portion.

Values obtained for tensile strength for our silicone-titania filled samples ranges between 2.79-4.89 MPa. These are higher than values obtained for blank samples M(0,0) and M(28,0). The unfilled PDMS has the lowest value for the tensile strength, 0.31 MPa, as expected. By adding 28 % silica, this value increases at 1.24 MPa. Instead, it seems that, the co-existence of the silica and titania has a synergistic effect on the tensile strength.

The Young modulus, E, determined from the stress-strain curve by calculating the ratio of stress to strain when this attains 10 % from the total elongation has values between 0.97 and 1.42 MPa. The modulus values of the silicone-silica-titania composites are almost double that of M(0,0) sample consisting of pure crosslinked PDMS and about five times higher than the sample M(0,10) based on crosslinked PDMS filled with TiO<sub>2</sub> only. Elongation increases from 312 % to 635 % when the titania content amounted from 2 to 50 % wt. The average hardness of the samples ranges from 72.6 to 86 ShA. By examining the hardness values it can be observed that this is conferred in principal by the presence of the silica as well as by the co-existence of the silica and titania. Single titania reduces the values of the material hardness, the samples based on the PDMS and titania only showing the lowest value for the hardness, 46.5 ShA.

#### 4.1.1.3. Dynamic mechanical analysis

This analysis provides the variation of the storage modulus ( $E'$ ), loss modulus ( $E''$ ) and loss tangent ( $\tan \delta$ ) as a function of temperature. The drops in  $E'$  curves and the peaks of  $E''$  and  $\tan \delta$  plots report on the relaxations in polymers. Some illustrative curves are presented in Figure 25, while the main parameters for all samples are centralized in Table 5. At very low temperatures, close to  $-150^\circ\text{C}$ , all the samples have the storage modulus ( $E'$ ) over  $10^8$  Pa, which indicates that all of them are in the glassy state. Until room temperature three important drops in the storage modulus take place. Broad loss modulus ( $E''$ ) and loss factor ( $\tan \delta$ ) peaks correspond to each descent of  $E'$ .

The first  $\tan \delta$  peak centered in the range  $-122^\circ\text{C} \div -126^\circ\text{C}$  can be associated with the  $\alpha$ -relaxation of PDMS chain segments. It can be seen that this value is not significantly influenced by the titania presence and content. It is not excluded that the PDMS sample contains chains segments with lower mobility. The presence of these chains explains the second  $\alpha$ -relaxation peak in the range  $-65^\circ\text{C} \div -45^\circ\text{C}$ . All filled samples have the melting temperature in the range  $-37^\circ\text{C} \div 41^\circ\text{C}$  and a slight decreasing of melting temperature can be observed by rising titania content.

Sample	$T_g$	$T_m$ ( $^\circ\text{C}$ )	$E'$ (Pa) at $-140^\circ\text{C}$	$E'$ (Pa) at $25^\circ\text{C}$
M(0,0)	- 125	-43	9.60E+08	2.53E+06
M(28,0)	- 125	-41	1.36E+09	5.11E+06
M(0,10)	- 122	-42	2.88E+09	4.65E+05
M(28,2)	- 126	-40	2.17E+09	1.63E+06
M(28,6)	- 123	-40	4.15E+09	1.73E+06
M(28,10)	- 124	-40	3.96E+09	1.20E+06
M(28,20)	- 124	-38	4.99E+09	1.61E+06
M(28,30)	- 125	-38	6.47E+09	2.05E+06
M(28,50)	- 125	-37	5.33E+09	2.58E+06

Table 7 - The main parameters of DMA curves

At room temperature, the  $E'$  values are situated around  $1-2 \cdot 10^6$  Pa, with very small differences between samples. The composites show good thermal stability until over  $150^\circ\text{C}$  (the limit of the experimental temperature). The temperature values included in the Table 5 correspond to the middle of the peaks on  $\tan \delta$  curve.

Although they are estimated by methods having different principles, the Young modulus and elastic modulus values are about the same order of magnitude: 0.97-1.42 and 1.20-2.58 MPa, respectively for the PDMS-silica-titania composites.

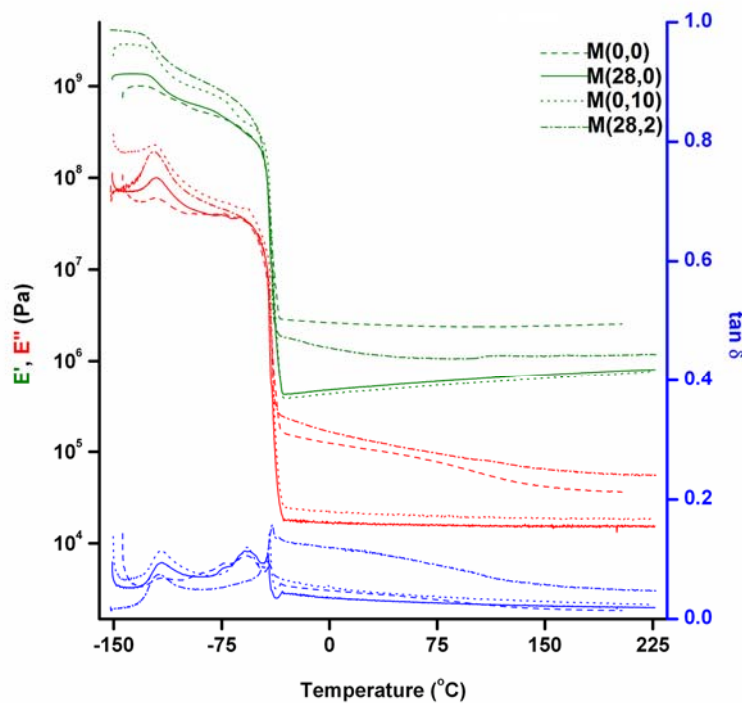


**Figure 42 - The dependence of storage modulus ( $E'$ ), loss modulus ( $E''$ ) and  $\tan \delta$  on temperature for samples: M(0,0); M(28,0); M(0,10); M(28,10).**

#### 4.1.1.4. Dielectric thermal analysis

The effects of the filler content on dielectric properties and on the segmental mobility associated with the glass transition were studied by dielectric spectroscopy for the silicone/titania composites.

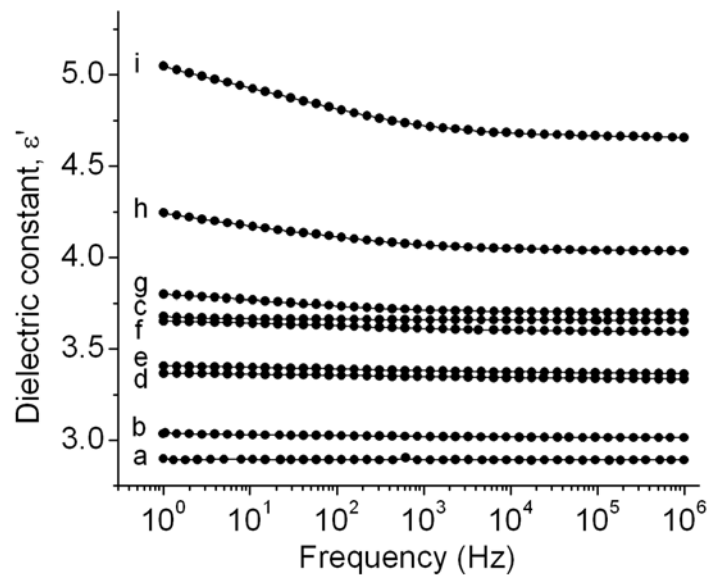


**Figure 43 - Dielectric permittivity  $\epsilon'$  as a function of frequency at room temperature for the samples: a-M(0,0); b-M(28,0); c-M(0,10); d- M(28,2); e- M(28,6); f- M(28,10); g- M(28,20); h- M(28,30); i- M(28,50).**

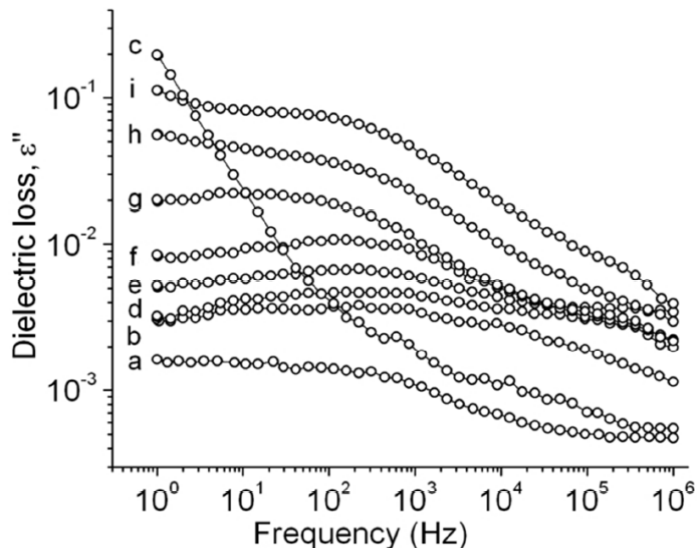


Figure 44 - Dielectric loss  $\epsilon''$  as a function of frequency at room temperature for the samples: a-M(0,0); b-M(28,0); c-M(0,10); d- M(28,2); e- M(28,6); f- M(28,10); g- M(28,20); h- M(28,30); i- M(28,50).

The polarizability of the Si-O bond constitutes a premise for a high dielectric constant. Indeed, this is higher as compared to organic nonpolar polymers (e.g., polyethylene), but not so much as it could be due to the nature of this chemical bond. This is the effect of the side methyl groups (in the case of PDMS), which prevent Si-O dipoles from approaching each other too closely. The situation does not change too much by replacing methyl groups with more polarizable ones. Instead, it has been found that the dielectric constant of PDMS increases with the polymerization degree of the siloxane backbone before quickly reaching a plateau value [63]. The dielectric properties of silicones are good, but not exceptional in comparison with organics. The success of silicone-based products is certainly related more to their stability over a wide range of temperature, humidity and frequency [63].

Figure 43 and Figure 44 show the comparison of dielectric constant ( $\epsilon'$ ) and dielectric loss ( $\epsilon''$ ) for blank samples and composites M(0,10), and M(28,2) to M(28,50) as a function of frequency from 1 Hz to 1 MHz at room temperature. For pure crosslinked PDMS (curve a), dielectric constant has a value of about 2.9, while for the composite with  $\text{SiO}_2$  (curve b) the value of dielectric constant is approximately 3 ( $\epsilon'_{\text{SiO}_2} \approx 3.9$ ). Dielectric constants for composites M(28,10) and M(0,10), having similar  $\text{TiO}_2$  content, are nearly equal, with slightly larger values for the sample M(0,10). It can be observed that, the dielectric constant of the composites with  $\text{TiO}_2$  is substantially increased with increasing filler content, because of the high dielectric constant of  $\text{TiO}_2$  ( $\epsilon'_{\text{TiO}_2} \approx 114$ ). Thus, values until about 4.5 were registered as  $\text{TiO}_2$  content raises at 50 pph.

Starting with composite M(28,20), dielectric constant and dielectric loss show an increase in the lower frequency range due to the Maxwell-Wagner-Sillars (MWS) polarization processes. The large frequency dependent contribution to the dielectric response, especially at low frequencies, comes from the separation of charges at interfaces with different dielectric characteristics [64]. This effect is more accentuated for the composites with higher  $\text{TiO}_2$  content due to the larger interfacial area. However, the observed dielectric loss values are almost one order of magnitude lower than other reported suitable for allowing sufficient transduction effects [65]. The limited MWS polarization phenomenon suggests a good compatibility between the different phases [66]. A different behaviour is observed for composite M(0,10), with a sharp increase of  $\epsilon''$  at low frequencies, due to a higher interfacial polarization. At intermediate frequencies and above, every increase of the filler volume fraction is coherently paired with a corresponding increase of  $\epsilon'$  (Figure 43).

As we already specified in the introductory part, different from most of the literature data [11],[65],[67]-[70] concerning to dielectric silicone elastomers, in this work we used a silicone with high temperature vulcanization (HTV). Only a very recent article [69] reported a similar system, namely PDMS/ $\text{BaTiO}_3$  nanocomposite as dielectric material, where polymer is high molecular one and is cured with peroxide. The dielectric constant values of about 6, more pronounced (until 13) at low frequency region, were reported at a filler loading until 70 pph. Instead, both tensile strength and elongation worsened as the filler load increased.

Apart from this, besides active TiO<sub>2</sub> filler, we incorporated silica this leading to high mechanical resistance (2.79 – 4.89 MPa), useful for harsh application conditions, and good elongation values (312-635 %).

The observed low values of the dielectric loss indicate minimal conversion of electrical energy to heat in the dielectric material and, as a result, the electrical signals will lose less of their intensity in the dielectric medium [72].

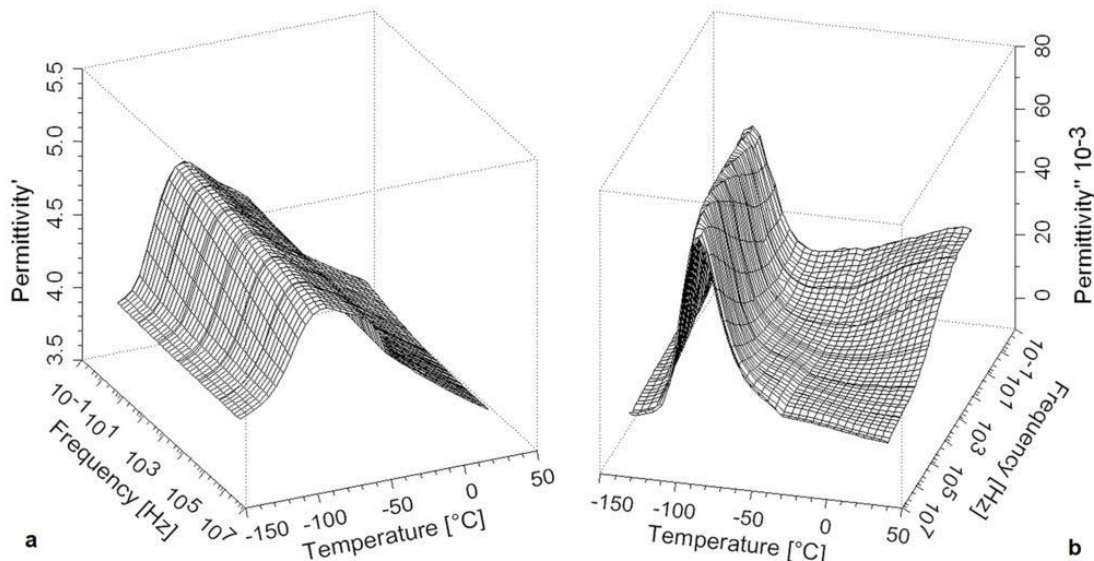


**Figure 45 - Dielectric constant (a) and dielectric loss (b) as a function of frequency and temperature for composite M(28,20).**

In Figure 45, the dielectric constant and dielectric loss are represented as a function of temperature and frequency for sample M(28,20). Around -120 °C, at 1 Hz,  $\epsilon'$  presents a steep increase and  $\epsilon''$  a peak which corresponds to the segmental  $\alpha$  relaxation associated with the glass transition of amorphous PDMS as was emphasized by DMA (Figure 42, Table 7). For higher frequencies, these peaks are shifted to higher temperatures, which is characteristic for dielectric relaxations. On further increasing the temperature,  $\epsilon'$  displays a decrease that could be due to a crystallization process that produces the immobilization and/or constraint of some fractions of the responding dipoles by increasing bulk crystallinity [72].

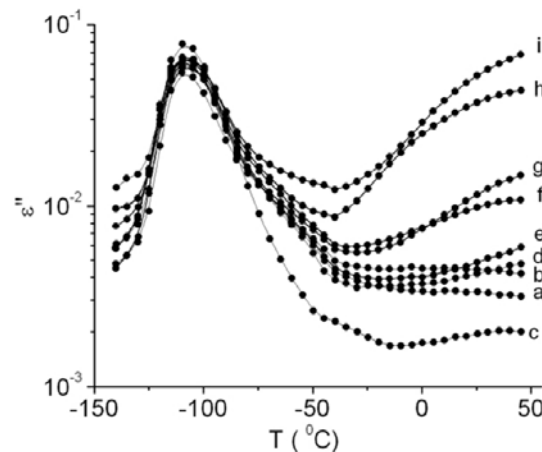


**Figure 46 - Temperature dependence of dielectric loss for the samples: a-M(0,0); b-M(28,0); c-M(0,10); d- M(28,2); e- M(28,6); f- M(28,10); g- M(28,20); h- M(28,30); i- M(28,50).**

Dielectric data recorded isothermally are replotted as  $\epsilon''$  versus temperature for 1 kHz in Figure 46, in order to facilitate comparison between composites M(0,10) and M(28,2)- M(28,50) (Figure 46, curves c-i) and blank samples M(0,0), M(28,0) (Figure 46, curves a,b). One can observe that the position and shape of

relaxation remains almost unchanged for all the compositions. This observation is valid for all the frequencies not represented here. Several studies [73] [74] on polymer nanocomposites show an increase of the glass transition temperature, suggesting that the mobility of the entire volume of the polymer is restricted by the presence of the nanoparticles. However, reduction of glass transition temperature has also been reported [75] in the case of weak interactions between filler and polymer, and in other cases the addition of nanoparticles causes no significant change to the glass transition of the polymer presumably because effects causing increase and decrease of polymer mobility are present simultaneously and effectively cancel out [76] [77]. At positive temperatures, dielectric loss increases with increasing filler content for samples M(28,2)- M(28,50) due to interfacial polarization mentioned above, while for M(0,0) and M(28,0),  $\varepsilon''(T)$  do not show large variations.

The temperature corresponding to  $\alpha$  peak was determined for frequencies taken at intervals of a decade and are represented in Figure 47. These values were the same for all the samples and it was found that their dependence is well described by the Vogel-Fulcher-Tamman equation [78] [79], characteristic for cooperative relaxations:

$$f_{\max} = f_0 \exp\left(-\frac{B}{T - T_0}\right) \quad (3)$$

where  $T$  is the temperature, expressed in K, that corresponds to maximum loss for frequency  $f_{\max}$ ,  $f_0$ , and  $B$  are temperature-independent empirical parameters.  $T_0$ , called Vogel temperature is the temperature at which the molecular movements associated with glass transition vanish. The best fitting was achieved for  $f_0 = 4.62 \times 10^{12}$ ,  $B = 0.76$  and  $T_0 = 130$  K. Similar  $\alpha$  relaxation was observed for the other composites not represented in Figures 46 and 47.

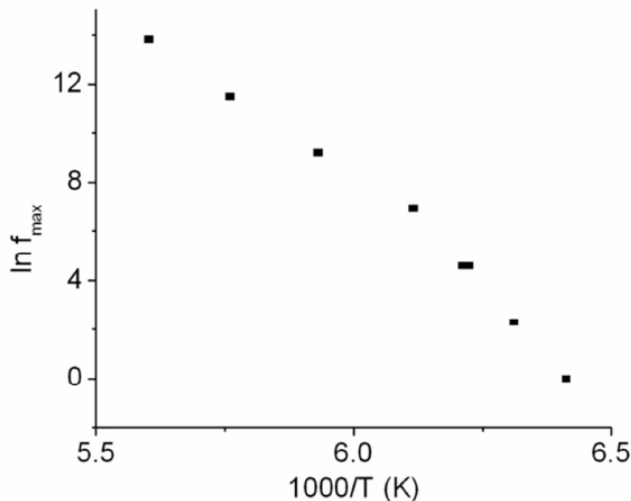


Figure 47 - Arrhenius plot representing  $\ln f_{\max}$  vs.  $1/T$  for all samples

#### 4.1.1.5. Vapor sorption capacity

The performance and long-term stability of the EAPs depend, among others, on the water exchange with the environment. Variation of the water content in EAPs will affect the permittivity and as result the actuation response. In addition, the water presence can contribute to corrosion. In certain cases, water sorption capacity is useful in sensors but this behavior must be known and controlled. Although silicones are known for their hydrophobicity and water repellence, by adding of silica or/and titania it would be expected to increase their hydrophilicity due to the presence of the OH groups on the surface of the particles. However, both fillers were hydrophobized prior to be incorporated in the silicone matrix, as the OH group's effect not to occur [63]. Therefore, it is important to verify the behavior of the resulted composites in variable humidity environment.

Water vapors sorption capacity for the samples at 25 °C in the 0-90 % relative humidity range (RH) was investigated. The vapors pressure was increased in 10% humidity steps, each having a pre-established

equilibrium time between 10 and 20 minutes. At each step, the weight gained was measured by electromagnetic compensation between tare and sample when equilibrium was reached. An anti-condensation system was available for vapor pressure very close to saturation. The cycle was ended by decreasing the vapor pressure in steps to obtain also the desorption isotherms.

The drying of the samples before sorption measurements was carried out at 25 °C in flowing nitrogen (250 mL/min) until the weight of the sample was in equilibrium at RH<1 %. The sorption/desorption isotherms registered in these conditions are presented in Figure 48.

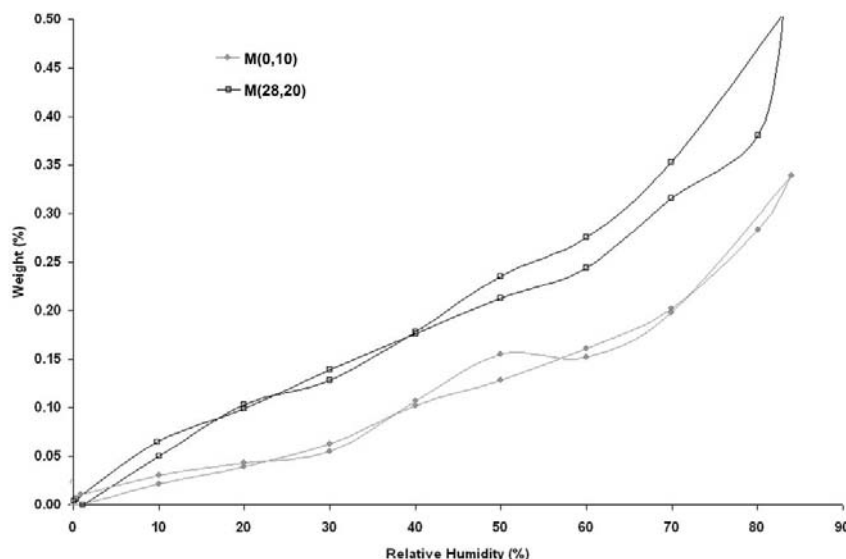


**Figure 48 - The illustrative shapes of the moisture sorption-desorption isotherms: M(0,10), M(28,20)**

As can be seen in Table 8, the maximum humidity sorption capacity has low values, between 0.10 and 0.68 wt. The neat crosslinked PDMS shows the lowest water sorption capacity, 0.10 wt%. By adding silica, the sorption capacity slightly increases up to 0.47 wt%. The small variations in the cases of the other samples do not seem to be correlated with the TiO<sub>2</sub> content. Low values of the water sorption capacity constitute a guarantee of good stability of the dielectric properties in an environment with variable humidity.

Sample	Weight (%d.b. <sup>a</sup> )
M(0,0)	0.10
M(28,0)	0.47
M(0,10)	0.34
M(28,2)	0.35
M(28,6)	0.68
M(28,10)	0.40
M(28,20)	0.51
M(28,30)	0.38
M(28,50)	0.43

**Table 8 - Maximum water vapor sorption capacity estimated on the basis of isotherms**

<sup>a</sup> dry basis

#### 4.1.1.6. Actuation and energy harvesting measurements

The considered actuation consists in the transformation of the electric energy directly into mechanical work producing large strains. The actuators are composed primarily of a passive elastomer film with thickness in the range 0.78-2.2 mm with two compliant electrodes on the surfaces, exhibiting a typical capacitor configuration. It is known that, in general the elastomers are incompressible (Poisson's ratio = 0.5)

and viscoelastic. When the electrical voltage is applied to the electrodes, an electrostatic force is generated between the electrodes. The force is compressive, and thus the elastomer film expands in the in-plane direction [80]. While most of the reported actuation experiments measure lateral strain resulted by electric field-induced thickness squeezing, we apply a non-contact measurement procedure by using the AGILENT 5529A system, which is able to measure the linear micro and nanodisplacement in cross-section with high resolution interferometer. This procedure is also considered better than contact ones by other authors [81]. The films were not prestrained before measurements. The parameters used to estimate actuation behavior were defined as follows:

The electric field :

$$E[V/mm] = \frac{U}{d} = \frac{\text{Voltage}[V]}{\text{Thickness}[mm]} \quad (4)$$

The resolution :

$$R_a[nm/V/mm] = \frac{a_{\max}[nm]}{E[V/mm]} \quad (5)$$

where  $a_{\max}$  - represents the maximum actuation to the maximum voltage of experiment (in our case  $U=500$  V).

The registrations were performed at a constant force by 22 cN. The variation of the displacement value in dependence on the applied voltage is presented in Figure 49 for all prepared samples. Although as expected, the displacement increases by applied voltage, this dependence seems to be not linearly one.

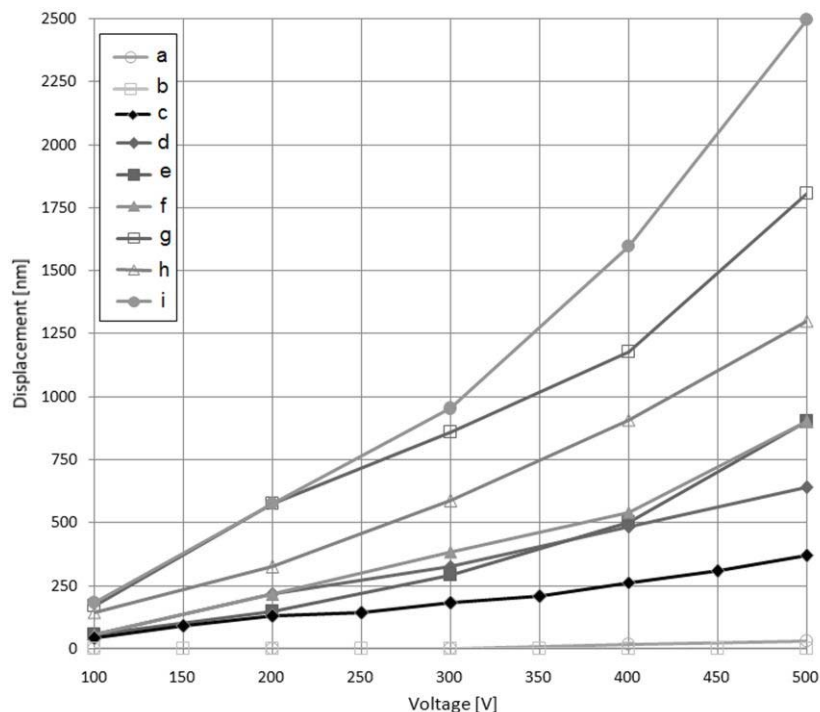


Figure 49 - The displacement versus applied voltage for the prepared samples: a-M(0,0); b-M(28,0); c-M(0,10); d-M(28,2); e-M(28,6); f-M(28,10); g-M(28,20); h-M(28,30); i-M(28,50).

In Table 9 are selected the specific experimental results of microactuation parameters for investigated elastomeric samples for 500 V applied voltage.

Sample	Actuation (at applied voltage U = 500 V)				Harvesting Voltage peak to peak, $U_{pp}$ [V]
	d Thickness [mm]	E Electric field [V/mm]	$R_a$ ( $a_{max}$ ) Resolution [nm/V/mm] (maximum actuation, nm)	% Traverse strain/[mV/mm]	
M(0,0)	1.60	313	0.10 (30 )	0.06	8
M(28,0)	2.22	226	0.04 (10)	0.00	6
M(0,10)	1.43	350	1.06 (370)	0.07	10
M(28,2)	1.03	485	1.24 (640)	0.13	20
M(28,6)	0.78	641	2.31 (900)	0.18	16
M(28,10)	0.98	510	1.84 (900)	0.18	15
M(28,20)	1.08	463	3.33 (1800)	0.36	14
M(28,30)	1.01	495	2.57 (1300)	0.26	12
M(28,50)	0.98	510	5.09 (2496)	0.50	14

**Table 9- The main actuation and energy harvesting parameters**

As expected, the actuation is improved as the titania content in the sample increases, being in direct correlation with mechanical (Figure 41, Table 6) and dielectric (Figures 42,43) parameters. For example, sample M(28,50) with highest titania content showed a gradient of 7.5 nm/V on the voltage range 300-500 V (Figure 49), which represent a very good performance in the field of electrostrictive actuation, regardless of materials [65],[82]. Transverse strain response of 3.25 % was reported for Dow Corning HSIII silicone films at a field of 28.0 MV/m [83], much higher than voltages applied by us (226-641 V/mm). By comparing with this response expressed as % traverse strain/[mV/mm], which results 0.11, our values obtained on blank samples M(0,0), M(28,0), and M(0,10) are lower (Table 9) due to the reduced elongation (90 – 160 %). Instead the samples containing silica and increasing amounts of TiO<sub>2</sub> showed better values for the electromechanical response, 0.14 – 0.55 % traverse strain/[mV/mm]. Our results are also good when compared with the maximum strain value of 4 % at 30 V/ $\mu$ m (30 000 V/mm) reported for composite based on PDMS having incorporated until 30 pph TiO<sub>2</sub> [70].

The harvesting test was realized to mechanical microimpulse: the fall of a microball (with the mass of m= 4.08 g) from a height of 0.5 m on the surface of the elastomeric membrane (Figure 40). The dynamic parameters taken into consideration in these conditions were:

- speed to the contact with the elastomeric membrane (the initial speed is 0):

$$v = \sqrt{2gh} = \sqrt{2 \cdot 9.8 \cdot 0.5} = 3.162[m/s] \quad (5)$$

- the mechanic impulse:

$$p = mv = 12.902 \cdot 10^{-3}[Ns] \quad (6)$$

- the kinetic energy in contact:

$$E = \frac{mv^2}{2} = 20.396 \cdot 10^{-3}[J] \quad (7)$$

- the microforce:

$$F = \frac{E}{h} = 0.0407[N] \quad (8)$$

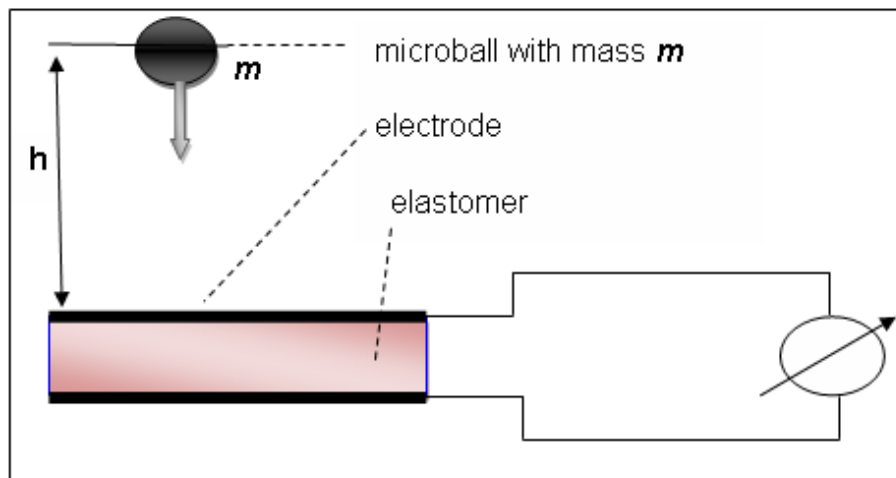


Figure 50 - Schematic energy harvester based on silicone elastomer film

The results of the harvesting experiment expressed as a peak to peak voltage for all samples (Table 9) indicate good values ranging between 6 and 20 V, comparable with those reported in literature on other materials [81],[83]-[86]. Thus, a level of 5.5 V was reported for the peak open-circuit voltage for a nanogenerator based on highly transparent PDMS/BaTiO<sub>3</sub> composite [83].

The developed electric micropower is ~ 7-10 µW with a density in the range 7.77- 11.00 µW/cm<sup>3</sup>. Based on the obtained values it seems that the co-existence of silica and titania enhances the harvesting capacity rather than each of them does alone.

#### 4.1.2. Composites with barium titanate

##### 4.1.2.1. Preparation of barium titanate and its characterization (XRD, TEM, SEM)

In order to synthesize cubic barium titanate, proper amount of TiO<sub>2</sub> (0.25 g) and BaCl<sub>2</sub> (0.65 g) were mixed together in 20 mL of 10 M NaOH [83]. The same amount of TiO<sub>2</sub> and BaCl<sub>2</sub> was used to synthesize barium titanate nanorods in a 5M NaOH solution. The resulting mixtures were transferred in stainless steel autoclaves coated with Teflon and kept for 72 h at 200°C in a Venticell 55 hydrothermal oven. Heating and cooling of samples was done with 1°C/min. After cooling, the resulted particles were washed with distilled water by centrifugation for 3 times at 6000 rpm and 15 min. Before analyses, particles were dried at 100°C over night in a laboratory oven.

Using the powder X-ray diffraction method we showed that the corresponding peaks for barium titanate nanorods are perfectly overlapping with those for commercial barium titanate (Figure 51). The same peaks appear in case of cubic particles (Figure 52). Peaks corresponding to 42° 2θ, 62° 2θ and 70° 2θ are for silicon wafer.

TiO<sub>2</sub> and BaCl<sub>2</sub> were used as precursors in basic medium. When a solution 10M NaOH was used as reaction medium the product as nanocubes of about 1 µm on each side resulted while at a lower basicity (NaOH 5M) nanotubes of about 200 nm in diameter and 2-3 µm in length were obtained as was determined by scanning and transmission electron microscopy (Figure 53). SEM image (Figure 53) reveals for commercial barium titanate prisms with high dispersity in size (between 1-7 µm).

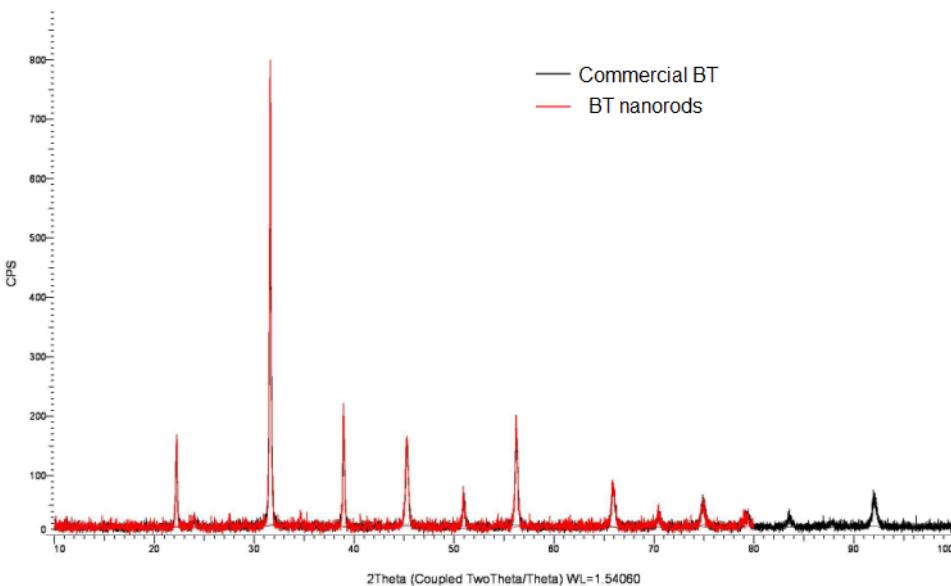


Figure 51 - X-ray powder diffraction spectra for commercial BT (black) and BT nanorods (red)

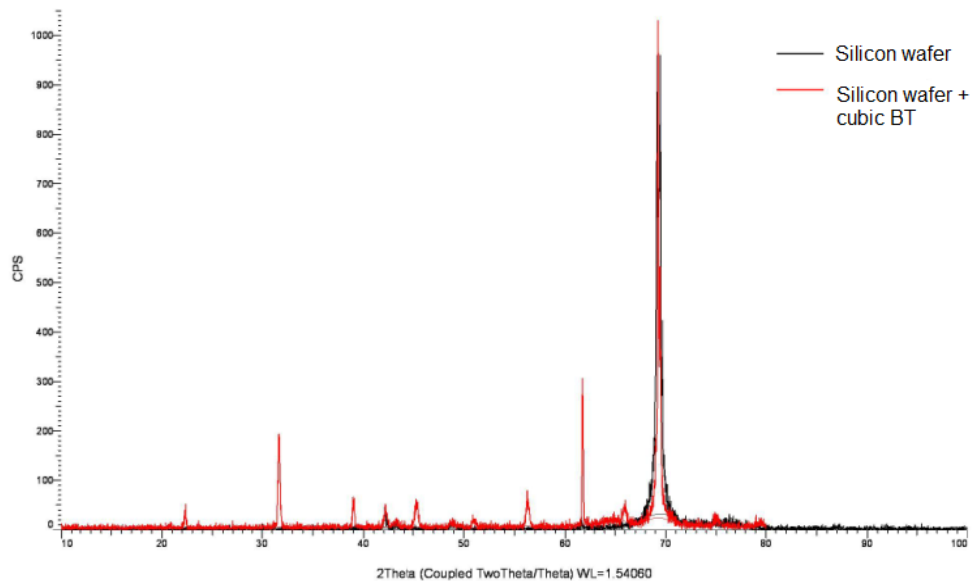


Figure 52 - X-ray powder diffraction spectra for silicon wafer (black) and cubic BT (red)

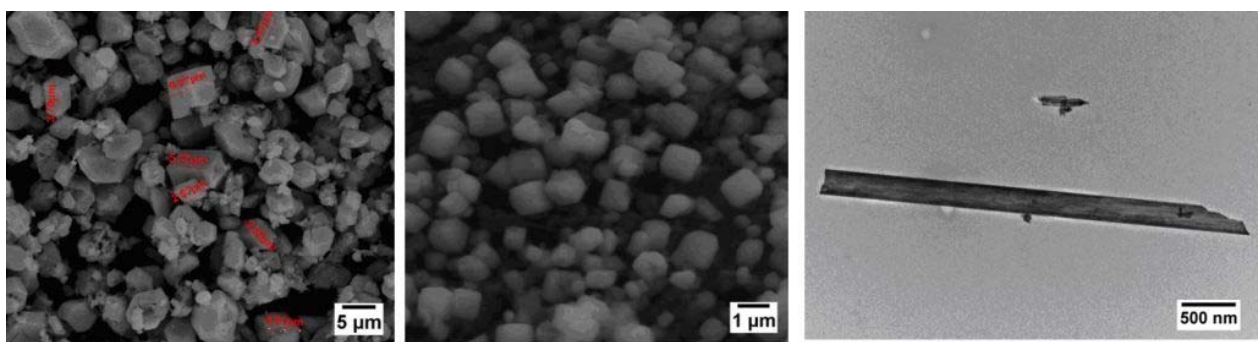


Figure 53 - SEM images of commercial barium titanate (left), cubic barium titanate (middle) and TEM image of barium titanate nanorods (right)

#### 4.1.2.2. Composites and film formation

**Procedure 1:** Barium titanate was grounded using an agate mortar and then mixed with a surfactant. Then crosslinker and catalyst were added and stirred thoroughly until the components formed a homogenous mixture. The resulted mixture was poured into a Teflon mould (15x5 cm). This was maintained in atmospheric humidity at room temperature for 24 h to allow crosslinking of the silicone matrix, after that the formed films with thickness between 0.5 and 0.7 mm were easily peeled off from the substrate.

The crosslinking occurred in thin films by condensation in presence of the atmospheric moisture and room temperature, according to figure 54.

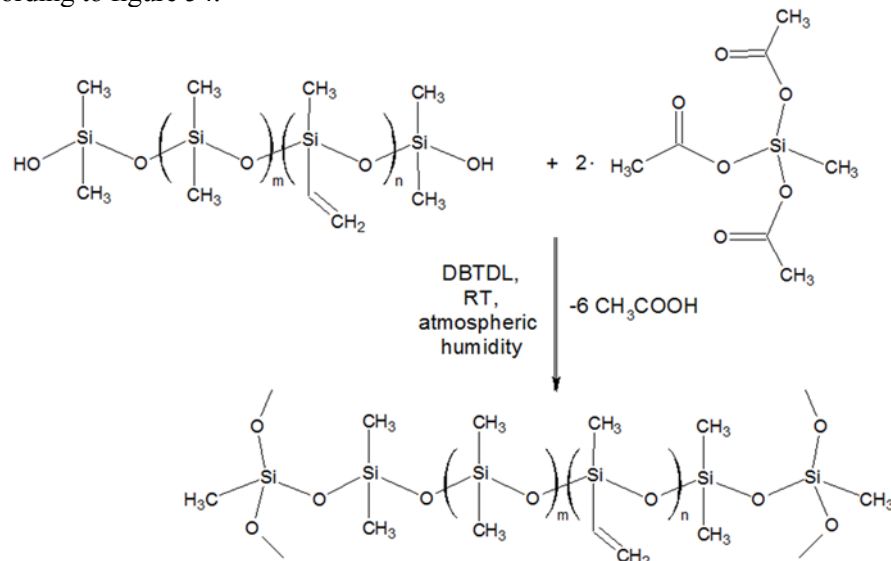


Figure 54 - Crosslinking pathway applied for poly(dimethylsiloxane)- $\alpha,\omega$ -diol

**Procedure 2:** The composites were prepared by mixing the siloxane polymer with fillers, in a Yanke - Kunkel laboratory mixer equipped with palettes in Dublex system and cooling mantle. The fillers, in different percents, were added to the polysiloxane under mixing. Finally the crosslinking catalyst (2, 4-dichlorobenzoyl peroxide) was also added.

A certain amount of composite (usually about 25 g) having incorporated catalyst was pressed in an iron mold 1x100x100 mm. This ensemble was kept 1 h at 100°C when the catalyst determines the crosslinking. Then, the film easily peeled off from the substrate was maintained another 3 h at 150°C in air stream to complete the crosslinking and for devolatilization.

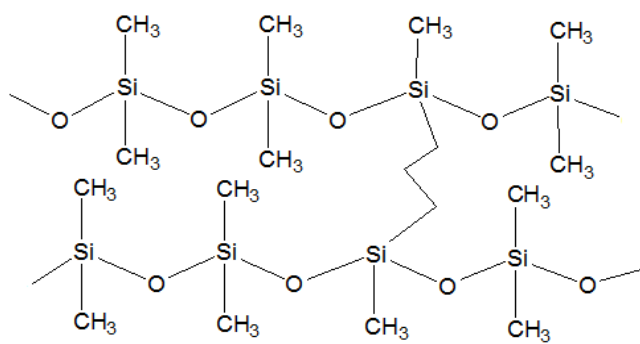


Figure 55 - A fragment of peroxidic crosslinked polymer.

#### 4.1.2.3. The effect of the barium titanate morphology on some properties of silicone composites

A high molecular weight polydimethylsiloxane- $\alpha,\omega$ -diol ( $M_n=438000$  g/mol) was prepared by bulk cationic ring-opening polymerization at room temperature and used to prepare crosslinked films for electromechanical applications. The neat crosslinked polymer and one filled with commercial barium titanate were prepared and used as reference to evaluate the influence of the barium titanate presence and its morphology on some characteristics (thermal and mixture behaviours, morphology) and properties of the resulted materials of interest for electromechanical applications (dielectric and mechanical parameters).

##### 4.1.2.3.1. Mechanical tests

The stress-strain tests (Figure 56, Table 10) reveal that the samples posses very good flexibility and this property is improved by the high molecular mass of the siloxane used. This is due to longer free fragments of siloxane chains being capable of sliding past one another when stretched. Fillers of any morphology decreased the strain, but very good elongations, around 900% and a higher Young modulus were still achieved.

Sample	Filler type	Young's modulus, MPa*	Tensile strength, MPa	Elongation at break, %	Dielectric permittivity, $\epsilon'$ (at 10 Hz, 25°C)	Dielectric loss, $\epsilon''$ (at 10 Hz, 25°C)
70C R	-	0.0930	0.20	2198	3.11	0.21
70C CO	Commercial BT	0.2325	0.17	1196	3.90	0.15
70C NR	BT nanorods	0.0194	0.14	894	9.04	0.30
70C CU	Cubic BT	0.1750	0.16	902	5.29	0.07

Table 10 - The main parameters of the mechanical and dielectric tests

\* Young's modulus was calculated from data at 15% strain.

Stress-strain cycles, with strains up to 100 % of initial length, show an elastic behaviour in all cases with a clearly visible hysteresis loop only at the first strain-release cycle. In the subsequent strain cycles the difference between strain and release was smaller than 1% of the stress value at each point, due to the fact that the siloxane chains are rearranged in the film.

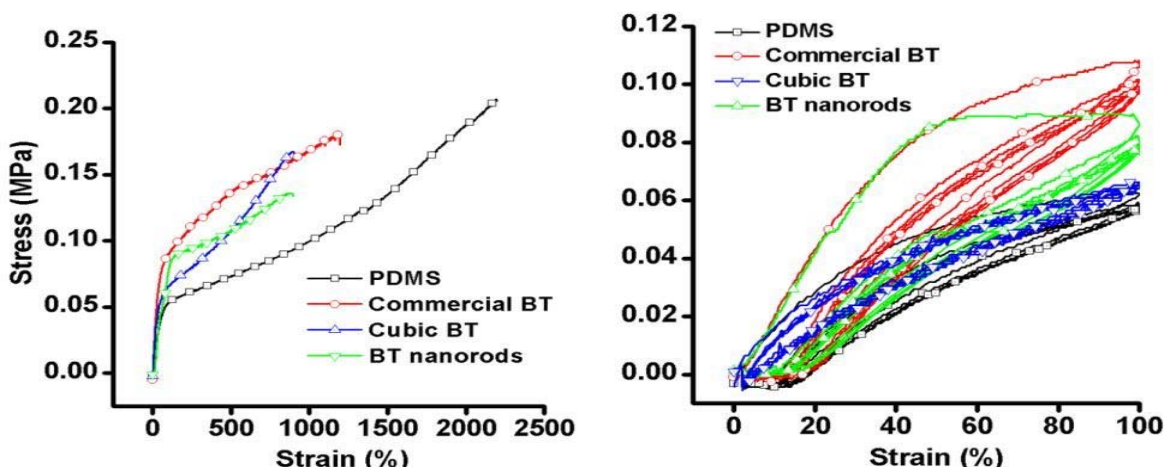
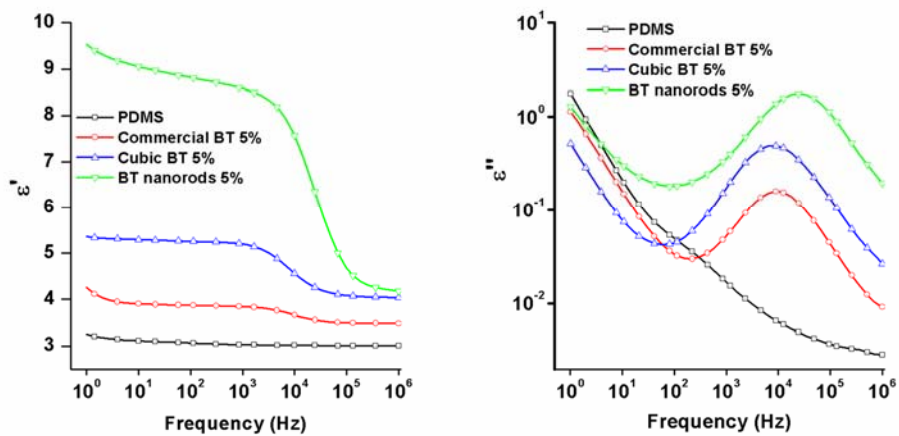


Figure 56 - Mechanical tests for the crosslinked films; stress-strain curves, left,

#### 4.1.3.4. Dielectric spectroscopy

The dielectric behaviour of the obtained composites is a normal one. As expected, the high aspect ratio of the filler resulted in increased values for permittivity. Thus, while pure crosslinked PDMS have  $\epsilon' = 3$ , this increase at 4, 5.4 and around 9 by incorporating commercial barium titanate, prepared cubic and nanorods particles, respectively (Figure 57). There is a sudden drop (the sharper as the value of the permittivity is greater) at about  $10^4$  Hz for dielectric constant  $\epsilon'$  accompanied with the maximum dielectric loss  $\epsilon''$ . This maximum represents the complete failure for the dipole to follow the oscillating electric field beyond which the dipole remains freeze with no effective contribution to the dielectric constant [87].

Dielectric loss results from the inability of polarization process in a molecule to follow the rate of change of the oscillating applied electric field. This arises from the relaxation time ( $\tau$ ) in a polymer which is the time taken for the dipoles to return to their original random orientation. This does not occur instantaneously and the polarization diminishes exponentially. If the relaxation time is smaller or comparable to the rate of oscillating electric field, then there would be no or minimum loss. However when the electric field oscillates well faster than the relaxation time, the polarization cannot follow the oscillating frequency resulting in the energy absorption and dissipation as heat [87].



**Figure 57 - Dielectric measurements for tested samples;**

#### 4.1.2.3.3. Vapor sorption capacity

The moisture sorption in polymers is very important for a variety of industries ranging from microelectronics to adhesives and coatings [88]. For further applications, i.e., in wave energy conversion, the elastomer should ensure a stable operation in different conditions of moisture and temperature. To verify this, the moisture sorption-desorption isotherms were registered in dynamic regime for the crosslinked composite films. Only a slight increasing in the moisture sorption capacity occurs using different types of barium titanate, which is hydrophilic (barium titanate microparticles are easily dispersed in water) (Figure 58). Thus, the maximum sorption capacity increases from 0.5 % in pure crosslinked PDMS to 1.18% for the composite with cubic BT, 1.47% for the composite with commercial BT and 3.53% in the composite with BT nanorods. This diminished effect could be assigned to the surfactant coating barium titanate particles combined with the known tendency of the polysiloxane to migrate at the interface material-air that will lead to a surface richer in hydrophobic siloxane component, which precludes water from entering the sample bulk. The slight increased sorption capacity of the composite with BT nanorods can be explained by their high contact surface area.

Following the IUPAC classification, the isotherms correspond to a type III – specific for non-porous hydrophobic materials with weak interactions between adsorbent-adsorbate. The kinetic curves (not shown) for water vapour sorption show the rate of desorption of water vapours are generally slower than the sorption rate, leading to a small hysteresis loop.

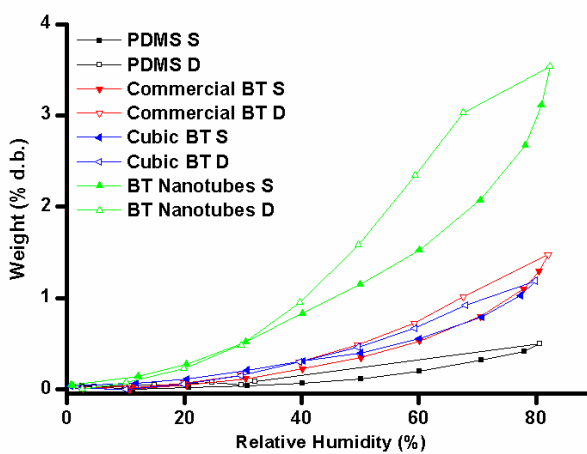


Figure 58 - Sorption-desorption isotherms of the composites registered at room temperature.

Thus, each type of nanoparticles leads to composite material with different mechanical and dielectric properties and this represents a way for further optimization of the properties of silicone-based dielectric actuators.

#### 4.1.2.4. The effect of the molecular mass of the polymeric matrix on some properties of silicone composites thereof

This study reveals the influence of the molecular mass and filler concentration on some properties of interest. For this purpose we synthesized 3 polymers by cationic ring opening ( $Mn_{AB8}=40\ 000\ g/mol$ ,  $Mn_{70B}=235\ 000\ g/mol$ ,  $Mn_{70A}=650\ 000\ g/mol$ ). After surface treatment with surfactant, commercial barium titanate was incorporated in polymer matrix under mechanical stirring. Curing occurs at room temperature under atmospheric humidity with a tri-functional silane (procedure 1, 4.1.2.2.). The resulted thin films were analysed by mechanical tests, dielectric spectroscopy, vapour sorption. We can see an improvement on dielectric properties with a higher molecular mass and a higher filler concentration, but a decent decrease in mechanical and vapour sorption properties

##### 4.1.2.4.1. Mechanical tests

Using a polymer with a high molecular mass (70A) and 10% commercial barium titanate, we achieved strains around 1150% and a 0.23 MPa stress ( $E=0.1MPa$ ). At lower molecular masses the strain is decreased using the same amount of filler. With the increase of filler content the mechanical properties decreases in all cases (Figure 59, Table 11).

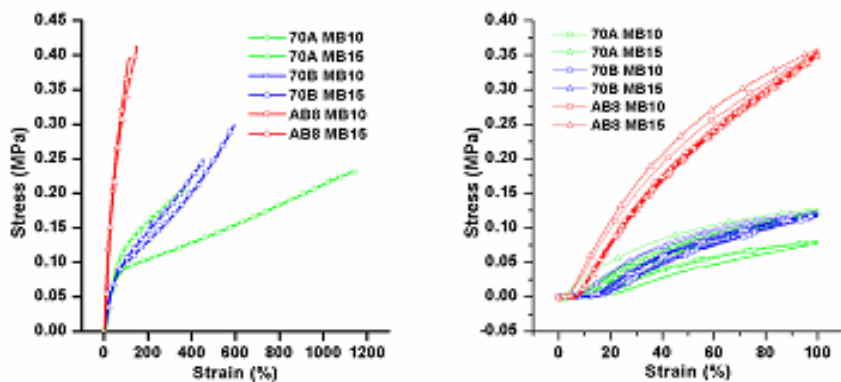


Figure 59 - Mechanical tests for the crosslinked films; stress-strain curves, left, and fatigue resistances, right.

Cod proba	Strain, %	Stress, MPa	E, MPa*	$\epsilon'$ (at 1 Hz, 25°C)	$\epsilon''$ (at 1 Hz, 25°C)
AB8 MB10	113.68	0.3966	0.6533	3.9011	0.9832
AB8 MB15	151.06	0.4120	0.3570	5.0593	0.0330
70B MB10	594.02	0.2980	0.2479	4.4920	0.4420
70B MB15	455.09	0.2480	0.0824	5.1844	0.3306
70A MB10	1149.69	0.2318	0.1901	5.0010	0.2024
70A MB15	374.46	0.2055	0.0562	5.9128	0.0381

Table 11 - The main parameters of the mechanical and dielectric tests

\* Young's modulus was calculated from data at 10% strain.

Stress-strain cycles, with strains up to 100% of initial length, show an elastic behaviour in all cases. A small clearly visible hysteresis loop appears only at the first strain-release cycle and in the later strain cycles the difference between strain and release was smaller than 1% of the stress value at each point.

#### 4.1.2.4.2. Dielectric spectroscopy

As expected, the increasing in content filler and molecular mass resulted in increased values for permittivity from around  $\epsilon'=4$ , for elastomer film with the smallest molecular mass and filler content, to  $\epsilon'=6$  for the elastomer film with the highest molecular mass and filler content. There is a sudden drop (the sharper as the value of the permittivity is greater) at about 10<sup>3</sup> Hz for dielectric constant  $\epsilon'$  accompanied with the maximum dielectric loss  $\epsilon''$ . This maximum represents the complete failure for the dipole to follow the oscillating electric field beyond which the dipole remains freeze with no effective contribution to the dielectric constant [87].

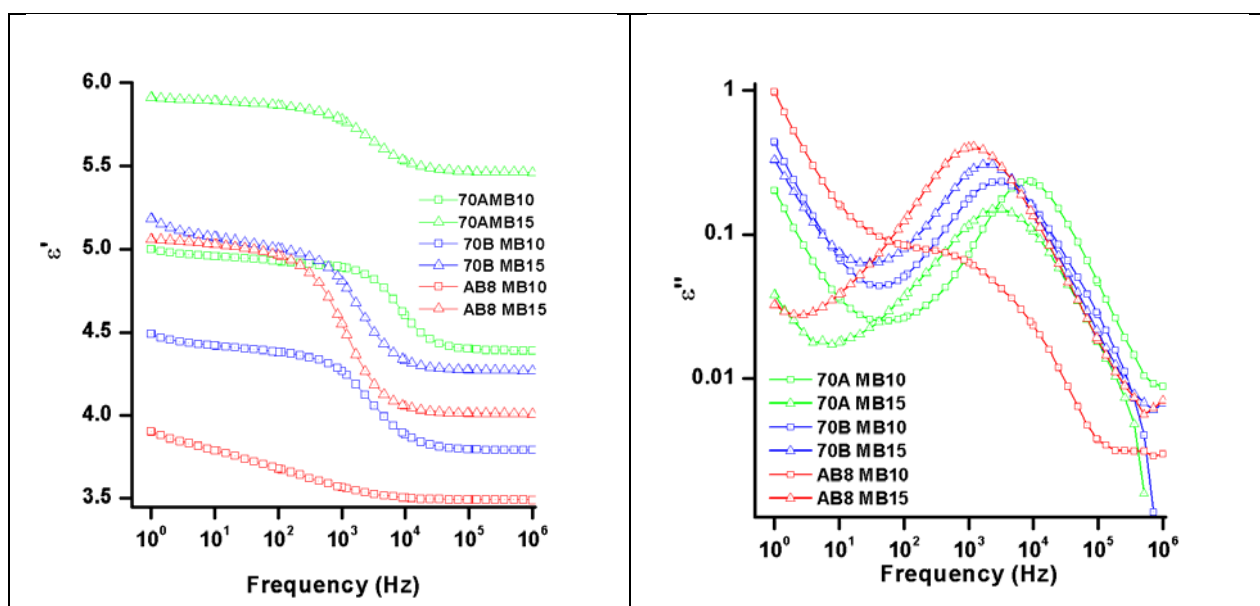


Figure 60 - Dielectric measurements for tested samples; dielectric constant (left) and dielectric loss (right) as a function of frequency

#### 4.1.2.4.3. Vapor sorption capacity

Only a slight increasing in the moisture sorption capacity occurs using the polymer with the lowest molecular mass (Figure 61). Thus, a bigger hysteresis loop is observed for polymer 70A, which possesses the highest molecular mass.

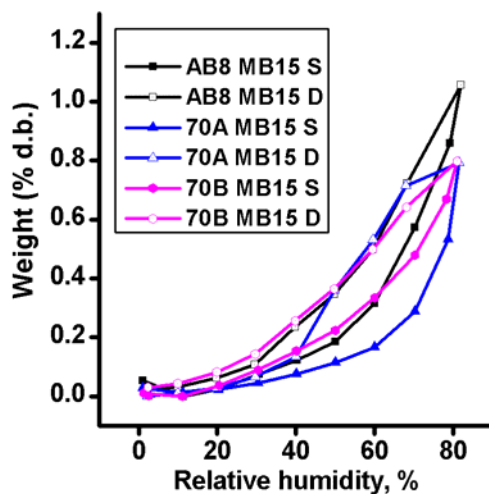


Figure 61 - Sorption-desorption isotherms of the composites with 15% barium titanate, registered at T=25°C.

The isotherms correspond to a type III – specific for non-porous hydrophobic materials with weak interactions between adsorbent-adsorbate. The kinetic curves (not shown) for water vapor sorption show the rate of desorption of water vapors are generally slower than the sorption rate.

#### 4.1.2.5. Polydimethylsiloxane-barium titanate composites as improved electroactive materials

Polydimethylsiloxane- $\alpha,\omega$ -diols with different molecular masses were used as matrix for barium titanate nanoparticles to obtain electroactive elastomeric nanocomposites. A trifunctional silane was used as a crosslinker. Barium titanate nanoparticles were previously treated with a surfactant to improve the compatibility with and dispersability in the matrix. The composites processed as films and crosslinked were investigated for morphology, surface properties, mechanical (stress-strain curves, Young modulus) and dielectric behaviour.

##### 4.1.2.5.1. Mechanical tests

The stress-strain tests (Figure 52, Table 12) reveal that the samples posses good flexibility and this property improves with the increase in the molecular mass of the siloxane used. The reinforcing effect of barium titanate particles is visible, since samples with the highest content of filler (5%), AB II MB 5 and AB IV MB 5, have the largest value for the stress for each siloxane polymer. However the increase in the molecular mass of the siloxane leads concurrently to a larger value of strain for sample AB IV MB 5, and this is due to longer free fragments of siloxane chains being capable of sliding past one another when stretched. In direct correlation, the Young's modulus values (Figure 53) decrease with increasing flexibility, as siloxane films are known for low values of Young modulus [89]. Since for each sample the subsequent standard deviations were less than 2% of the average value, the graphs present only the average value for each type of film.

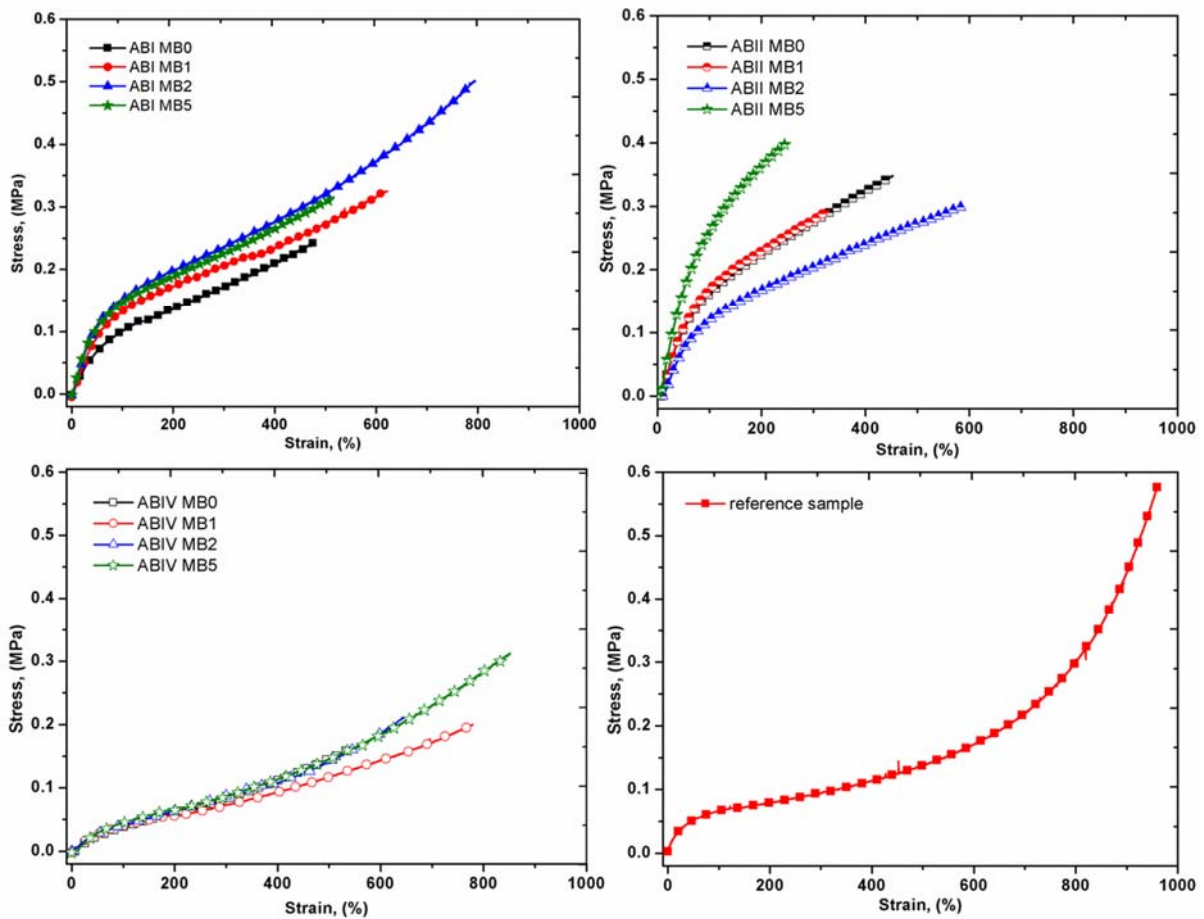


Figure 62 - Stress-strain behaviour for tested samples; reference = 3M VHB

Sample	Young's modulus, <sup>a</sup> MPa	Tensile strength, MPa	Elongation at break, %	Dielectric permittivity, $\epsilon'$ (at 10 Hz, 20 °C)	Dielectric loss, $\epsilon''$ (at 10 Hz, 20 °C)
AB I MB0	0.052	0.248	480	3.20	0.04
AB I MB1	0.053	0.325	621	3.26	0.48
AB I MB2	0.063	0.500	795	4.00	1.14
AB I MB5	0.061	0.316	516	4.17	0.44
AB II MB0	0.077	0.348	452	3.06	0.01
AB II MB1	0.090	0.294	330	3.26	0.05
AB II MB2	0.052	0.300	585	3.55	0.01
AB II MB5	0.160	0.399	249	3.85	0.01
AB IV MB0	0.033	0.180	543	3.17	0.15
AB IV MB1	0.026	0.202	780	3.57	0.51
AB IV MB2	0.036	0.225	641	3.73	0.68
AB IV MB5	0.038	0.320	850	3.98	0.52
3M VHB	0.060	0.58	950	3.30	0.04

Table 12 - The main parameters of the mechanical and dielectric tests

<sup>a</sup> Young's modulus was calculated from data at strain up to 10%.

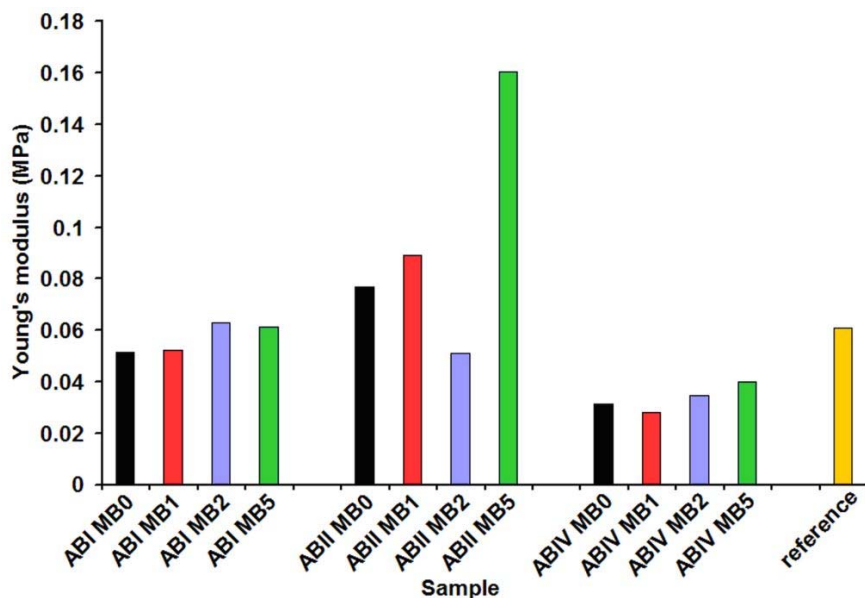


Figure 63 - Young's modulus for the tested samples; reference = 3M VHB

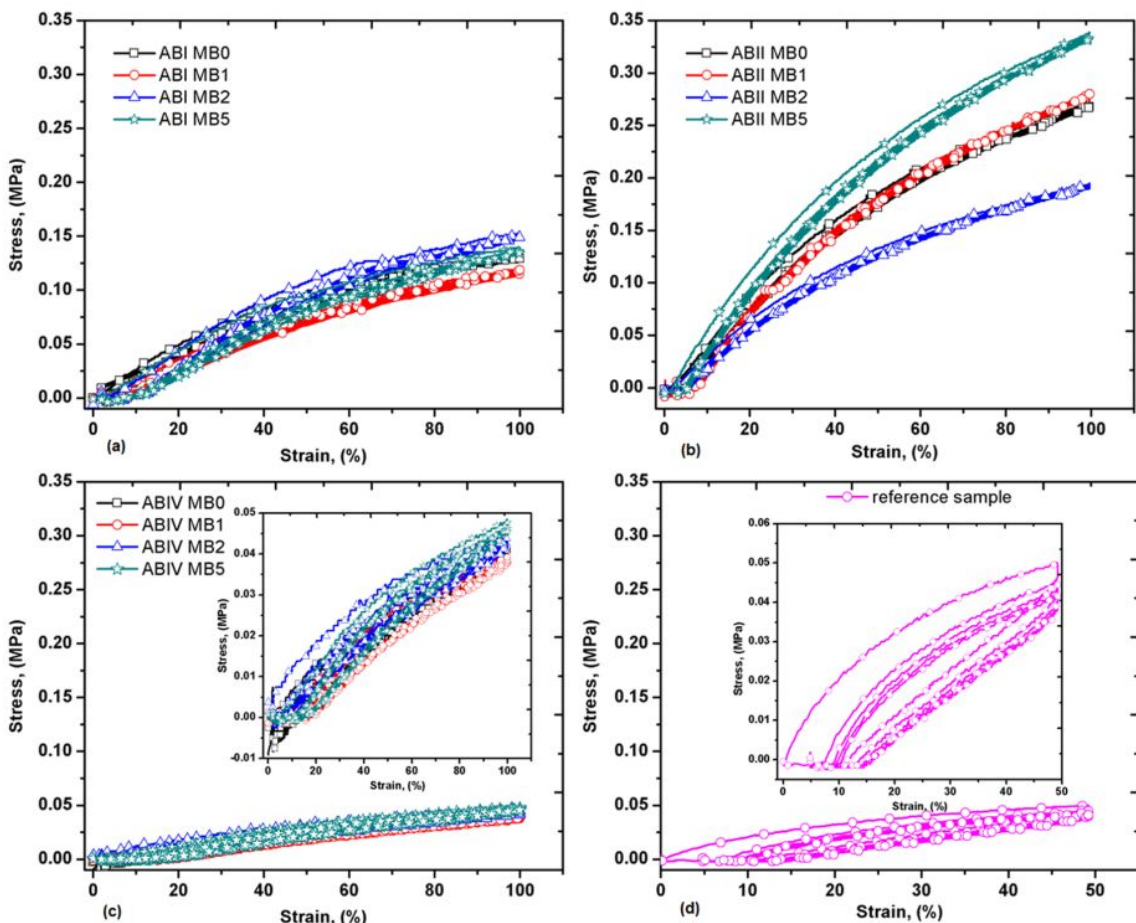


Figure 64 - Testing for cycles of stress-strain on the crosslinked films: (a) samples with polymer AB I; (b) samples with polymer AB II; (c) samples with polymer AB IV; (d) sample based on commercial 3M VHB.

When tested for cycles of stress-strain, with strains up to 100 % of initial length, the samples were clearly different (Figure 64). The samples based on polysiloxane presented an elastic behaviour, with a clearly visible hysteresis loop only at the first strain-release cycle, then the difference between strain and release was

smaller than 1% of the stress value at each point. The sample based on acrylic polymer 3M VHB presented a viscoelastic behaviour (Figure 64d) with nonlinear behaviour for cycles with strains above 50% therefore the cycles were made with only 50% strain and a clear loss of strain energy by viscous component is visible in the curves.

#### 4.1.2.5.2. Dielectric spectroscopy

There exists a distinct, although small, enhancement in dielectric constant with increasing filler content. However the increase of the  $\epsilon'$  value is not as large as expected, probably due to interactions between the layer of surfactant and the particles. The  $\epsilon'$  values of the films decrease with increasing frequency.

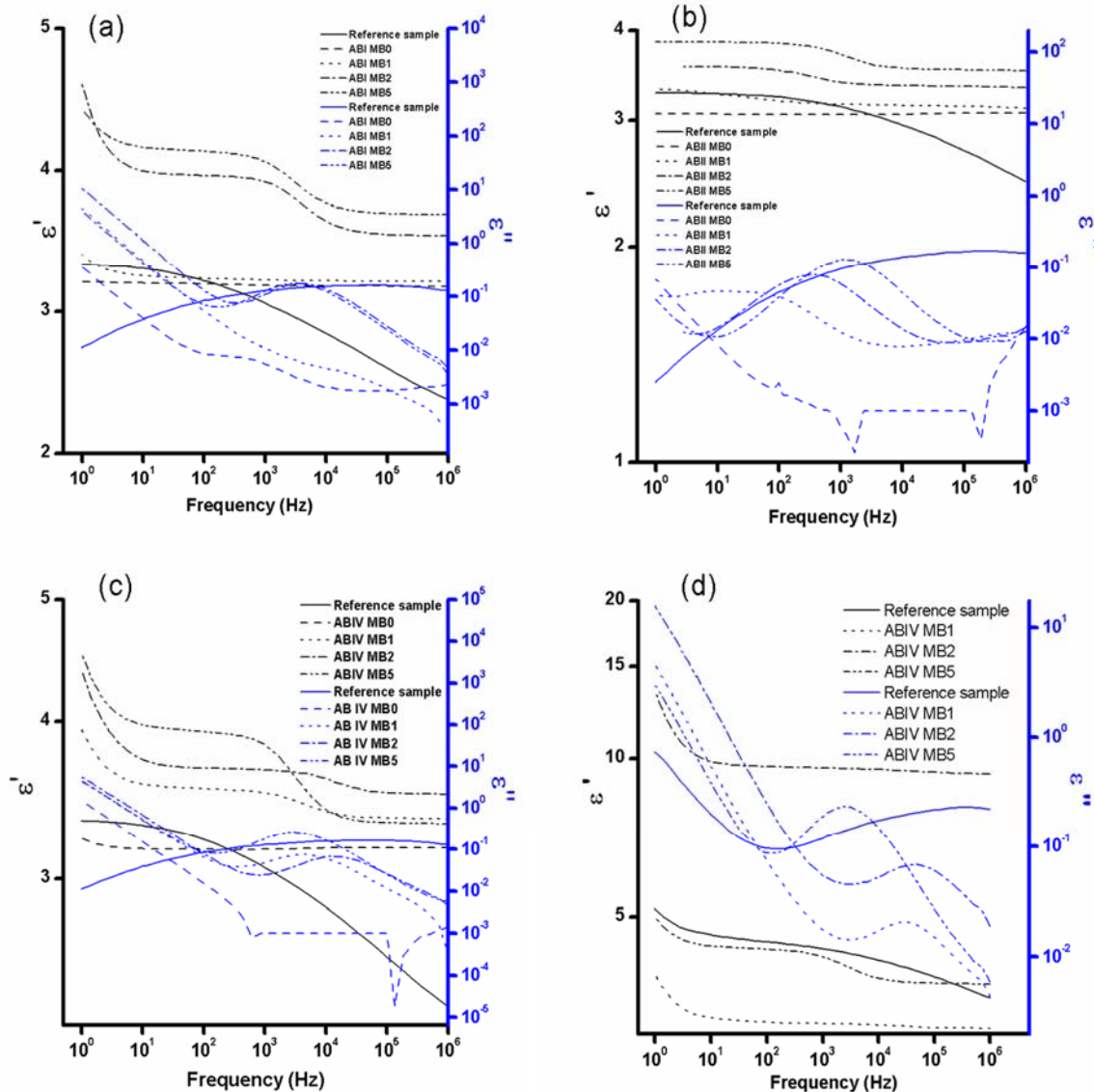


**Figure 65 - Dielectric spectroscopy results for the tested samples with dielectric constant and dielectric loss values at: (a) AB I at  $T = 20^\circ\text{C}$ ; (b) AB II at  $T = 20^\circ\text{C}$ ; (c) AB IV at  $T = 20^\circ\text{C}$ ; (d) ABIV films at  $T = 20^\circ\text{C}$  prestrained with 50% in both axes. reference=3M VHB**

A significant drop in  $\epsilon'$  occurs when the frequency reaches  $10^3$  Hz. In this case, the dipole relaxation in the composite films lags behind the change of applied fields. The characteristic relaxation peaks of the siloxane matrix in  $\epsilon''$  curves (AB II MB 0 and AB IV MB 0) disappear with the introduction of barium titanate particles (Figure 65 b, c) as this leads to the decrease of free volume in the polymer matrix and an increase of density of polar groups [90]. A higher degree of siloxane crosslinking would lead to increased values for permittivity since the free volume fraction would decrease, but this would negatively affect the

capability of the films to stretch with high percentages [90]. However, the data presented in Figure 65 and Table 12 do not permit us to draw a clear conclusion about the influence of the molecular mass of the polymer on the dielectric constant of the crosslinked films.

#### 4.1.2.5.3. Thermal analysis

DSC experiments (Figure 49) highlight the transitions occurring in the sample by temperature modification and associated heat capacity change ( $\Delta C_p$ ). It can be seen that all samples show glass transition around -120-(-123) °C regardless of the molecular weight of PDMS and the filler content. The samples based on polymers ABI and ABII exhibit nearly identical DSC traces, suggesting that BaTiO<sub>3</sub> particles have negligible influence on the thermal behavior of the samples.

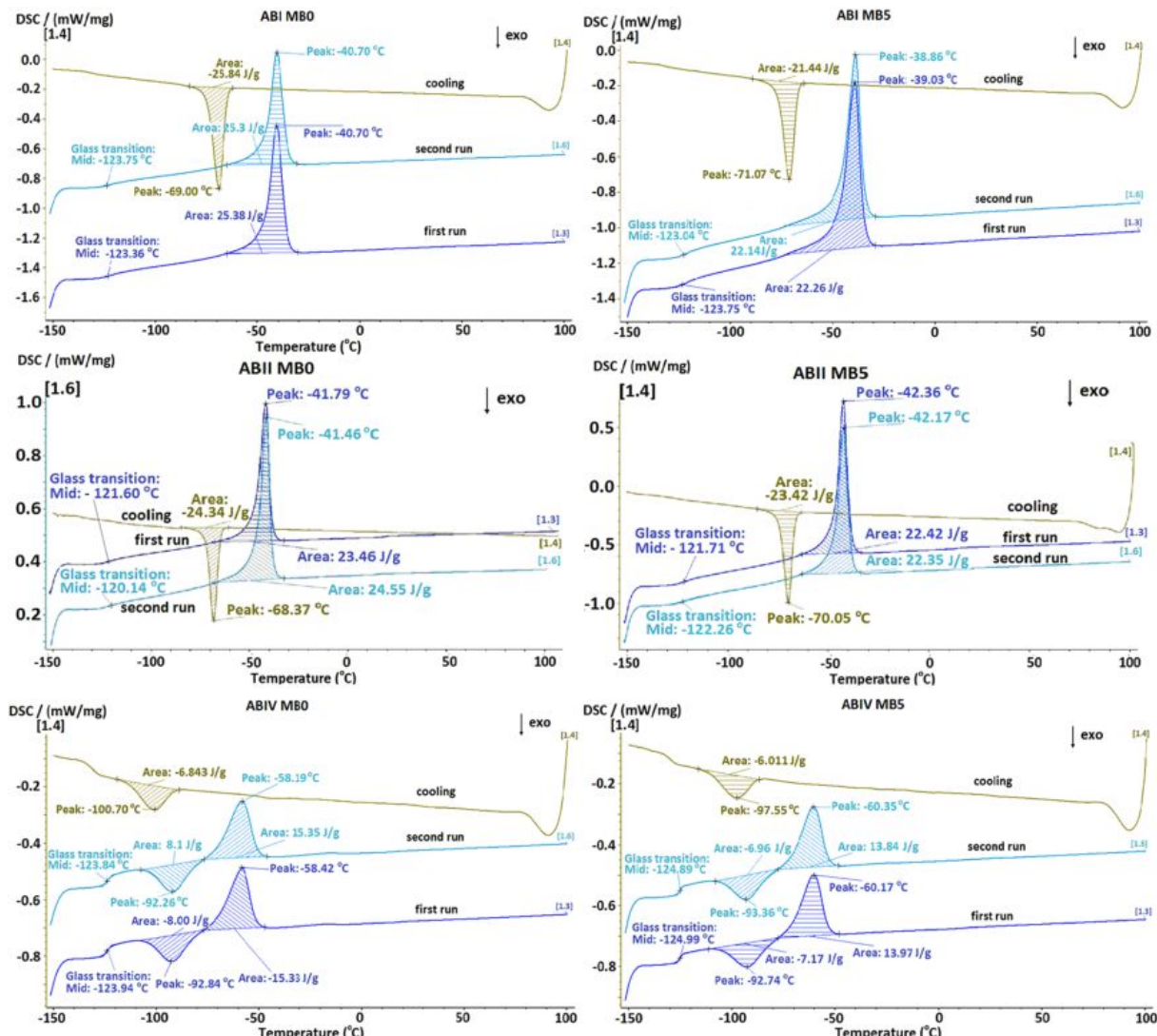


Figure 66 - DSC results for the tested samples

Thus, they show a reproducible endothermic peak at about -40 °C on the first and second heating curves assigned to melting, while on the cooling curve, an exothermic peak assigned to cold crystallization at about -70 °C develops. Instead, in the sample based on higher molecular weight PDMS, ABIV, a heating crystallization process is visible around -92 °C, while the melting and cold crystallization occur at lower temperatures (-60 and -100 °C, respectively) as compared with samples based on polymers ABI and ABII. The high length of the polymer chain ( $M_n=142\ 000\ g/mol$ ) and, as a result, the higher distance between crosslinks, permits occurrence of this process.

The TG-DTG data (Figure 67, Table 13) reveal the onset of degradation at higher temperatures for silicone samples (degradation onset at 397 °C), in comparison with acrylic polymer sample (220 °C). The thermal decomposition mainly occurs in a single step.

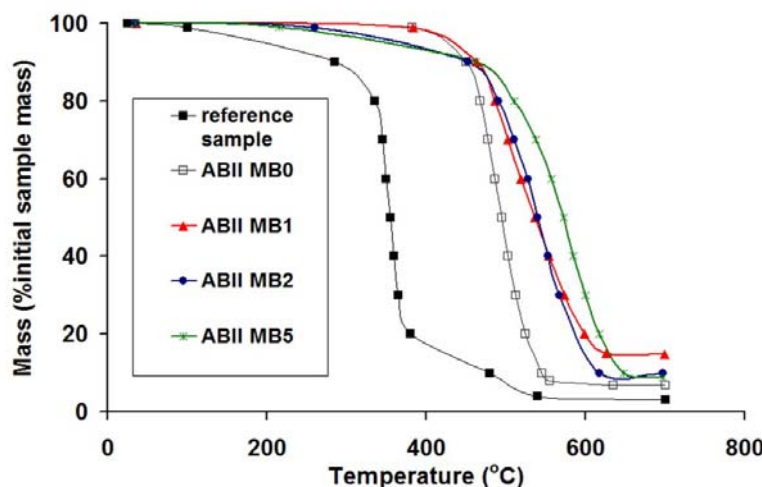


Figure 67 - Thermogravimetric curves for the crosslinked samples; reference = 3M VHB

The addition of barium titanate microparticles has a positive effect on the thermal resistance of the materials, as the onset temperature increases, although not very fast, up to 437 °C for sample with 5% BaTiO<sub>3</sub> (AB II MB5). The low value for the residue of degradation in inert atmosphere is due to breaking of the siloxane bond at high temperature and the formation of siloxane oligomers with low vaporization temperature and such chemical species are outgassing from the samples in the test crucibles [91].

Sample	T <sub>onset</sub>	T <sub>end</sub>	Peak (°C)	Residual mass (%)
AB II MB 0	397	549	491	7
AB II MB 1	419	614	499	13.8
AB II MB 2	430	609	546	9.4
AB II MB 5	436	630	582	8.4
3M VHB	220	540	380	3

Table 13 - Thermogravimetical data for the samples tested

#### 4.1.2.5.4. Vapor sorption capacity

The moisture sorption-desorption isotherms were registered in dynamic regime for the crosslinked composite films. Only a slight increasing in the moisture sorption capacity occurs by raising the content of barium titanate which is hydrophilic (barium titanate microparticles are easily dispersed in water) (Figure 68). Thus, the maximum sorption capacity increases from 0.22 % in pure crosslinked PDMS to 0.76 % in the composite with 5% BaTiO<sub>3</sub>, but the later value is lower as compared with that registered for commercial VHB sample (1.28 %) taken as reference.

Overall the isotherms correspond to a type III – specific for nonporous hydrophobic materials with weak interactions between sorbed and sorbing materials. The kinetic curves (not shown) for water vapor sorption show the rate of desorption of water vapors are generally slower than the sorption rate, leading to a small hysteresis loop.

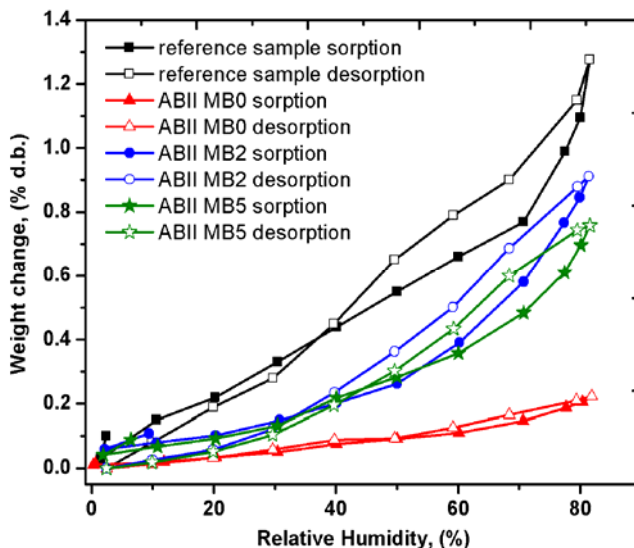


Figure 68- Sorption/desorption isotherms for the prepared samples as compared with a reference sample (commercial acrylic 3M VHB)

#### 4.1.3. Composites with lead zirconate

##### 4.1.3.1. Preparation of lead zirconate and its characterization (XRF, XRD, TEM, SEM)

The nanoparticles of lead zirconate were prepared by using a modified procedure from the one used by Oren et al. [92]. Namely, in a homogeneous precipitation method a mixture of cation stock solutions of lead and zirconium chlorides was (Figure 69). Then a solution of urea was mixed with the cation stock solution, leading to a clear solution that was further heated at 90 °C for ~2 hours. Then a solution of sodium hydroxide was added. After continuous heating, the precipitation started in ~10 minutes, when turbidity appeared in the clear solution. Precipitates were aged at 90-95 °C without stirring. Afterwards, the precipitates were separated by centrifugal filtration at 6000 rpm and the recovered material was washed with distilled water and the procedure was repeated twice. The washed material was oven-dried at 90 °C for 2 hours, followed by calcination.

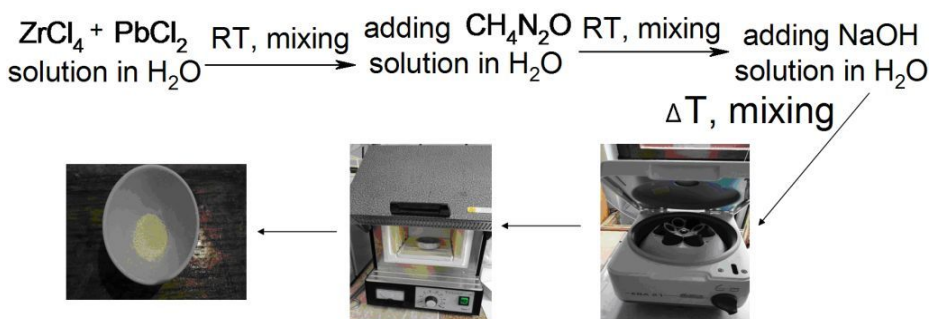


Figure 69 - Preparation of lead zirconate nanoparticles

Transmission electron microscopy (TEM) investigations of the nanoparticles were made with Hitachi High-Tech HT7700 Transmission Electron Microscope, operated in high contrast mode at 100 kV accelerating voltage. Samples were cast from diluted dispersion (1g/L) on 300 mesh carbon coated copper grids and vacuum dried. The analysis shows the formation of nanoparticles with average diameters of 50-100 nm.

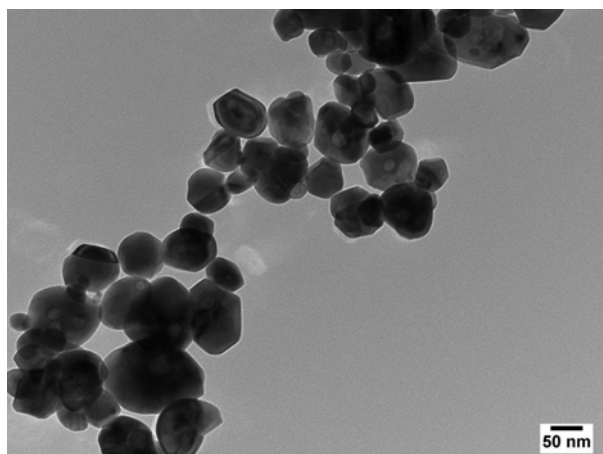


Figure 70 - TEM image of the LZ nanoparticles

For complete characterization of the lead zirconate nanoparticles, X-ray diffraction analysis of the powders was performed using a BRUKER D8 ADVANCE diffractometer (XRD). The XRD data (Figure 71) show the reflections and splitting of (2 4 0) peak at 41°, indicating that the crystal structure of the tested material is that of orthorhombic perovskite.

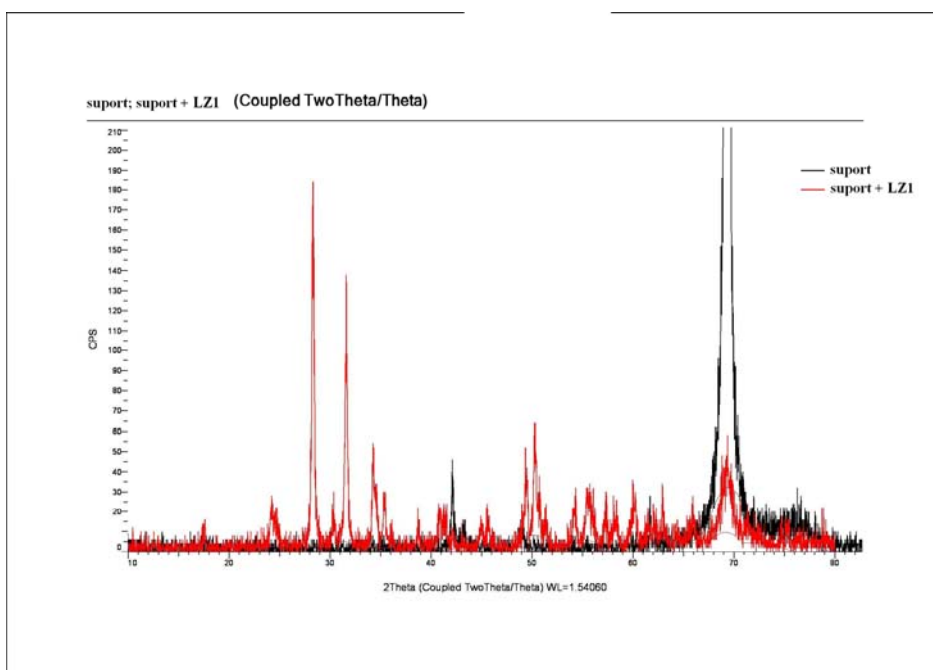


Figure 71 - XRD patterns of the LZ nanoparticles

When compared with the XRD spectrum for lead zirconate powders prepared by different authors [93] [94] the peaks are shifted to lower values for  $2\theta$  angles, due to the material being poor in lead content and enriched in Zr. Therefore the ceramic nanoparticles do not have the classic structure of  $\text{PbZrO}_3$ , but the brute formula was calculated from EDX measurement as being  $\text{Pb}_{0.1}\text{Zr}_{1.5}\text{O}_3$ .

#### 4.1.3.2. Composites and film formation

The lead zirconate powder was used as filler for elastomer films based on silicones, with the purpose of improving the dielectric and mechanical properties of these films, while simultaneously trying to preserve in the new composites the softness and the high stretch capability specific for films made with pure siloxane. The siloxane polymer used was polydimethylsiloxane- $\alpha,\omega$ -diol (PDMS) and it was synthesized according to the already described procedure [18],[95]: cationic ring-opening polymerization of

octamethylcyclotetrasiloxane in the presence of a cation exchanger as catalyst. Molecular mass was estimated on the basis of GPC analysis as being 142000 for the polymer.

The siloxane was mixed in a double roll Yanke - Kunkel laboratory mixer equipped with palettes in Dublex system and cooling mantle, with appropriate amounts of dielectric powder (lead zirconate) and the crosslinking agent methyl(triacetoxy)silane (MTS) (Table 14). After an uniform mixture was formed, it was cast in teflon mold where it was allowed to crosslink for two weeks in a sol-gel process, using the water vapours in atmosphere as hydrolysis agent for the silane. The films were then manually peeled off from the surface of the mold.

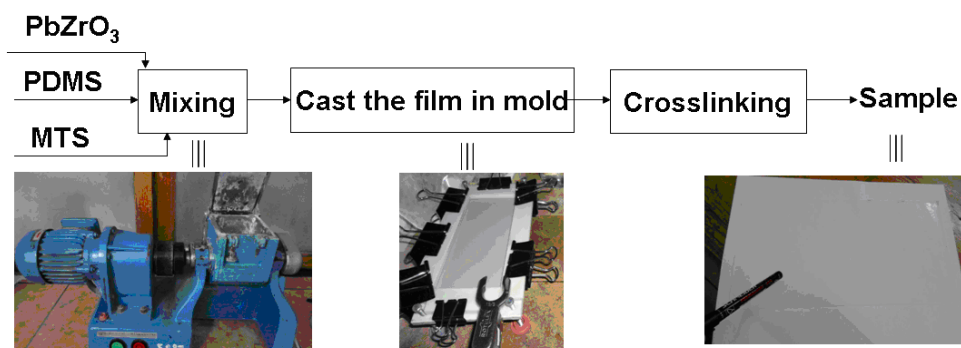


Figure 72- Procedure for preparation of composite films

Sample	Reagent (mass relative to siloxane)		
	PDMS	LZ	MTS
S1	100	0	5
S2	100	2	5
S3	100	6.5	5

Table 14 - The composition of the prepared films

#### 4.1.3.3. Mechanical tests

Tensile strength tests were performed at room temperature using an Instron Single Column Systems tensile testing machine (model 3345) equipped with a 5 kN load cell and activated grips, which prevented slippage of the sample before break. The crosshead speed used was  $50 \text{ mm min}^{-1}$ . Specimens for tensile measurements were cut out from thick films using a V cutter. At least five identical dumbbell-shaped specimens for each sample were tested, and their average mechanical properties are reported. The reported errors are the subsequent standard deviations.

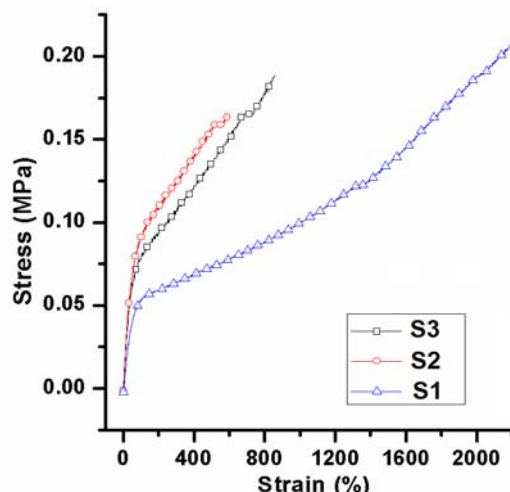


Figure 73 - Stress-strain curves for elastomer films containing LZ nanoparticles

The samples containing lead zirconate nanoparticles have a reduced value for breaking strain, since a small percentage of the nanoparticles forms agglomerates with micrometer size and the surface of these agglomerates acts as stress concentrator. Also the presence of lead zirconate nanoparticles introduces defects in the siloxane polymeric network leading to reduced value for the breaking stress when compared with the reference sample S1. However, the value for the breaking strain is larger than 400 %, making these membranes suitable for use as dielectric elastomers.

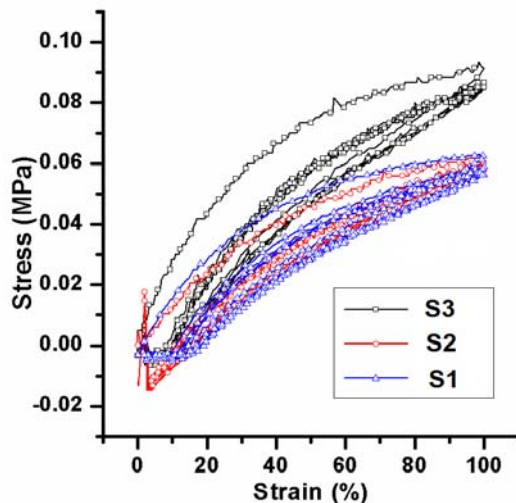


Figure 74 - Cyclic stress-strain films for elastomers containing LZ nanoparticles

The membranes prepared with lead zirconate nanoparticles have small hysteresis loops at cyclic stress-strain, making these suitable for use in flexible piezoelectric devices; also the value of the stress at a certain percentage of strain is larger than the corresponding value for the reference samples with pure siloxane.

#### 4.1.3.4. Dielectric spectroscopy

Dielectric spectroscopy was performed using the Novocontrol “Concept 40” broadband dielectric spectrometer (Hundsangen, Germany). In this experiment, the dielectric constant ( $\epsilon'$ ) and losses ( $\epsilon''$ ) were recorded in the frequency domain of six decades (log scale) of frequency, i.e. 1–100000 Hz, at constant temperature of 25 °C.

When the ceramic nanoparticles are introduced in the composition of the membranes the value of the dielectric constant increases – with up to 26 % for the sample S3 compared with reference S1. There is a relaxation at higher frequencies ( $5 \times 10^3$  Hz) due to charge accumulation at the interface between the nanoparticle surface and the polymer matrix.

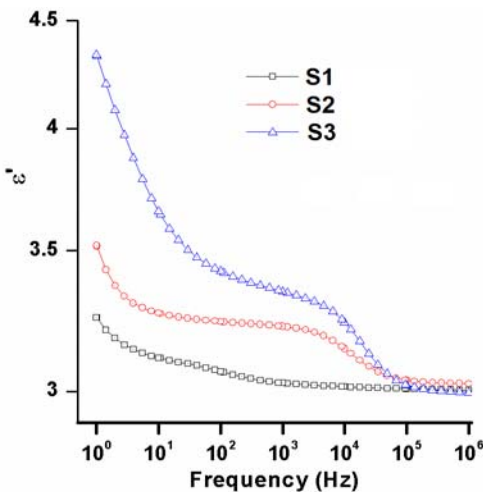


Figure 75 - The variation of dielectric constant for elastomers with LZ

The loss factor maintains reduced values when the nanoparticles are introduced in the polymer matrix. There is a clear relaxation visible at high frequencies ( $4 \times 10^4$  Hz) determined by charge accumulation at the interface between the nanoparticle surface and the polymer matrix.

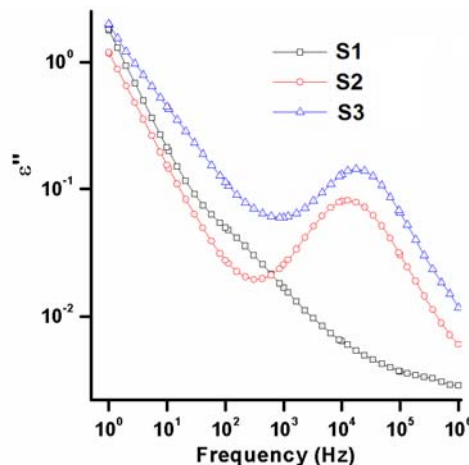


Figure 76 - The variation of dielectric loss for elastomers with LZ

#### 4.1.3.5. Thermal analysis

Thermal analyses within inert gas atmosphere were performed with an STA 449 F1 Jupiter (Netzsch, Germany) for TG/DSC analysis coupled with a Bruker Vertex 70 FTIR spectrometer. The TG chamber was purged with nitrogen (99.99% purity) at  $50 \text{ mL min}^{-1}$ . The temperature range was 30–700 °C, using a heating rate of  $10 \text{ K min}^{-1}$ .

DSC experiments (Figure 77) highlight the heat capacity change ( $\Delta C_p$ ) associated with the glass transition around -124 °C, and also one exothermic peak at about -70/-72 °C and an endothermic peak at -38/-39 °C, assigned to the phenomenon of cold crystallization and for melting of crystalline phase.

The peak corresponding to melting (-38 °C) is larger than the one corresponding for crystallization (-70 °C) and this indicates that a significant amount of crystalline phase develops during the cooling scan. This is a consequence of the mobility of PDMS chains and this property enables a three-dimensional arrangement of chains needed to develop the crystalline phase. The DSC curves of samples S2 and S3 are very similar, overlapping for heating scans. This behaviour suggests the ceramic particles have negligible influence on the thermal behavior of the samples.

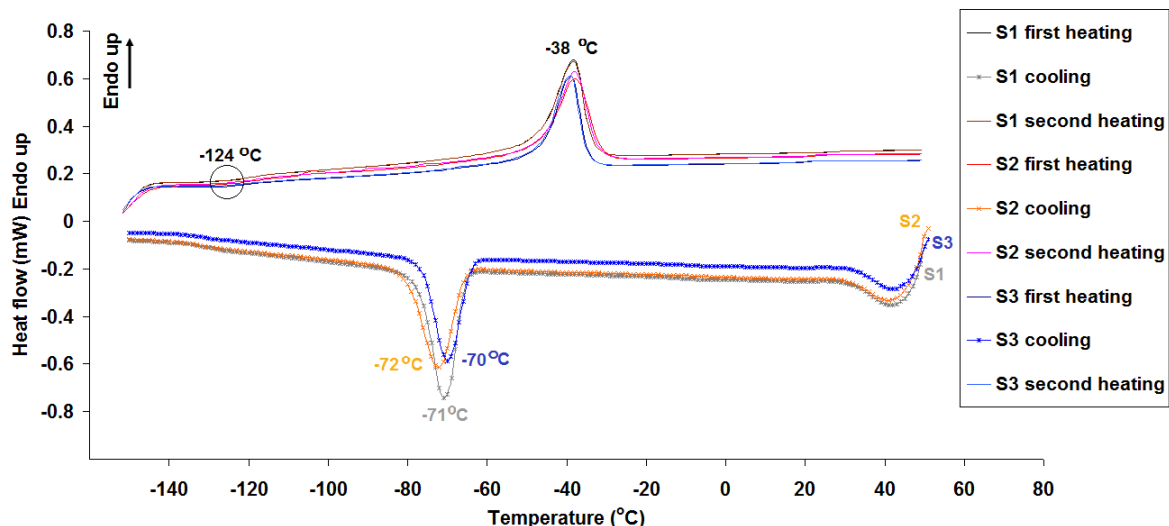


Figure 77 - The differential scanning calorimetry curves for elastomers with LZ

#### 4.1.3.6. Vapor sorption capacity

When materials are designed for use in electronic devices, the elastomer should ensure a stable operation and therefore the characteristics of interest must be stable in different conditions of moisture and temperature. There occurs an increase of in the moisture sorption capacity with the rising of the content of lead zirconate nanoparticles (Figure 77) and the maximum sorption capacity increases from 0.45 % in pure crosslinked PDMS to 1.35 % in the material with 6.5% lead zirconate, and this value is comparable with the ones obtained for other materials used as dielectric elastomers such as acrylic rubber 3M VHB (1.3 %).

The isotherms correspond to a type III material and show the membranes are nonporous hydrophobic materials with weak interactions between sorbed and sorbing materials.

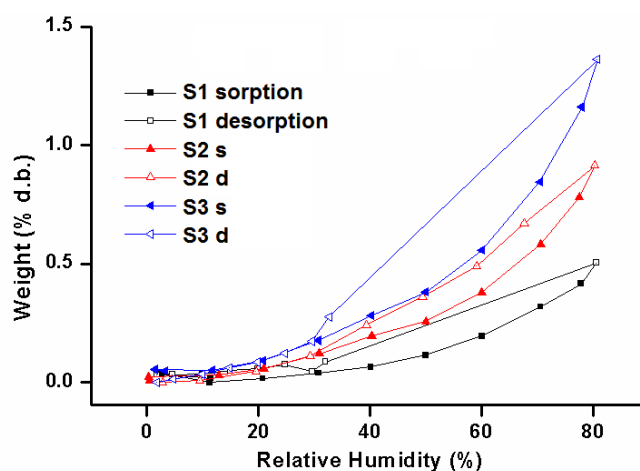


Figure 78 - Dynamic vapour sorption isotherms for the elastomers containing LZ nanoparticles

## Section 5: Conclusions

### 5.1 Discussion

A series of commercial polymeric films were characterized by appropriate techniques to obtain information of interest for potential application in energy harvesting: Fourier Transform Infrared spectroscopy, mechanical testing, dielectric spectroscopy, differential scanning calorimetry, dynamic vapour sorption capacity. The results are centralized in Annex 1. The measurements were performed by using the same equipments and by working in the same conditions. Due to high differences between their chemical structures, very different values for these characteristics were obtained for the analysed samples.

In order to use the polymers for building wave energy transducers it is necessary that these materials satisfy certain quantifiable conditions. Some conditions are related to the mechanical properties, such as:

- a) low mass density ( $\sim 1000 \text{ kg/m}^3$ ), similar with the density of the seawater;
- b) large deformability ( $\sim 700\%$ ) in order to be able to pre-stretch and to stretch under the action of the waves;
- c) reasonable values for Young's modulus ( $>0.1 - 20 \text{ MPa}$ );

There are conditions related to the electrical properties of the elastomers whose fulfilment is necessary in the construction of wave energy transducers. These conditions are as follows:

- a) high energy density ( $0.1-3.5 \text{ kJ/kg}$ );
- b) large break-down strength: usually  $20-400 \text{ MV/m}$ ;
- c) moderate (relative) dielectric permittivity: 1.8-7;
- d) good electro-mechanical conversion efficiency: 60-90%;

The most used classes of polymers for tests of direct mechanical wave energy conversion to electricity are natural rubber, silicones, acrylic rubber and polyurethanes. Regarding natural rubber, results do not appear particularly promising: increases in dielectric constant have been accompanied by increases in dielectric loss and reductions in dielectric breakdown strength [96]-[98] and the value of the elastic modulus is affected by the addition of filler [99]. For acrylic rubber the necessity of adding bulky support frames for maintaining the films restrained means there are significant increases of the mass of devices based on VHB acrylic and it reduces their effective energy densities from the ideal theoretical value of  $\sim 3.5 \text{ MJ/m}^3$  to values similar with other dielectric elastomers and plastics ( $<1 \text{ MJ/m}^3$ ). VHB acrylic sheets of polymer suffer from viscoelastic effects which limit their maximum response frequency to the 10–100 Hz range and their viscoelastic nature also limits their overall efficiency and leads to time dependent strain that can make their performance erratic. Silicones have the disadvantage of low tear strength and very low value for Young modulus ( $<0.1 \text{ MPa}$ ). The use of polyurethanes has been overshadowed by other classes of elastomers.

A short overview of mechanical and chemical properties and behaviour for various classes of elastomer rubbers is presented in Table 15 (the entire table in Annex I).

Property, characteristic	NR <sup>1</sup>	SBR <sup>2</sup>	Neoprene	Butyl	Nitril	EPDM <sup>3</sup>	PU <sup>4</sup>	S <sup>5</sup>	FC <sup>6</sup>	CSPE <sup>7</sup>	Acryl <sup>8</sup>
Specific gravity [95]	0.93	0.94	1.23	0.92	1.00	0.85	1.05	1	1.85	1.1	1.09

Table 15 - Mechanical and chemical properties of different types of elastomers

<sup>1</sup>-Natural rubber; <sup>2</sup>-Styrene butadiene rubber; <sup>3</sup>-Ethylene propylene diene monomer rubber; <sup>4</sup>-Polyurethane; <sup>5</sup>-Silicones; <sup>6</sup>-Fluorocarbon rubber; <sup>7</sup>-chlorosulfonated polyethylene synthetic rubber; <sup>8</sup>-Acrylic rubbers; <sup>9</sup>-At 80 Hz unless otherwise stated

The dielectric properties for different elastomer rubbers are presented in Table 15 (the entire table in Annex I).

## 5.2 Conclusion

Three types of silicone composites were prepared and studied in the first year of the project implementation, as following:

- A polydimethylsiloxane- $\alpha,\omega$ -diol of high molecular mass was prepared, characterized and used as matrix to prepare composites followed by crosslinking. Silica and titanium dioxides were used as fillers to improve mechanical characteristics and dielectric constant, respectively. A net increasing of the mechanical characteristics (Young modulus, tensile strength, elongation, and hardness) resulted by incorporation of 28 wt% silica, while the subsequent adding of the titania led to the increasing of the dielectric constant, and also contributes to the increasing of tensile strength and elongation. A slight decreasing of the melting temperature values and increasing of storage modulus was emphasized by DMA while glass transition is not affected by the presence of the fillers. The low dielectric and mechanical losses of the investigated silicone/titania composites make them candidates as actuator materials, where a short response time is required. The dielectric constant of composites increased with increasing filler content, while retaining the flexibility of the matrix. Low values of the water vapor sorption capacity are a guarantee of good stability of the dielectric properties in an environment with variable humidity. The actuation effect expressed as section displacement and estimated with high resolution interferometer ranges between 0.04-5.09 nm/V/mm, in general increasing by raising titania content. The energy harvesting capacity determined from the fall of a miniball on the surface of elastomeric film gave promising results.

The robustness of these composites supported by their thermal, mechanical and surface properties recommends them for use inclusively in harsh environmental conditions, when their behavior is not significantly affected.

- Siloxane composites based on polydimethylsiloxane- $\alpha,\omega$ -diols having different chain length as matrices and barium titanate powder as filler added in different percents (1, 2, and 5 wt%) were prepared and crosslinked in films. Samples without filler were prepared for comparison in similar conditions. DSC study reveals that the presence and amount of the filler do not affect the thermal transition of the crosslinked structures, these being influenced mainly by the polymer chain length. A slight increasing in the thermostability of the samples due to the filler effect was emphasized by thermogravimetric analysis. The presence of the barium titanate leads to increasing in moisture sorption in the material. Considering the intended use for energy conversion, the key parameters are the ultimate strain, the elastic behaviour and the relaxation at repeated strain cycles and the voltage generated under tension. In general, slight increases are registered both in mechanical parameters (Young modulus, tensile strength and elongation), although not regulate enough, and dielectric permittivity values by the incorporation of barium titanate as compared with samples without filler. The highest value for Young modulus was registered for the sample based on the polymer with shortest chain and as a result the highest crosslinking density. Sample based on the longest chain and highest filler content showed the highest elongation value. The dielectric permittivity value increases from 3.20, 3.06, and 3.17 to 4.17, 3.85, and 3.98, respectively by variation of the filler content from 0 to 5 wt%. The siloxane-based films show superior performance in elastic behaviour in testing cycles as compared with an acrylic commercial sample.

It have been observed an improvement in dielectric properties by increasing molecular mass of the polymeric matrix and filler concentration, besides a slight decreasing in mechanical and vapour sorption properties. It has also been found that the using of nanoparticles with different morphologies leads to composite material with different mechanical and dielectric properties and this represents a way for further optimization of the properties of silicone-based dielectric actuators.

- Polydimethylsiloxane- $\alpha,\omega$ -diols were also used as matrix to incorporate lead zirconate in order to obtain new silicone composites with increased dielectric permittivity. The lead zirconate (LZ) nanoparticles with average diameters of 50-100 nm were home-prepared by using a modified procedure reported in literature. The crosslinked elastomer membranes having incorporated LZ nanoparticles have small values for water sorption, preserving the hydrophobic character of the siloxane membranes. There is a decrease of the maximum strain for elastomers with LZ when compared with elastomers made with pure siloxane, due to discontinuities introduced in the elastomer volume by LZ nanoparticles. The value of dielectric constant

increases with the increase in the content of LZ, improving the dielectric behaviour and the membranes with nanoparticles have small hysteresis loops at cyclic stress-strain, making these suitable for use in flexible piezoelectric devices. Also the dielectric loss at small frequencies (100 Hz) is similar for all membranes – the nanoparticles do not lead to increase of dielectric losses.

As can be seen from Table 15 (Annex 1) from previous subsection, several conclusions can be drawn regarding the mechanical and chemical properties of commercial siloxane based elastomers that have been the focus of our research for wave energy transducers:

- the specific gravity of siloxane based elastomers (~1 for pure siloxane elastomer and ~1.2 for siloxane with ceramic nanoparticles) is close to values for other elastomers;
- the value of tensile strength is lower for siloxane rubber when compared with other elastomers;
- the hardness values for crosslinked samples of siloxane elastomers with ceramic nanoparticles is very good (60-100 Shore A); these have also some of the best behaviour among elastomers regarding properties such as abrasion resistance, atmospheric aging resistance, oxidation resistance, heat resistance, low temperature flexibility and moisture resistance, all of which are important when constructing wave energy transducers;
- the permeability of siloxanes is smaller than that of other elastomers and it is necessary in order to insulate the electrical devices;
- the mechanical loss factor has a small value (0.05) due to the elastic behaviour of siloxanes, with almost no viscous component;

Based on the data from Table 15 (Annex1) from previous subsection, several conclusions can be drawn regarding the dielectric and mechanical properties of siloxane based elastomers both commercial ones (reported in literature) and prepared by PPIMC team during first year of the project:

- siloxane elastomers have excellent strain capability (up to 1000%) but this property is accompanied by low values for Young modulus (<0.1 MPa). This indicates a soft material that is easily deforming under an external force, which is a desired property for the construction of wave energy transducers, mainly the water column type where it must be avoided the build up of air pressure when the wave surges;
- dielectric constant values for different samples of siloxane elastomers with nanoparticles are between 4 and 9, an increase when compared with values specific for pure siloxane films (3-3.5 – daca e corect, inseamna ca trebuie precizat la ce frecventa s-au luat toate aceste valori!) and the dielectric loss factor at low frequencies is as low as 0.066 making these films suitable for the desired application.

### **5.3 Future Works**

- Study on the influence of the filler-matrix compatibilization agent/procedure;
- Optimization of the elastomeric silicone composites for wave energy harvesting.

For building wave energy transducers with good efficiency, it is necessary to have elastomers that combine a series of rather contradictory properties: soft materials with low viscous component, very large strains (>500% compared with initial length) but with decent values for Young modulus (>0.1 MPa) and a combination of highest possible value for dielectric constant and high breakdown electric field (> 50 MV/m). In order to comply with these demands, the team of researchers at Petru Poni Institute of Macromolecular Chemistry will develop the best formulations obtained in the first year; PPIMC will also focus in the following year on creating and testing new formulations for siloxane elastomers which are of interest in the field of wave energy transducers, such as:

- siloxanes reinforced with diversified ceramic nanoparticles;
- silicone composites having incorporated metal complexes;
- siloxanes with other organic substituents to the silicon atom within siloxane backbone;
- interpenetrated polymer networks with siloxanes and other polymers.

All these options for research will be tested for obtaining new elastomers with improved properties, taking into consideration the materials obtained in the last year of research in the frame of PolyWEC.

## References

- [1]. Pelnine, R.; Kornbluh, R.; Eckerle, J.; Jeuck, P.; Oh, S.; Pei, Q.; Stanford, S.; *Dielectric Elastomers: Generator Mode Fundamentals and Applications*; In Proc. SPIE (Vol. 4329, pp. 148-156); 2001.
- [2]. Koh, S.J.A., Zhao, X., Suo, Z.; *Maximal Energy that can be Converted by a Dielectric Elastomer Generator*; Applied Physics Letters 94, 262902; 2009.
- [3]. Koh, S.; Keplinger, C.; Li, T.; Bauer, S.; Suo, Z.; *Dielectric Elastomer Generators: how much Energy can be converted?*; IEEE Transactions on Mechatronics, 16(1): 33-41; 2011.
- [4]. Jean-Mistral, C.; Basrour, S.; Chaillout, J.-J.; *Modelling of Dielectric Polymers for Energy Scavenging applications*; Smart Mater. Struct. 19, 105006, 2010.
- [5]. Rosset, S., Shea, H. R. (2013). Flexible and stretchable electrodes for dielectric elastomer actuators. *Applied Physics A*, 110(2), 281-307.
- [6]. Cech, T. V.; *Principles of Water Resources: History, Development, Management, and Policy*, 3rd Edition; Wiley, September 2009
- [7]. Chiba, S.; Waki, M.; Kornbluh, R.; Pelnine, R.; *Innovative power generators for energy harvesting using electroactive polymer artificial muscles*; Proc. SPIE 2008, 6927, 692715
- [8]. Jones, W. D.; *Ocean power catches a wave*; IEEE Spectr. 2008, 45, 14
- [9]. Carpi, F.; Rossi, D. D.; Kornbluh, R.; Pelnine, R. Sommer-Larsen, P. (Eds.); *Dielectric Elastomers as Electromechanical Transducers*; New York: Elsevier, 2008.
- [10]. Maas, J.; Graf, C.; Dielectric elastomers for hydro power harvesting, *Smart Mater. Struct.* 2012, 21, 064006
- [11]. Brochu, P.; Pei, Q. Advances in Dielectric Elastomers for Actuators and Artificial Muscles, *Macromolecular Rapid Communications*, 2010, 31, 10-36
- [12]. McKay, T.G.; O'Brien, B.M.; Calius, E.P.; Anderson, I.A. Soft generators using dielectric elastomers, *Appl. Phys. Lett.* 2011, 98, 142903
- [13]. Greve, H.-H.; *Rubber, 2. Natural*, in *Ullmann's Encyclopedia of Industrial Chemistry*, 2000, Wiley-VCH, Weinheim.
- [14]. Roentgen, W. C.; *About the Changes in Shape and Volume of Dielectrics Caused by Electricity*; ser. Annual Physics and Chemistry Series, Vol. 11, sec III, G. Wiedemann, Eds., J. A. Barth Leipzig, Germany 1880, p. 771
- [15]. James E. Mark, Burak Erman (eds.); (2005); *Science and technology of rubber*. p. 768.
- [16]. Kinetic Model for Vulcanization,  
[https://engineering.purdue.edu/CCD/index.php?page=vulcanization\\_kinetic\\_model](https://engineering.purdue.edu/CCD/index.php?page=vulcanization_kinetic_model), accessed 10.18.2013.
- [17]. Engels, H-W.; Weidenhaupt, H-J; Pieroth, M.; Hofmann, W.; Menting, K-H.; Mergenhagen, T.; Schmoll, R.; Uhrlandt, S.. *Rubber, 4. Chemicals and Additives*, in *Ullmann's Encyclopedia of Industrial Chemistry* 2004, Wiley-VCH, Weinheim.
- [18]. Cazacu, M, Marcu, M., *J. Macromol. Sci. Part A*, 1995, 32, 1019-1025
- [19]. Pouget, E.; Tonnar, J.; Lucas, P.; Lacroix-Desmazes, P.; Ganachaud, F.; Boutevin, B. Well-Architected Poly(dimethylsiloxane)-Containing Copolymers Obtained by Radical Chemistry, *Chem. Rev.* 2010, 110, 1233–1277
- [20]. Skalsky, M.; Vaughan, J. D.; Chapman, R. E. In: Planck H, Syre I, Davner M, Egbers G, Eds. *Progress in biomedical engineering*, vol. 3. *Polyurethanes in biomedical engineering II*. New York: Elsevier; 1987, p. 75
- [21]. Tillet, G.; Boutevin, B.; Ameduri, B.. Chemical reactions of polymer crosslinking and post-crosslinking at room and medium temperature, *Progr. Polym. Sci.* 2011, 36, 191–217
- [22]. Bosman, A. W.; Janssen, H. M.; Van Gemert, G. M. L.; Verstegen, R. M.; - Meijer, E. W.; Sijbesma, R. P. (Suprapolix B.V., Netherlands) WO 2004052963, 2004
- [23]. Sijbesma, R. P.; Beijer, F. H.; Brunsved, L.; Folmer, B. J. B.; Hirschberg, J. H. K. K.; Lange, R. F. M.; Lowe, J. K. L.; Meijer, E. W. Reversible Polymers Formed from Self-Complementary Monomers Using Quadruple Hydrogen Bonding, *Science* 1997, 278, 1601-1604
- [24]. Lehn, J. M. *Supramolecular Chemistry: Concepts and Perspectives*; VCH: Weinheim, Deutschland, 1995
- [25]. Saam, J. C.; Falender, J. R. (Dow Corning Corp., USA) DE 2717192, 1977

- [26]. Falender, J. R.; Saam, J. C.; Mettler, C. M. (Dow Corning Corp., USA) DE 2717227, **1977**
- [27]. Ahmad, S.; Gupta, A. P.; Sharmin, E.; Alam, M.; Pandey, S. K. Synthesis, characterization and development of high performance siloxane-modified epoxy paints, *Prog. Org. Coat.* **2005**, *54*, 248–255
- [28]. Adhikari, R.; Dao, B.; Hodgkin, J.; Mardel, J.; *Synthesis, structures and membrane properties of siloxane-imide co-polymers produced by aqueous polymerization*; Eur. Polym. J., **2011**, *47*(6), 1328-1337
- [29]. Wei, S.-Q.; Bai, Y.-P.; Shao, L.; *A novel approach to graft acrylates onto commercial silicones for release film fabrications by two-step emulsion synthesis*; Eur. Polym. J. **2008**, *44*, 2728–2736
- [30]. Hagenaars, A. C.; Bailly, Ch.; Schneider, A.; Wolf, B. A., *Preparative fractionation and characterization of polycarbonate/eugenol-siloxane copolymers*; Polymer, **2002**, *43*(9), 2663-2669
- [31]. Keddie, D. J.; Grande, J. B.; Gonzaga, F.; Brook, M. A.; Dargaville, T. R., Amphiphilic Silicone Architectures via Anaerobic Thiol-Ene Chemistry, *Org. Lett.*, **2011**, *13*(22), 6006–6009
- [32]. Mark, J. E.; Allcock, H. R.; West, R.; *Inorganic Polymers*, Second Edition; Oxford University Press, Inc., New York, **2005**, p. 186
- [33]. Noll, W. *Chemistry and Technology of Silicones*; Academic Press: New York, 1968
- [34]. Voronkov, M. G.; Mileshkevich, V. P.; Yuzhelevskii, Y. A. *Studies in Soviet Science. The Siloxane Bond: Physical Properties and Chemical Transformations*; Plenum Publishing Corporation: New York, **1978**
- [35]. Robert A. Norwood, Manfred Eich, Mark G. Kuzyk, Editors, *Linear and Nonlinear Optics of Organic Materials IV*; Proc. of SPIE Vol. 5517, SPIE, Bellingham, WA, **2004**, p.117
- [36]. Kai, Su; Jon, V. DeGroot, Jr.; Norris, Ann W.; Lo, Peter Y. *Siloxane Materials for Optical Applications*, in: *ICO20: Materials and Nanotechnologies*, Wei Lu, Jeff F. Young, Eds. Proc. of SPIE Vol. 6029, 60291C, **2005**, 60291C-1 – 60291C-8
- [37]. Gubbels, F. *11. Silicones in the Electronics Industries, Chapter 2. Silicones in Industrial Applications in Inorganic Polymers*, Nova Science Publishers, Roger De Jaeger; Mario Gleria,Eds. **2007**, ISBN: 1-60021-656-0
- [38]. McAfee, LaRuth C. *Polysiloxane-Based Liquid Crystal Block Copolymers for Piezoelectric and Mechano-Optical Applications*, Ph. D. Thesis, Submitted at MIT, June **2005**
- [39]. Bellas, V.; Tegou, E.; Raptis, I.; Gogolides, E.; Argitis, P.; Iatrou, H.; Hadjichristidis, N.; Sarantopoulou, E.; Cefalas, A. C.; *Evaluation of siloxane and polyhedral silsesquioxane copolymers for 157 nm lithography*; *J. Vac. Sci. Technol. B* **2002**, *20*(6), 2902-2909
- [40]. Owen, M. J. *Why Silicones Behave Funny*, Dow Corning Corporation, [http://www.dowcorning.co.kr/ko\\_KR/content/publishedlit/01-3078-01.pdf](http://www.dowcorning.co.kr/ko_KR/content/publishedlit/01-3078-01.pdf)
- [41]. Dumitriu S., Ed. *Polymeric biomaterials*. New York: Marcel Dekker; **1993**
- [42]. Kothandaraman. Rubber Materials. Ane Books India. **2008**, p. 68. ISBN 978-81-8052-224-6.
- [43]. Rubber selection – A guide to outline properties, [http://www.merl-ltd.co.uk/2003\\_materials/rubber12.shtml#acm](http://www.merl-ltd.co.uk/2003_materials/rubber12.shtml#acm) , retrieved 2008-12-25.
- [44]. Acrylic rubbers, [https://www.tut.fi/ms/muo/vert/5\\_rubber\\_chemistry/SR\\_acrylic\\_rubbers.htm](https://www.tut.fi/ms/muo/vert/5_rubber_chemistry/SR_acrylic_rubbers.htm) , retrieved 2013-10-10
- [45]. Whelan, T.; *Polymer Technology Dictionary*; Springer. **1994**, p. 13. ISBN 978-0-412-58180-9.
- [46]. Gent, A. N.; *Engineering with Rubber: How to Design Rubber Components*; Hanser Verlag. **2001**, p. 18. ISBN 978-1-56990-299-8.
- [47]. Irlich, H.; *Chemistry and Technology of Isocyanates*; New York: John Wiley & Sons, Inc. **1996**, ISBN 0-471-96371-2
- [48]. Nipol®AR (Acrylic Rubber), [http://www.zeon.co.jp/business\\_e/enterprise/rubber/rubber\\_acm.html](http://www.zeon.co.jp/business_e/enterprise/rubber/rubber_acm.html) , retrieved 14.10.2013
- [49]. REDCO Rubber Information, <http://redco1.com/rubber-information/acrylic-rubber> , retrieved 14.10.2013
- [50]. Zhang, Q. M.; Su, J.; Kim, C. H.; Ting, R.; Capps, R.; *An experimental investigation of electromechanical responses in a polyurethane elastomer*; *J. Appl. Phys.* **1997**, *81*, 2770-2776
- [51]. Gum, W.; Riese, W.; Ulrich, H.; *Reaction Polymers*; New York: Oxford University Press. **1992**, ISBN 0-19-520933-8.
- [52]. Harrington, R.; Hock, K.; *Flexible Polyurethane Foams*; Midland: The Dow Chemical Company, **1991**

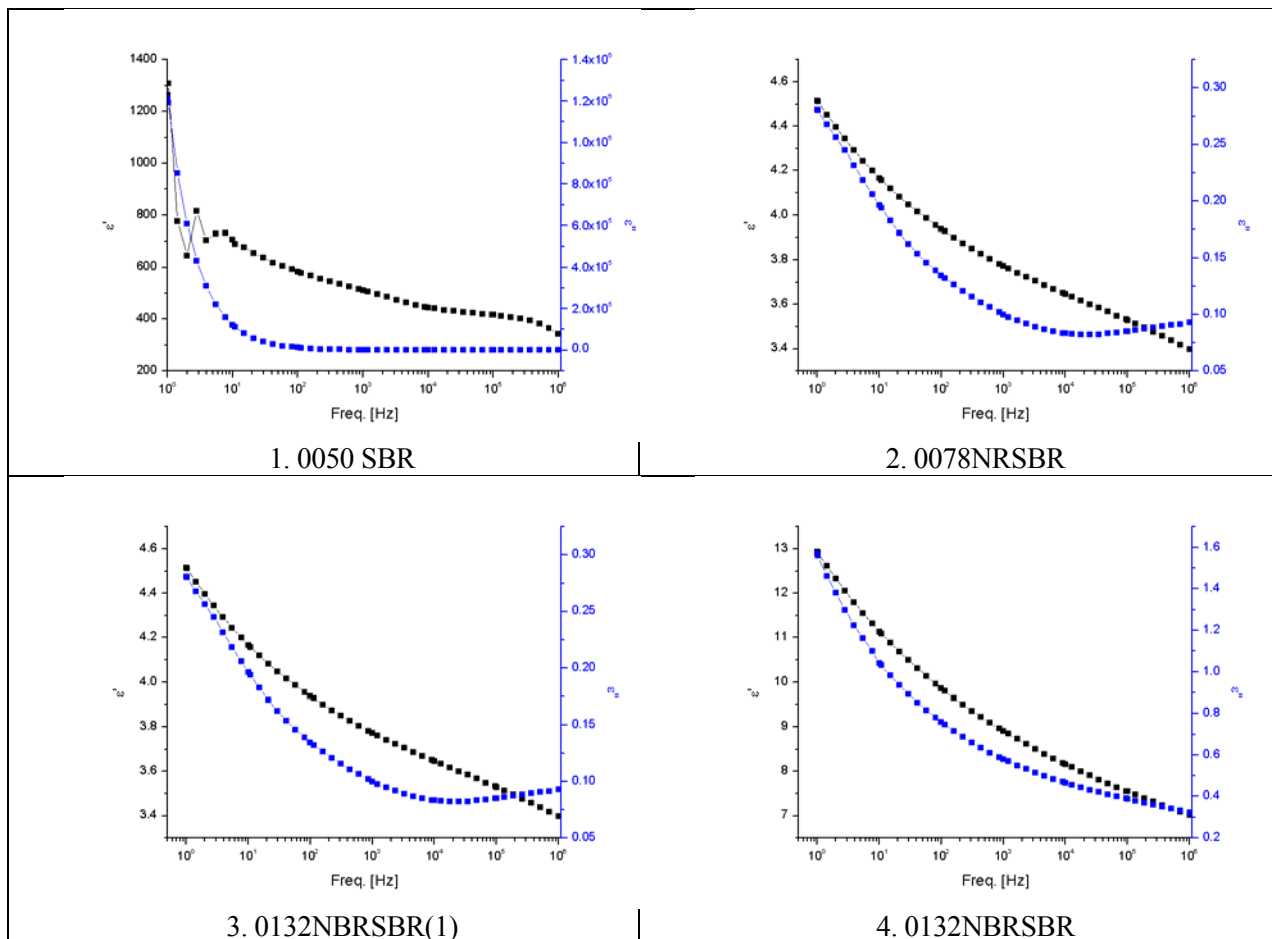
- [53]. Kaushiva, Byran D. *Structure-Property Relationships of Flexible Polyurethane Foams*. PhD Thesis. Virginia Polytechnic Institute, August 15, **1999**
- [54]. Dernehl, C. U. Health Hazards Associated with Polyurethane, *Journal of Occupational and Environmental Medicine*, February **1966**, 8(2), 59-62
- [55]. Health Alert: Polyurethane exposure, <http://www.nssga.org/safetyhealth/polyurethaneexposure0204.pdf>, retrieved 15.10.2013.
- [56]. *The Socio-Economic Impact of Polyurethanes in the United States from the American Chemistry Council*; The Polyurethanes Recycle and Recovery Council (PURRC), a committee of the Center for the Polyurethanes Industry. February **2004**. Retrieved 2013-10-19.
- [57]. Valentine, C.; Craig, T. A.; Hager, S. L.; *Inhibition of the Discoloration of Polyurethane Foam Caused by Ultraviolet Light*; J. Cellular Plastics **1993**, 29(6), 569–590.
- [58]. Newman, C. R.; Forciniti, D.; *Modeling the Ultraviolet Photodegradation of Rigid Polyurethane Foams*; Ind. Eng. Chem. Res. **2001**, 40(15), 3336–3352. doi:10.1021/ie0009738.
- [59]. Blair, G. R.; Dawe, B.; McEvoy, J.; Pask, R.; de Priamus, M. R.; Wright, C.; *The Effect of Visible Light on the Variability of Flexible Foam Compression Sets*; Orlando, Florida: Center for the Polyurethane Industry, **2007**.
- [60]. Behrendt, G.; Naber, B. W.; *The Chemical Recycling of Polyurethanes*; Journal of the University of Chemical Technology and Metallurgy, **2009**, 44(1), 3-23
- [61]. Russell, J. R.; Huang, J.; Pria, A.; Kucera, K. et al.; *Biodegradation of Polyester Polyurethane by Endophytic Fungi*; Appl. Environ. Microbiol. September **2011**, 77(17), 6076-6084
- [62]. Cazacu, M.; Antohi, M.; Racles, C.; Vlad, A.; Forna, N.; *Silicone-based composite for lining of removable dental prosthesis*; J. Compos. Mater. **2009**, 43(19), 2045-2055
- [63]. Gubbels, F.; *Silicones in Industrial Applications*. In: De Jaeger, R.; Gleria, M. (eds) *Inorganic Polymers*, Nova Science Publishers, **2007**, pp. 61-162 (chapter 2)
- [64]. Kremer, F.; Schönhals, A.; Luck, W.; *Broadband Dielectric Spectroscopy*. – Springer-Verlag, **2002**
- [65]. Gallone, G.; Galantini, F.; Carpi, F.; *Perspectives for new dielectric elastomers with improved electromechanical actuation performance: composites versus blends*; Polym. Int. **2010**, 59, 400–406
- [66]. Moulson, A. J.; Herbert, J. M. *Electroceramics: materials, properties and applications*. London: Chapman & Hall, **1990**
- [67]. Babar, A. A.; Bhagavati, V. A.; Ukkonen, L.; Elsherbeni, A. Z.; Kallio, P.; Sydanheimo, L.; *Performance of High-Permittivity Ceramic-Polymer Composite as a Substrate for UHF RFID Tag Antennas*; Int. J. Antennas Prop. **2012**, ID 905409, 1-8
- [68]. Khastgir, D.; Adachi, K.; *Rheological and dielectric studies of aggregation of barium titanate particles suspended in polydimethylsiloxane*; Polymer **2000**, 41, 6403–6413
- [69]. Nayak, S.; Chaki, T. K.; Khastgir, D.; *Development of poly(dimethylsiloxane)/BaTiO<sub>3</sub> nanocomposites as dielectric material*; Adv. Mater. Res. **2012**, 622 – 623, 897-900
- [70]. Zhao, H.; Wang, D.-R.; Zha, J.-W.; Zhao, J.; Dang, Z.-M.; *Increased electroaction through a molecular flexibility tuning process in TiO<sub>2</sub>-polydimethylsilicone nanocomposites*; J. Mater. Chem. A, **2013**, (I), 3140-3145
- [71]. Hamciuc, C.; Hamciuc, E.; Cazacu, M.; Okrasa, L.; *Poly(ether-imide) and poly(ether-imide)-polydimethyl-siloxane containing isopropylidene groups*; Polym. Bull. **2008**, 59, 825–832
- [72]. Alexandru, M.; Cazacu, M.; Nistor, A.; Musteata, V.E.; Stoica, I.; Grigoras, C.; Simionescu, B.C.; *Polydimethylsiloxane/silica/titania composites prepared by solvent-free sol-gel technique*; J. Sol-Gel Sci. Technol. **2010**, 56, 310–319
- [73]. Chen, K.; Yang, S.; *Synthesis of epoxy-montmorillonite nanocomposite*; J. Appl. Polym. Sci. **2002**, 86, 414–421
- [74]. Liu, X.; Wu, Q. Pp/clay nanocomposites prepared by grafting-melt intercalation. *Polymer* **2001**, 42, 10013–10022
- [75]. Ash, B.; Schadler, L.; Siegel, R.; *Glass transition behavior of lumina/polymethylmethacrylate nanocomposites*; Mater. Lett. **2002**, 55, 83–87
- [76]. Bershtein, V.; Egorova, L.; Yakushev, P.; Pissis, P.; Sysel, P.; Brozova, L. Molecular dynamics in nanostructured polyimide-silica hybrid materials and their thermal stability. *J. Polym. Sci. Part B: Polym. Phys.* **2002**, 40, 1056–1069

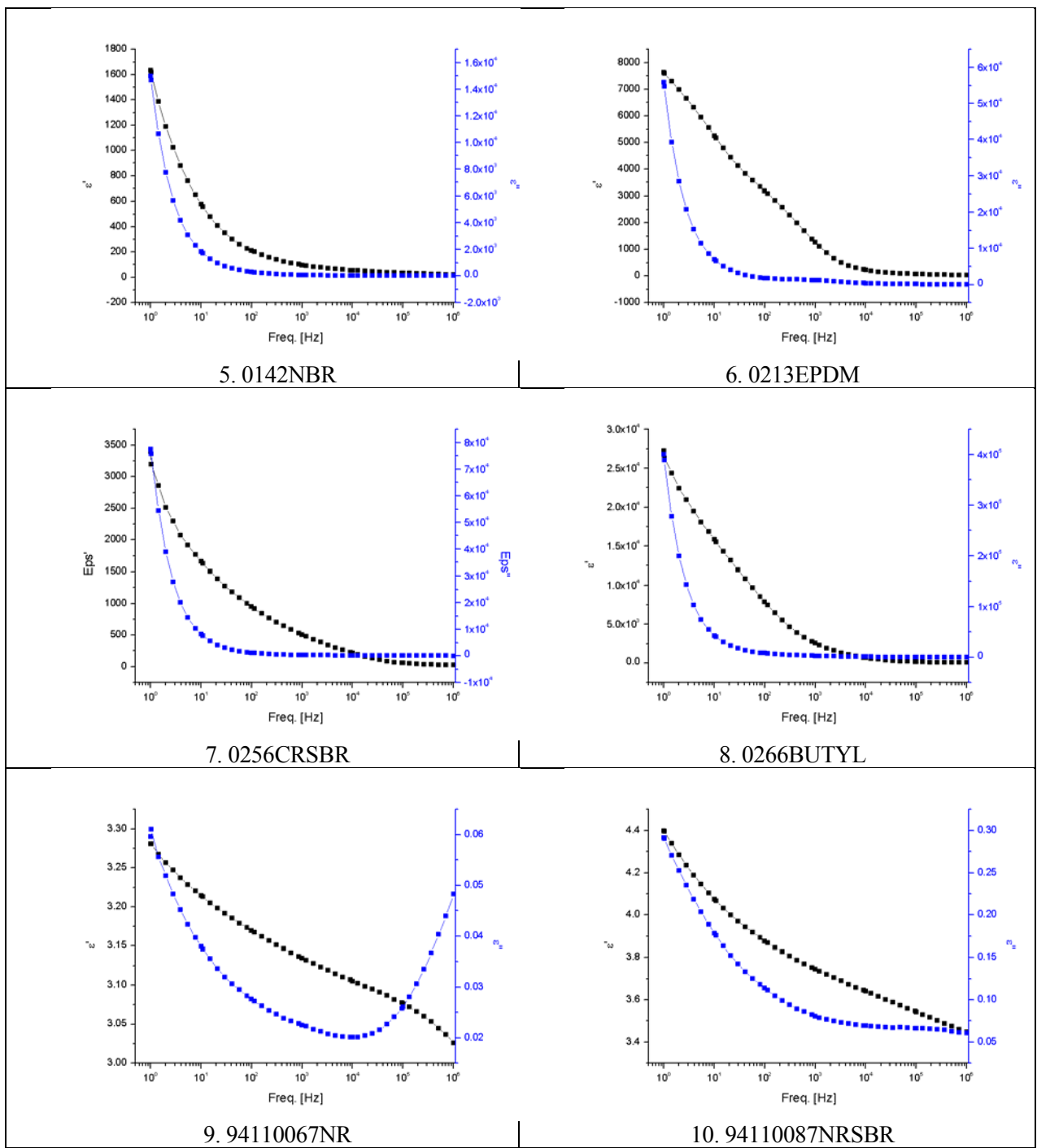
- [77]. Fragiadakis, D.; Pissis, P.; Bokobza, L. Glass transition and molecular dynamics in poly(dimethylsiloxane)/silica nanocomposites. *Polymer* **2005**, *46*, 6001–6008
- [78]. Vogel, H. Das Temperaturabhängigkeitgesetz der Viskosität von Flüssigkeiten. *Physik Z.* **1921**, *22*, 645–646
- [79]. Liedermann, K. A simple formula for the temperature dependence of the relaxation frequency in glassy systems. *Colloid Polym. Sci.* **1996**, *274*, 20–26
- [80]. Sabourin, C. L.; Carpenter, J. C.; Leib, T. K.; Spivack, J. L. Biodegradation of dimethylsilanediol in soils. *Appl. Environ. Microb.* **1996**, *62*(12), 4352–4360
- [81]. Yang, G.; Ren, W.; Akhras, G.; Mukherjee, B.K. Transverse strain of silicone dielectric elastomer actuators. *J. Adv. Sci.* **2005**, *18*(1/2), 166–169
- [82]. Nam, J. D.; Choi, H. R.; Koo, J. C.; Lee, Y. K.; Kim, K. J. *Dielectric elastomers for artificial muscles*. In: Kim, K. J.; Tadokoro, S. (eds.) *Electroactive polymers for robotic applications, artificial muscles and sensors*; Springer-Verlag London Limited **2007**, pp. 37–48
- [83]. Lin, Z.-H.; Yang, Y.; Wu, J. M.; Liu, Y.; Zhang, F.; Wang, Z. L. BaTiO<sub>3</sub> Nanotubes-Based Flexible and Transparent Nanogenerators. *J. Phys. Chem. Lett.* **2012**, *3*, 3599–3604
- [84]. Kwon, D.; Rincon-Mora, G. A. A rectifier-free piezoelectric energy harvester circuit. *Proceedings of ISCAS* **2009**, 1085–1088
- [85]. Granstrom, J.; Feenstra, J.; Sodano, H. A.; Farinholt, K. Energy harvesting from a backpack instrumented with piezoelectric shoulder straps. *Smart Mater. Struct.* **2007**, *16*, 1810–1820
- [86]. Liu, Y.; Liu, L.; Zhang, Z.; Jiao, Y.; Sun, S.; Leng, J. Analysis and manufacture of an energy harvester based on a Mooney-Rivlin-type dielectric elastomer. *Europhys. Lett.* **2010**, *90*, 36004 p1–p6
- [87]. Zulkifli Ahmad, Polymeric Dielectric Materials, **2012**, DOI: 10.5772/50638
- [88]. Racles, C.; Cazacu, M.; Fischer, B.; Opris, Dorina M. Synthesis and characterization of silicones containing cyanopropyl groups and their use in dielectric elastomer actuators, *Smart Mater. Struct.*, **2013**, *22*, 000000 (10 pages)
- [89]. Ogawa, T.; Takei, S.; Willson, C. G. Ultraviolet curable branched siloxanes as low-k dielectrics for imprint lithography, *J. Vac. Sci. Technol. B*, **2013**, *31*, 011601–011606
- [90]. Stiubianu, G.; Racles, C.; Cazacu, M.; Simionescu, B. C. Silicone-modified cellulose. Crosslinking of cellulose acetate with poly[dimethyl(methyl-H)siloxane] by Pt-catalyzed dehydrogenative coupling, *J. Mater. Sci.*, **2010**, *45*, 4141–4150
- [91]. Stiubianu, G.; Nicolescu, A.; Nistor, A.; Cazacu, M.; Varganici, C.; Simionescu, B. C. Chemical modification of cellulose acetate by allylation and crosslinking with siloxane derivatives, *Polym. Int.*, **2012**, *61*, 1115–1126
- [92]. Oren, E. E.; Taspinar, E.; Tas, A. C. Preparation of Lead Zirconate by Homogeneous Precipitation and Calcination, *J. Am. Ceram. Soc.*, **1997**, *80*(10), 2714–2716
- [93]. Usa, Sukkha; Rangson, Muanghlua; Surasak, Niemcharoen; Banjong, Boonchoma; Naratip, Vittayakorn. Antiferroelectric–ferroelectric phase transition in lead zinc niobate modified lead zirconate ceramics: crystal studies, microstructure, thermal and electrical properties, *Appl. Phys. A* **2010**, *100*, 551–559
- [94]. Kong, L. B.; Ma, J.; Zhu, W.; Tan, O. K. Preparation and characterization of lead zirconate ceramics from high-energy ball milled powder, *Mater. Lett.* **2001**, *49*, 96–101
- [95]. Marcu, M.; Simionescu, M.; Cazacu, M.; Lazarescu, S.; Ibanescu, C. Obtaining poly(dimethylsiloxane)-diols using the heterogeneous catalysis. The optimization of the reaction conditions *Iran. J. Polym. Sci.* **1994**, *3*, 95–104
- [96]. Huang, C.; Zhang, Q. M.; deBotton, G.; Bhattacharya, K. All-organic dielectric-percolative three-component composite materials with high electromechanical response. *Appl. Phys. Lett.* **2004**, *84*, 4391.
- [97]. Gallone, G.; Carpi, F.; De Rossi, D.; Levita, G.; Marchetti, A. Dielectric constant enhancement in a silicone elastomer filled with lead magnesium niobate–lead titanate. *Mater. Sci. Eng. C* **2007**, *27*, 110–116
- [98]. Zhang, Z.; Liu, L.; Fan, J.; Yu, K.; Shi, L.; Leng, J. New silicone dielectric elastomers with a high dielectric constant. *Proc. SPIE* **2008**, *6926*, 692610, 10 p.
- [99]. Lotz, P.; Matysek, M.; Lechner, P.; Hamann, M.; Schlaak, H. F. Dielectric elastomer actuators using improved thin film processing and nanosized particles. *Proc. SPIE* **2008**, *6927*, 692723

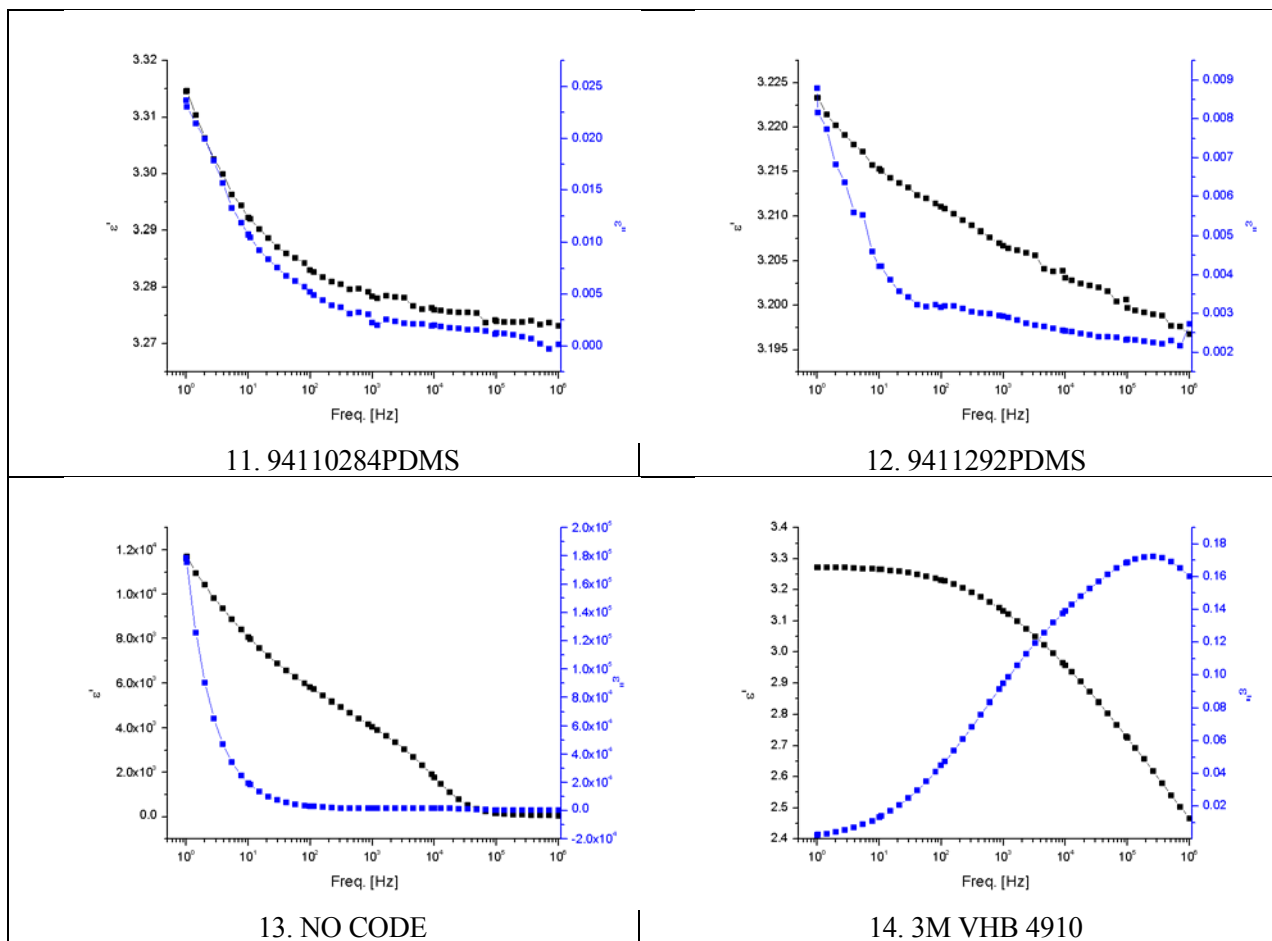
## ANNEX I

### Section 3.2.

No.	Sample	Dielectric constant ( $\epsilon'$ )			Dielectric loss ( $\epsilon''$ )		
		1Hz	1kHz	1MHz	1Hz	1kHz	1MHz
1.	0050 SBR	1262.9	511.7	342.2	1200000	1235.1	113.8
2.	0078NRSBR	4.51	3.77	3.39	0.28	0.1	0.09
3.	0132NBRSBR(1)	870.83	530	33.6	22719	88.41	27.96
4.	0132NBRSBR	12.93	8.9	7.01	1.57	0.57	0.32
5.	0142NBR	1633.7	97.31	20.96	14987	67.23	6.85
6.	0213EPDM	7636	1258.2	32.56	55887	1171.7	18.71
7.	0256CRSBR	3392.7	507.92	23.49	77548	311.71	15
8.	0266BUTYL	27266	2544.3	54.96	399980	2594.4	50.65
9.	94110067NR	3.28	3.13	3.02	0.059	0.022	0.04
10.	94110087NRSBR	4.39	3.74	3.44	0.29	0.08	0.06
11.	94110284PDMS	3.31	3.27	3.27	0.02	0.002	0.0001
12.	9411292PDMS	3.22	3.2	3.19	0.008	0.002	0.002
13.	NO CODE	11610	4046.3	40.07	178820	1468.3	60.9
14.	3M VHB 4910	3.27	3.13	2.46	0.002	0.009	0.16

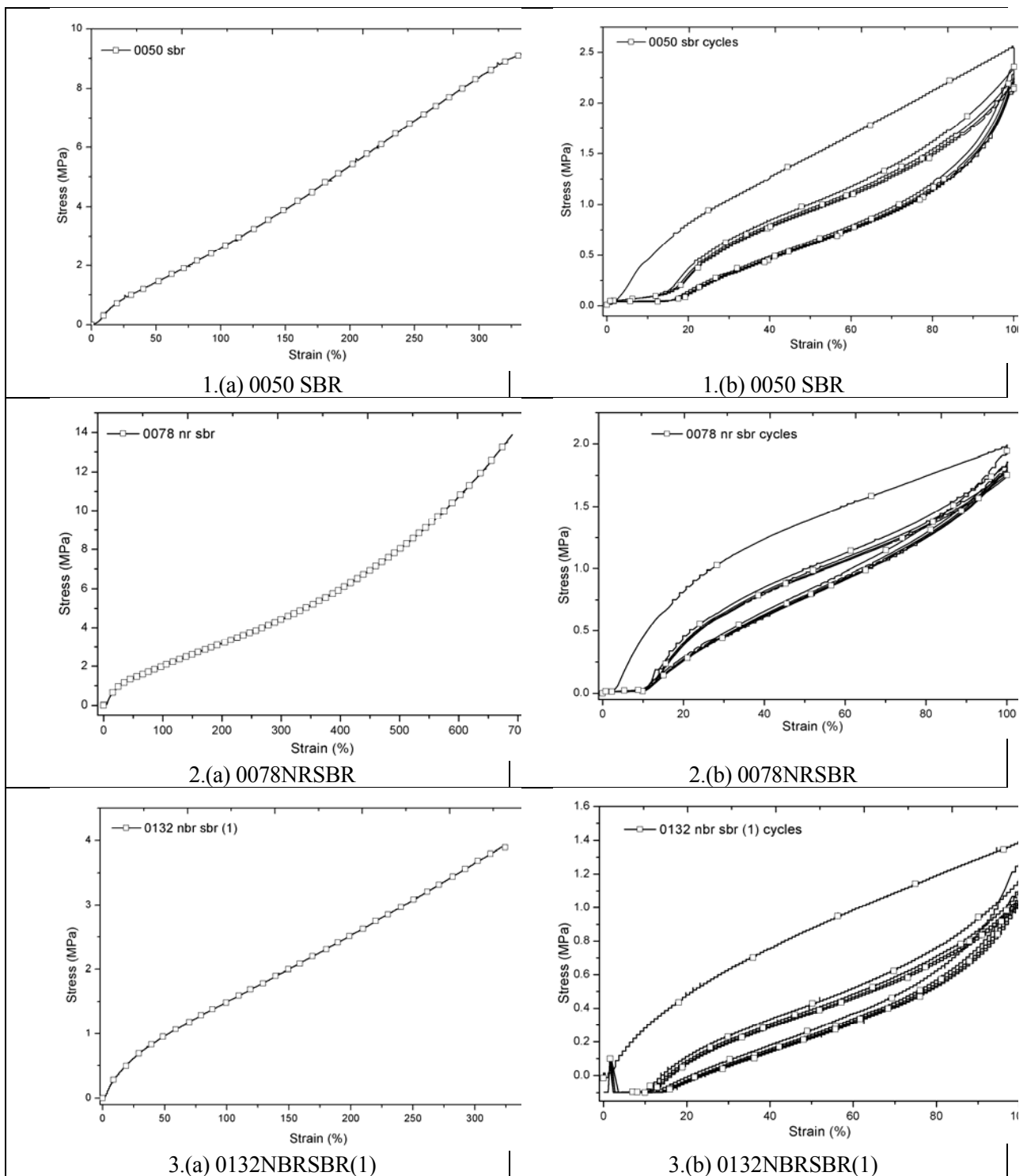


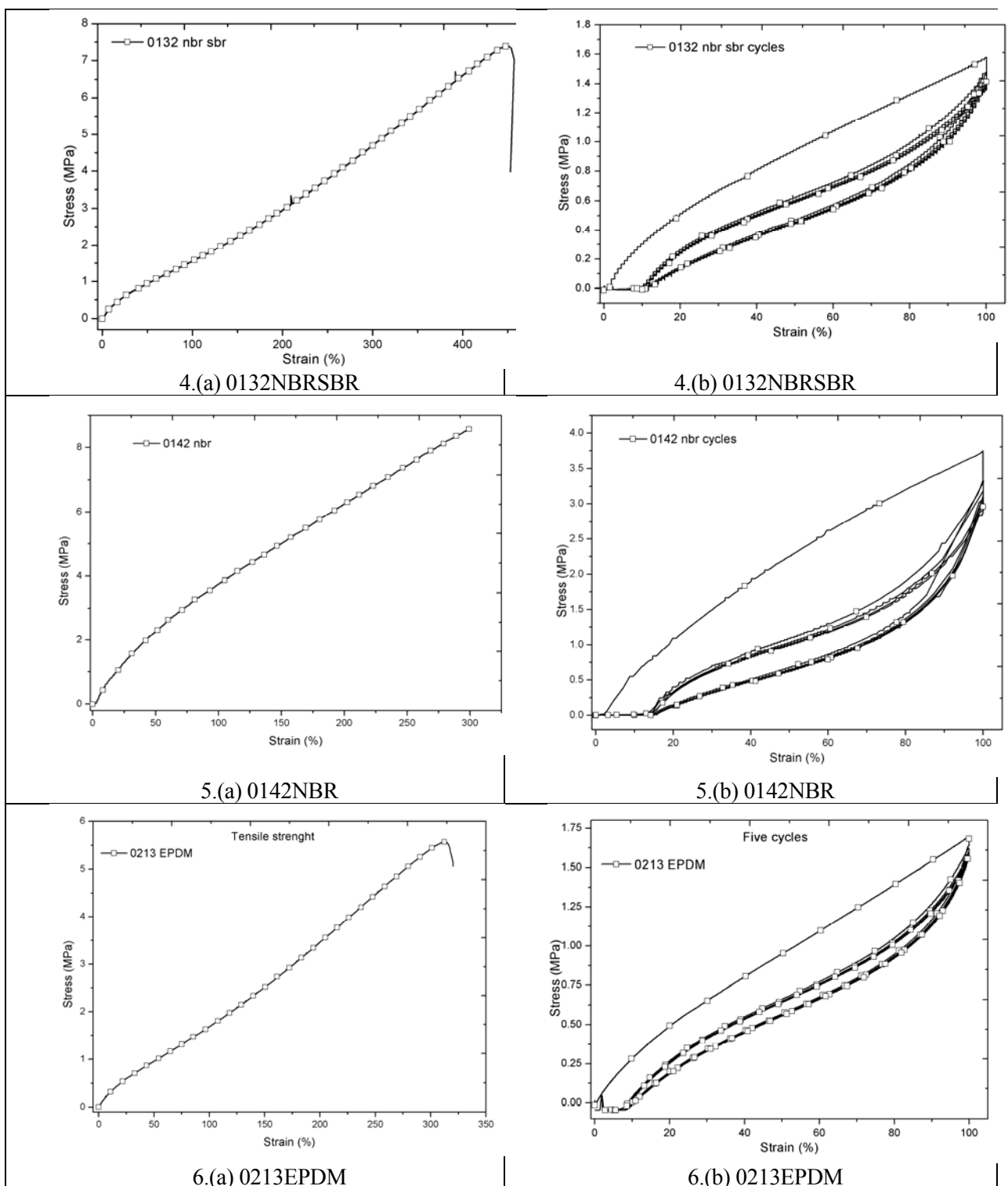


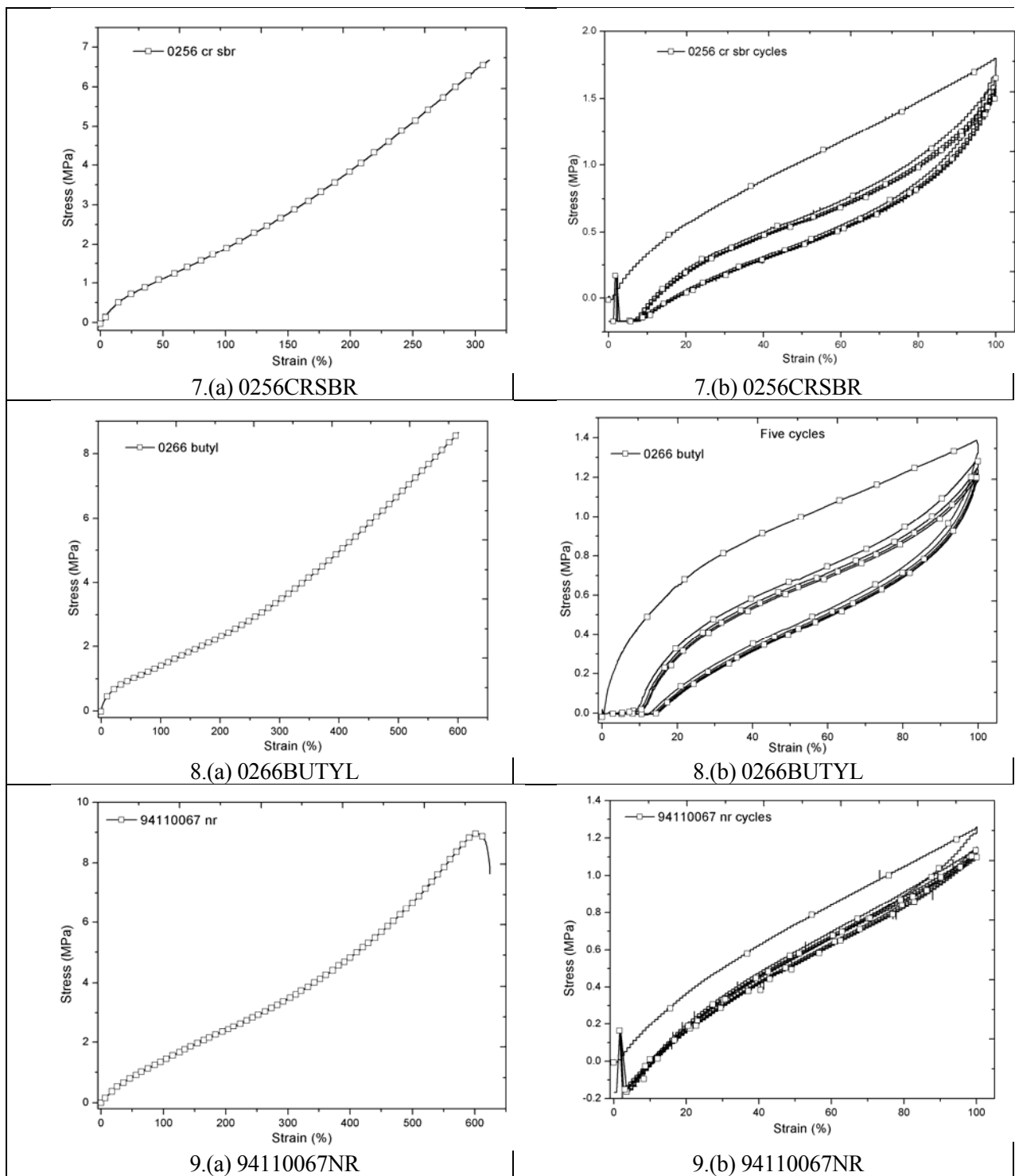


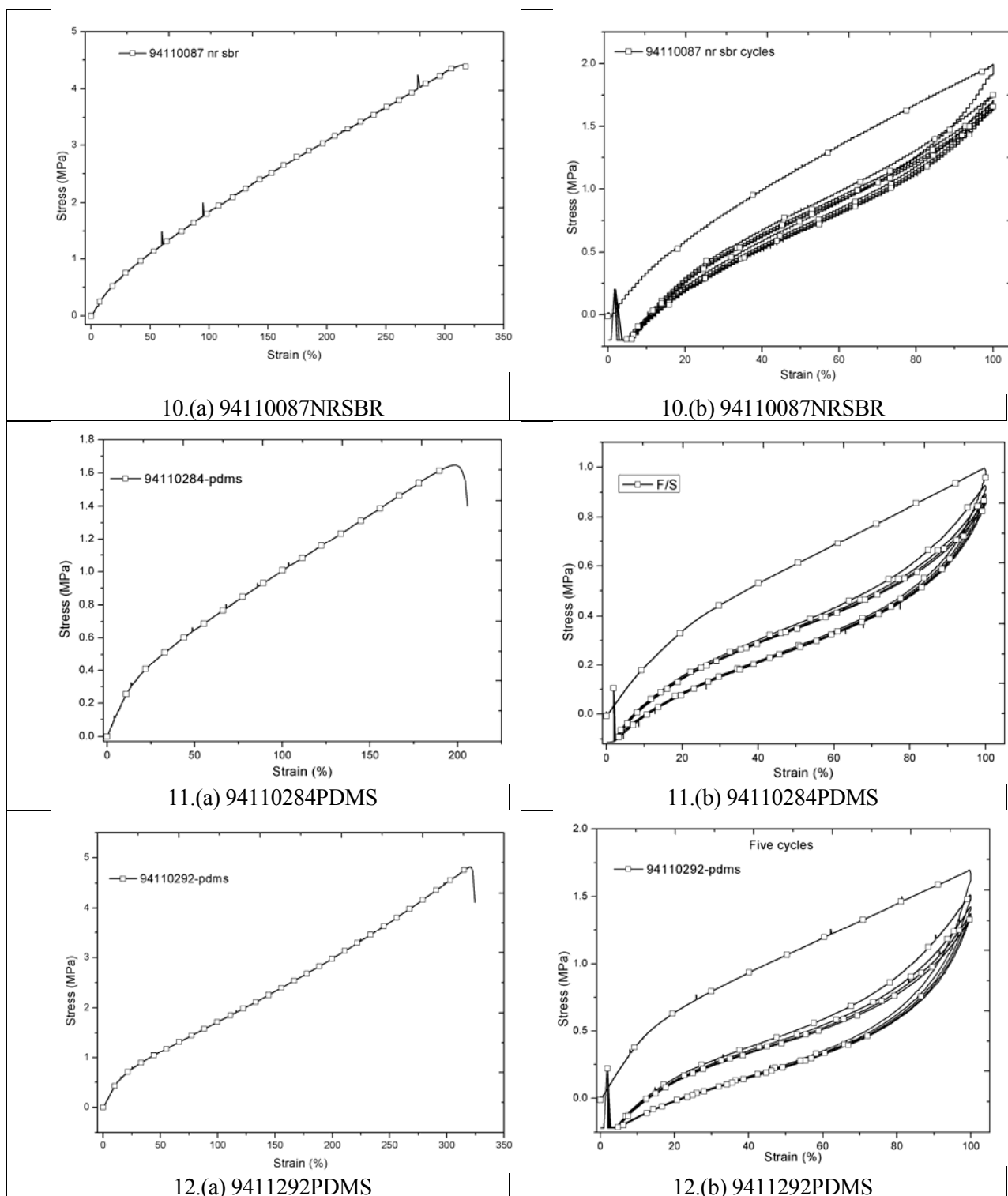
### Section 3.4.

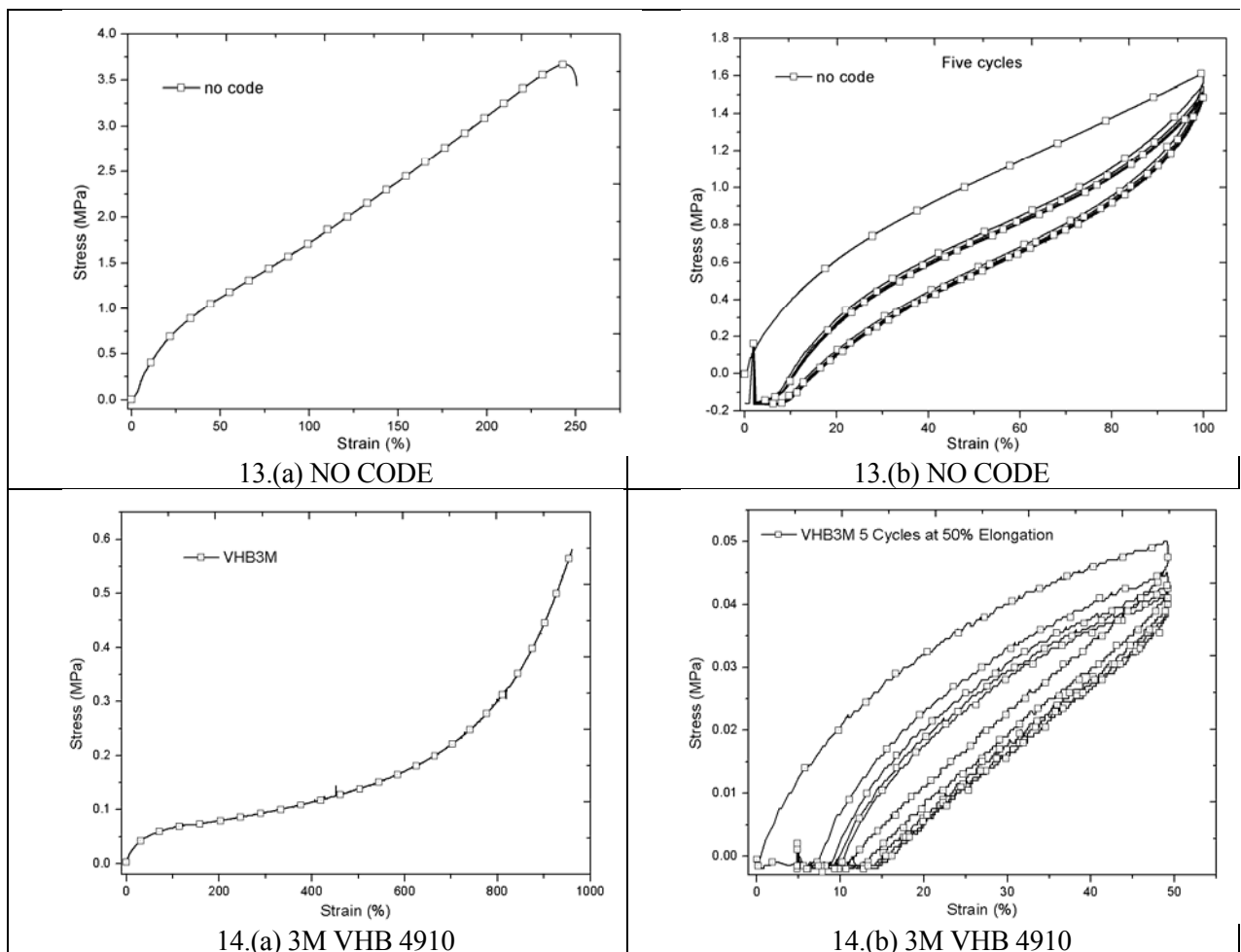
No.	Sample	Stress (MPa)	Strain (%)	Young's modulus (MPa)
1.	0050 SBR	9.15	341	2.68
2.	0078NRSBR	13.87	690	2.01
3.	0132NBR(SBR(1))	3.86	324	1.19
4.	0132NBR(SBR)	7	457	1.53
5.	0142NBR	8.6	300	2.87
6.	0213EPDM	5.06	320	1.58
7.	0256CRSBR	6.66	311.4	2.14
8.	0266BUTYL	8.65	601	1.44
9.	94110067NR	8.13	622	1.31
10.	94110087NRSBR	4.39	317	1.38
11.	94110284PDMS	1.64	200	0.82
12.	9411292PDMS	4.8	321	1.50
13.	NO CODE	3.43	250	1.37
14.	3M VHB 4910	0.58	961	0.06





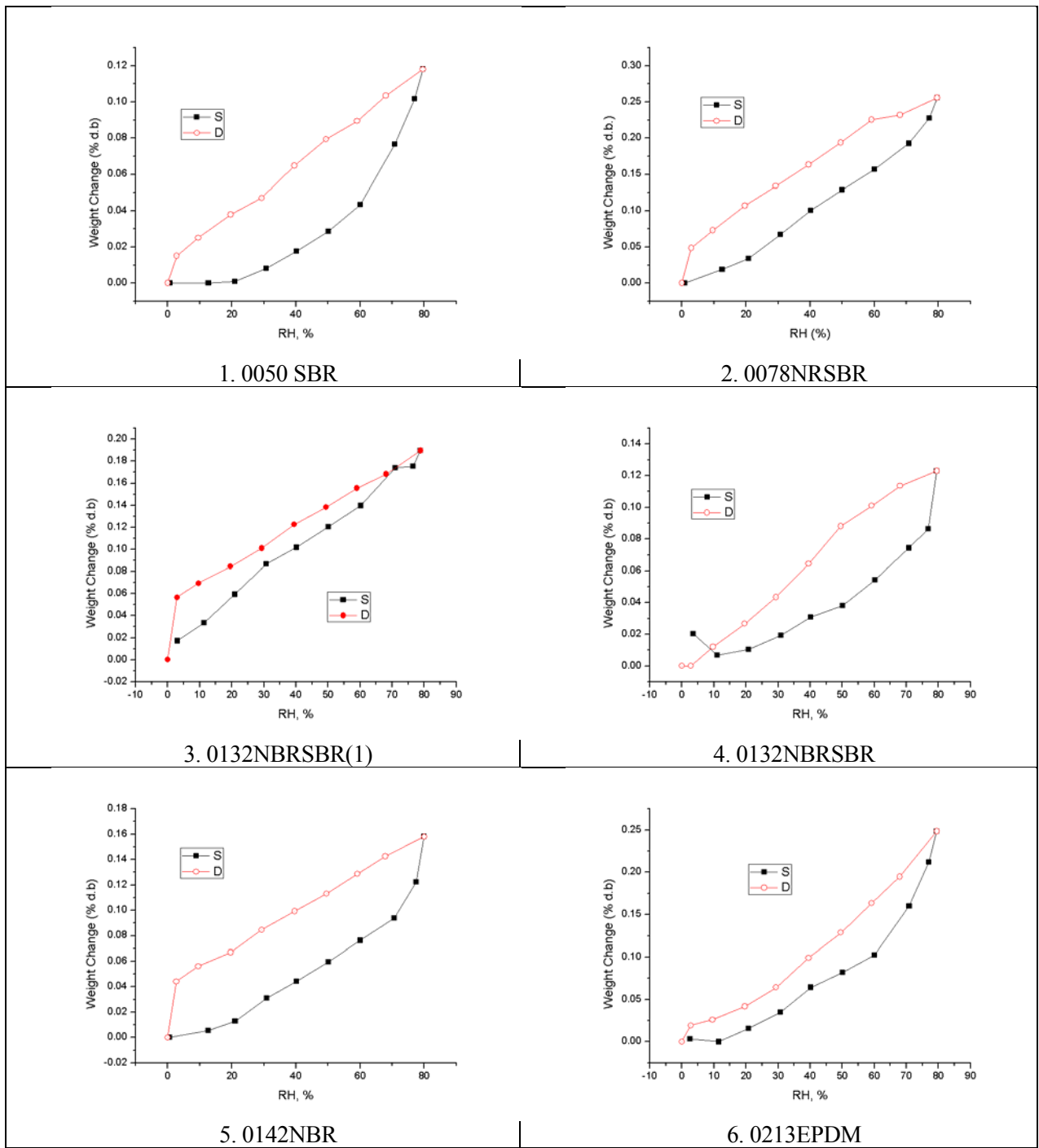


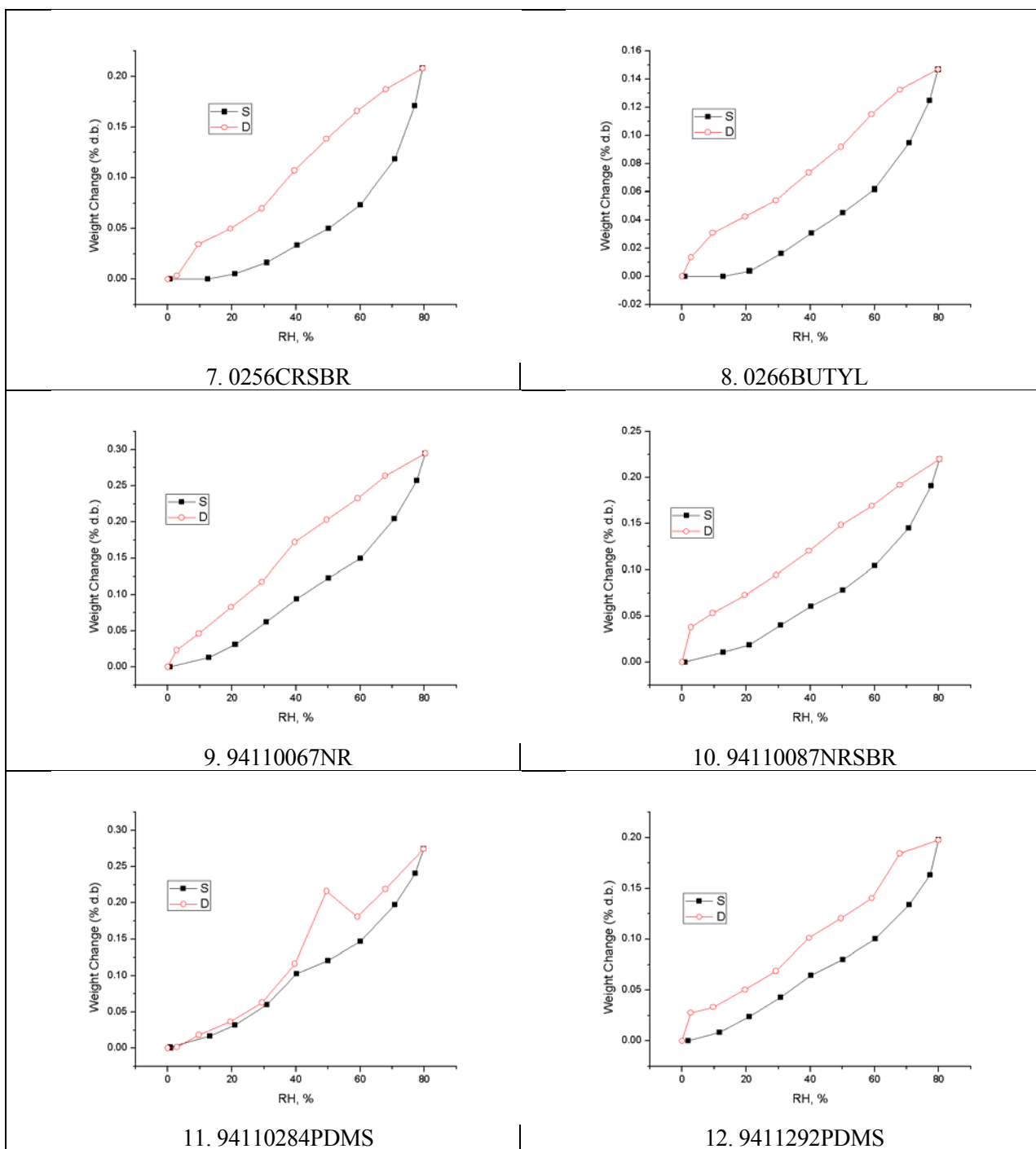


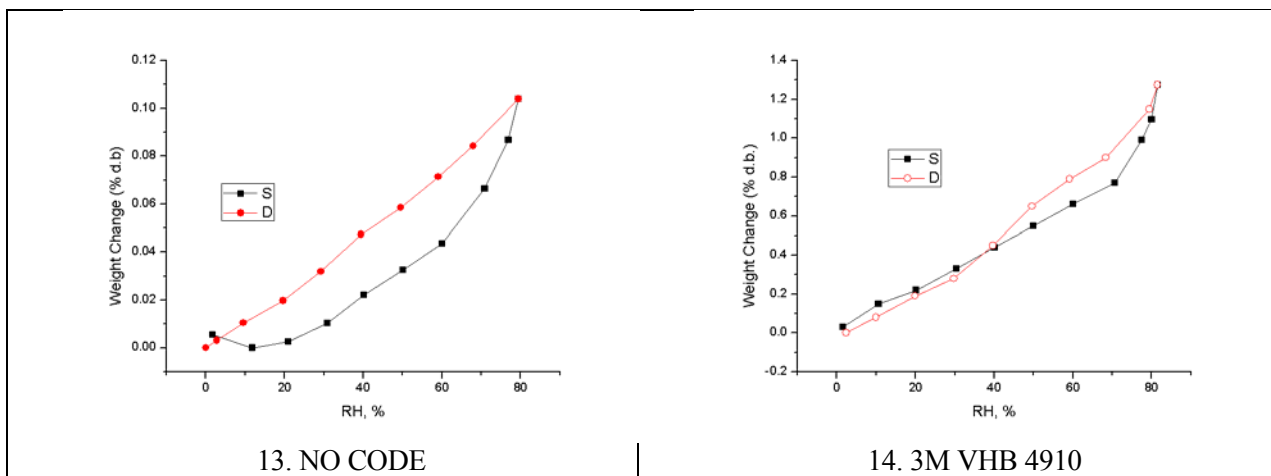


### Section 3.5.

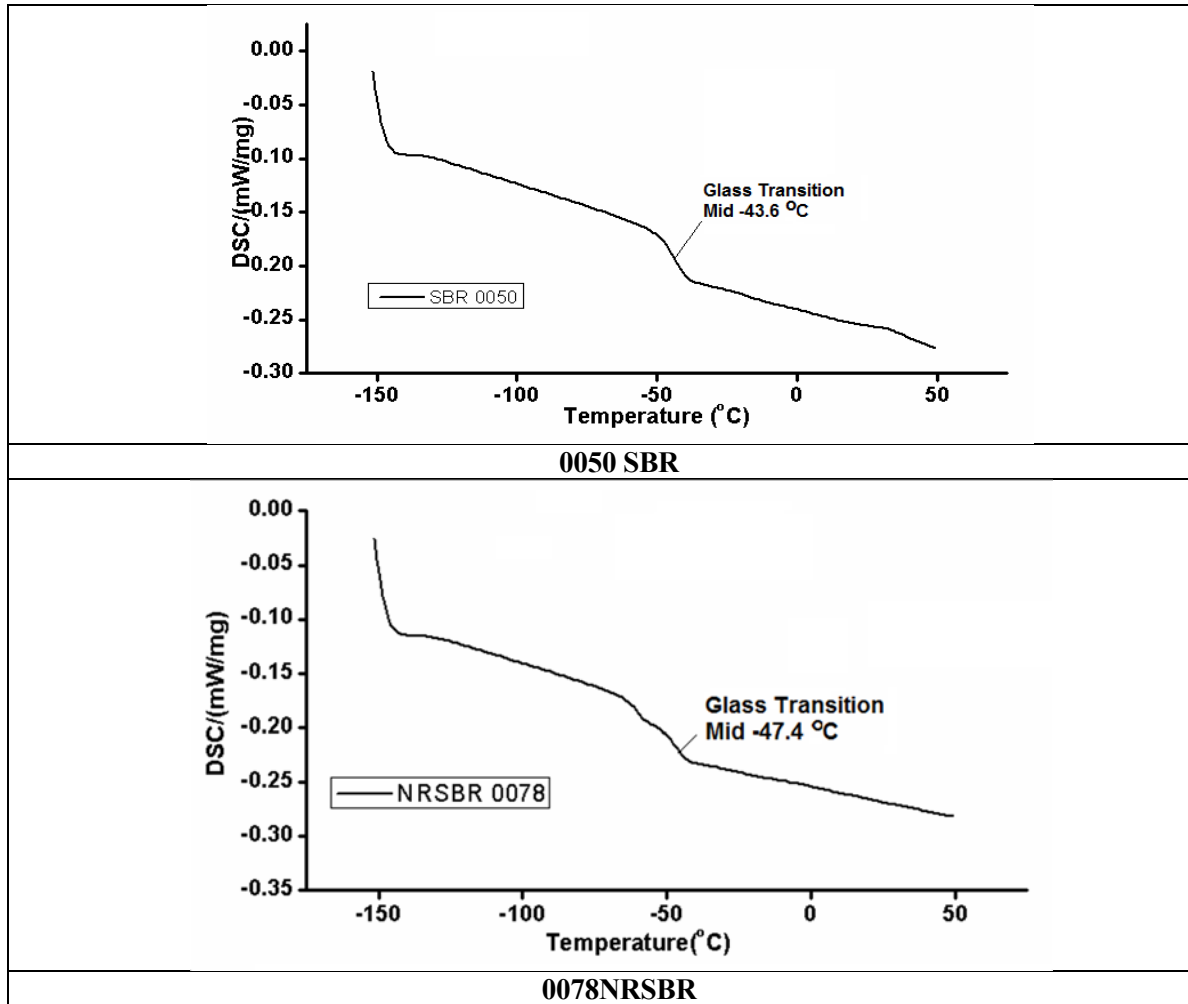
No.	Sample	Max. Weight (% dry basis)
1.	0050 SBR	0.12
2.	0078NRSBR	0.25
3.	0132NBR(SBR)(1)	0.19
4.	0132NBR(SBR)	0.123
5.	0142NBR	0.158
6.	0213EPDM	0.248
7.	0256CRSBR	0.2
8.	0266BUTYL	0.147
9.	94110067NR	0.294
10.	94110087NRSBR	0.22
11.	94110284PDMS	0.274
12.	9411292PDMS	0.197
13.	NO CODE	0.104
14.	3M VHB 4910	1.275

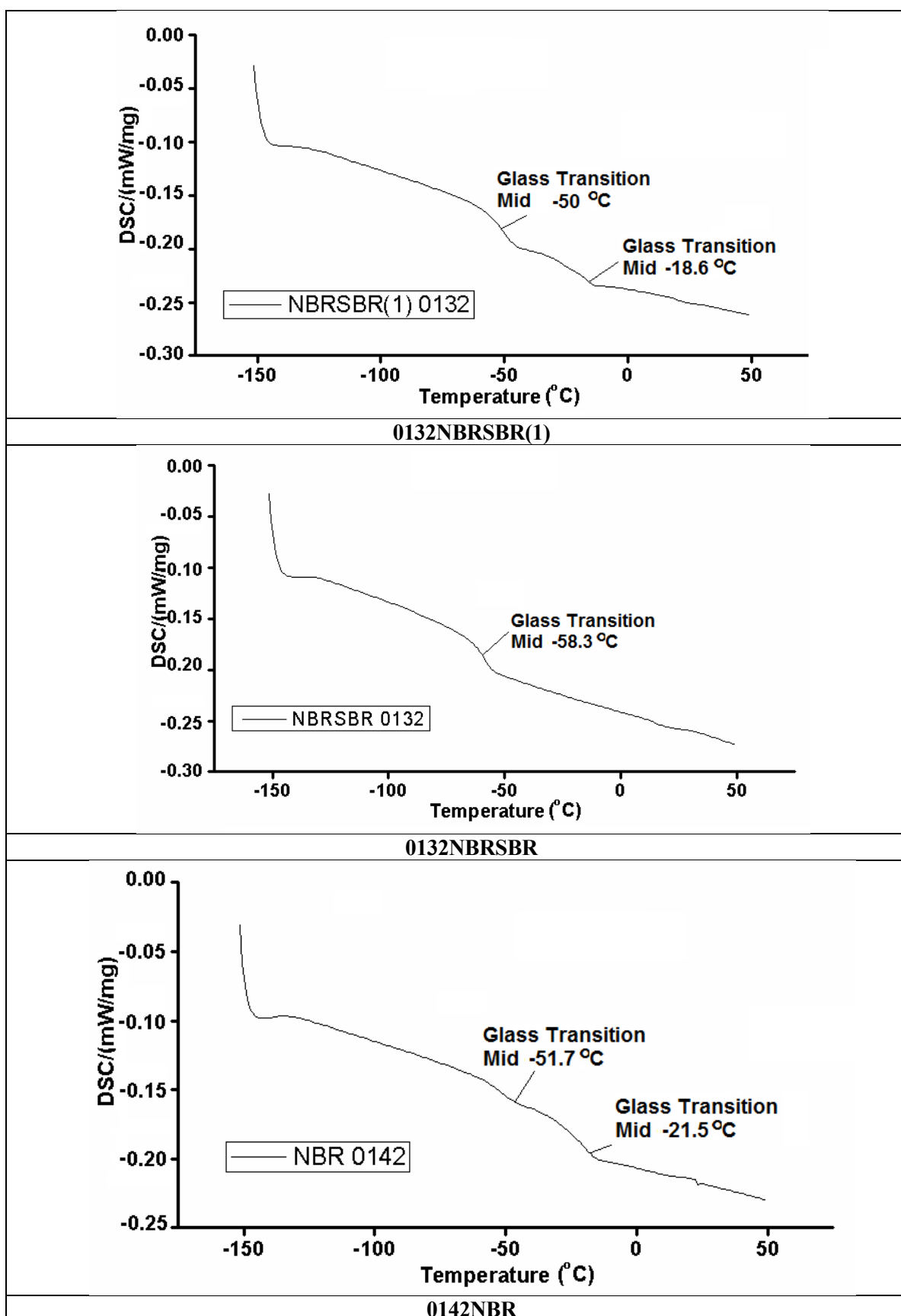


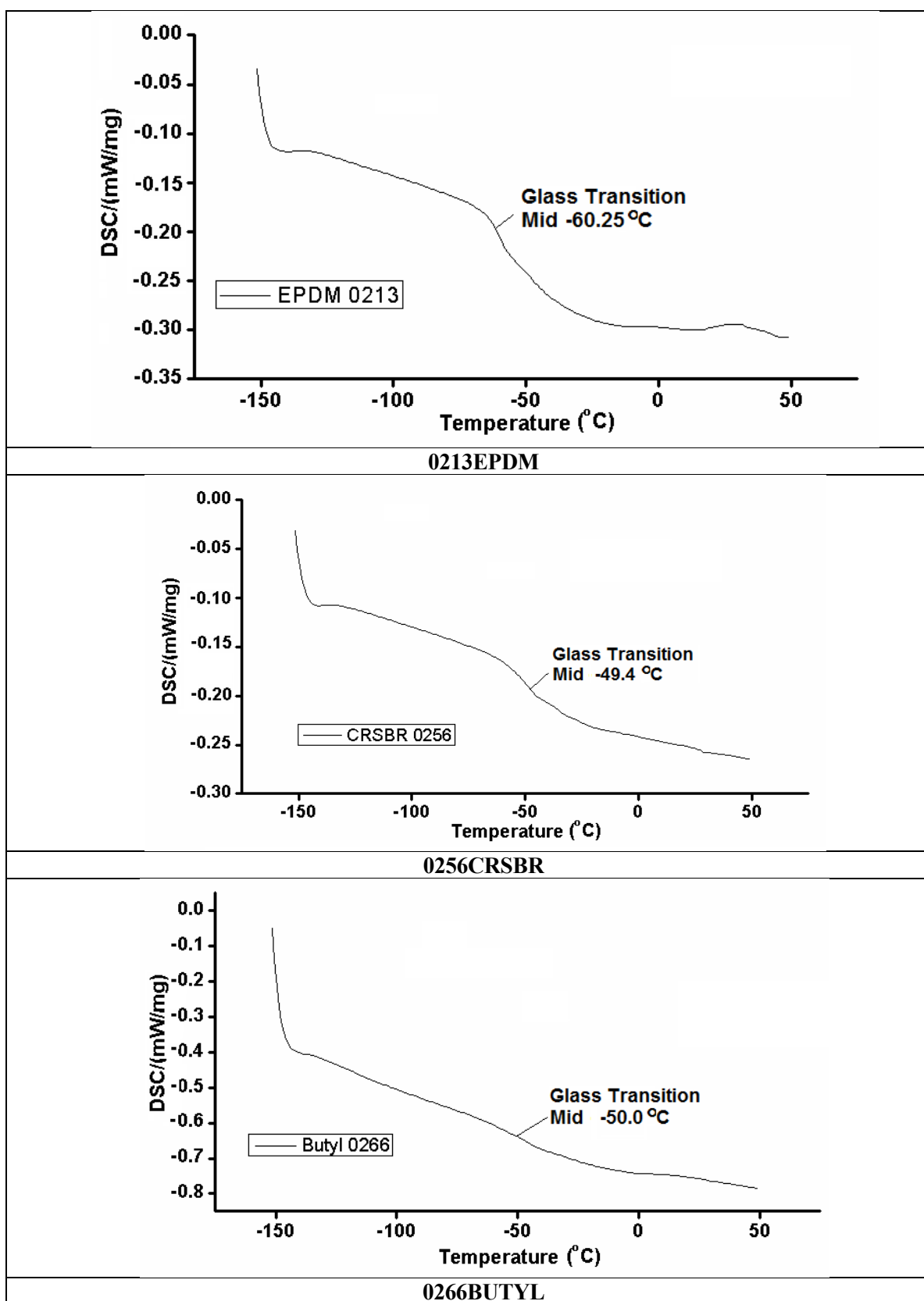


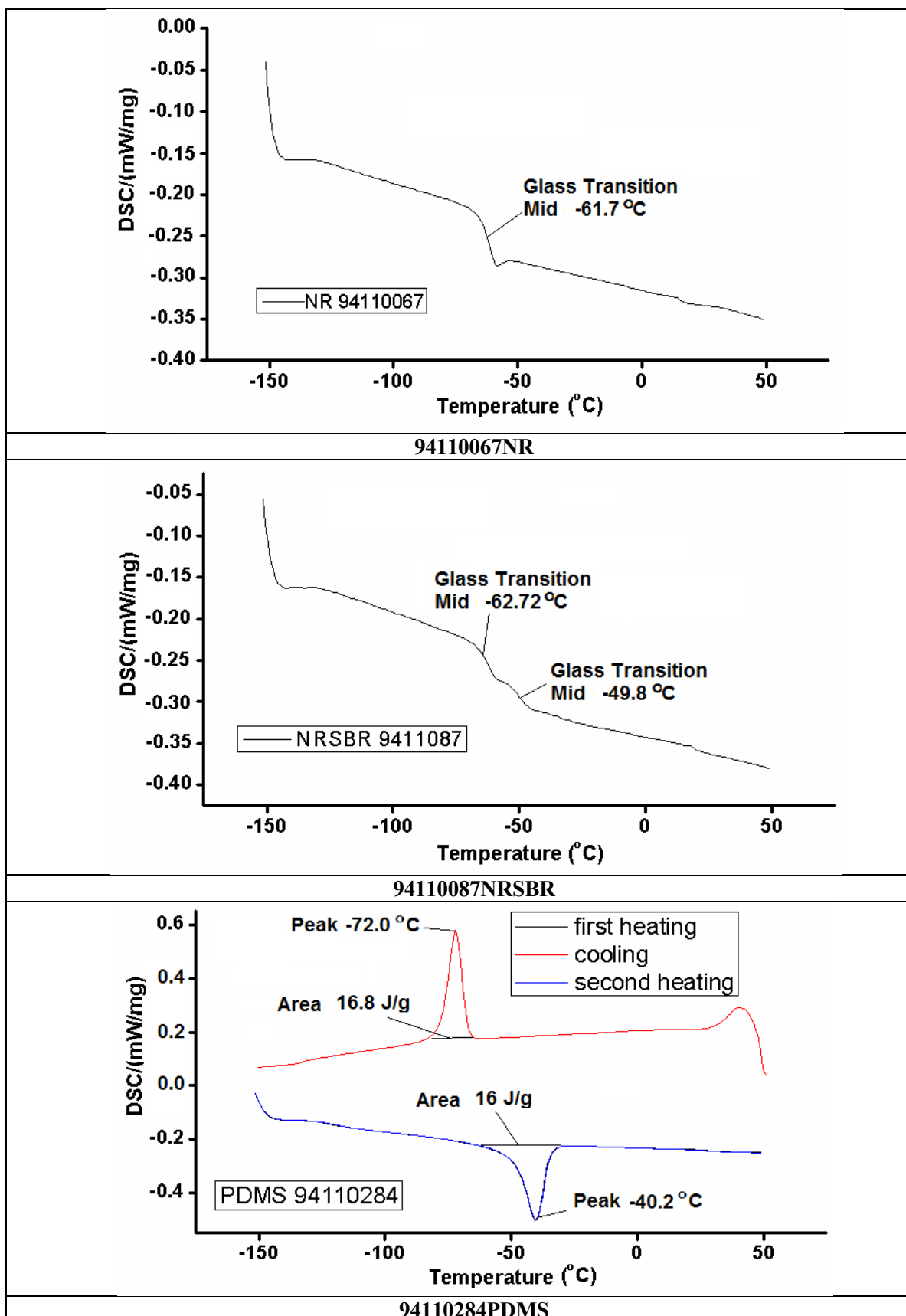


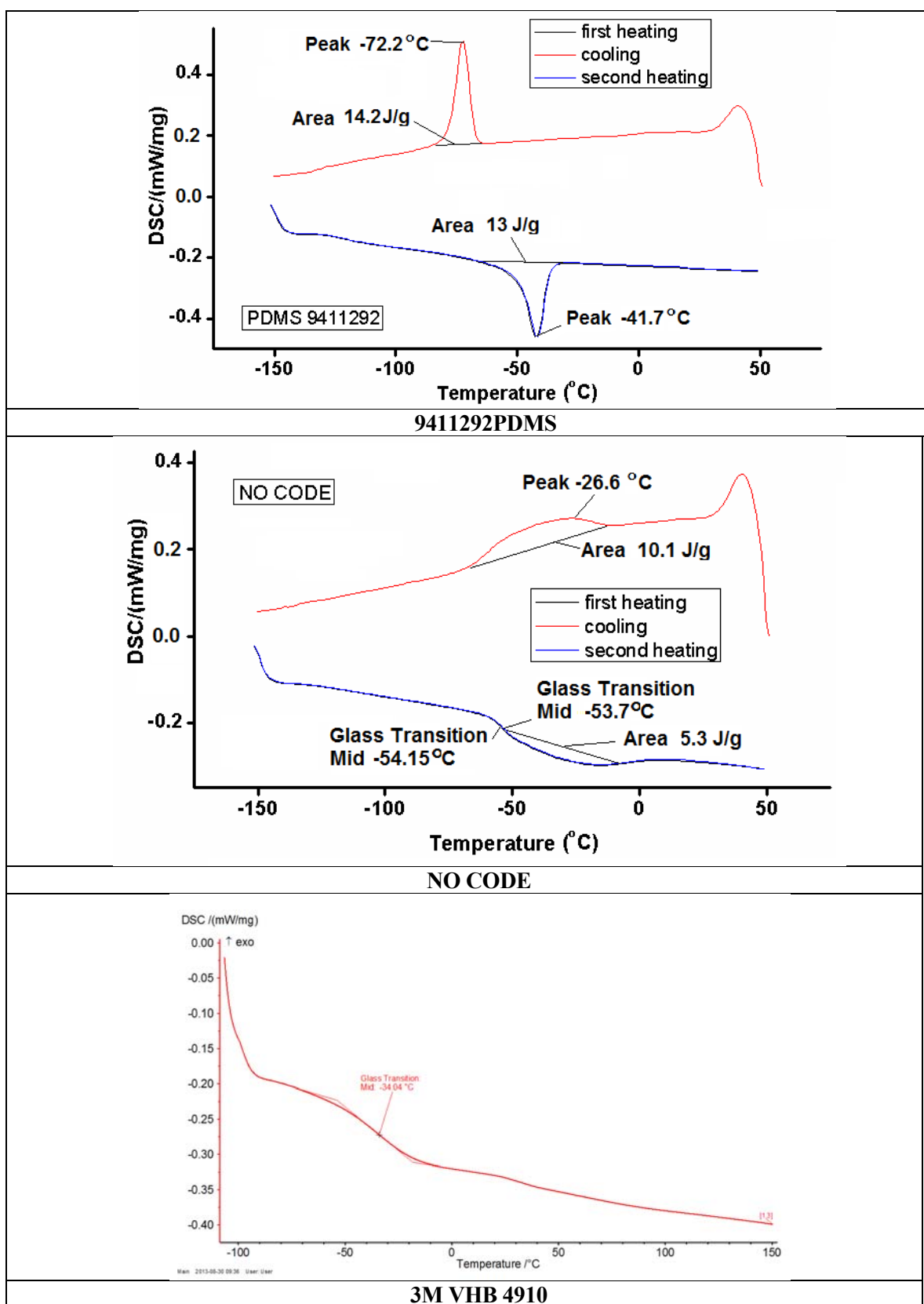
### Section 3.7.











**Tabel 14.** Mechanical and chemical properties of different types of elastomers

Property, characteristic	NR <sup>1</sup>	SBR <sup>2</sup>	Neoprene	Butyl	Nitril	EPDM <sup>3</sup>	PU <sup>4</sup>	S <sup>5</sup>	FC <sup>6</sup>	CSPE <sup>7</sup>	Acryl <sup>8</sup>
Specific gravity [95]	0.93	0.94	1.23	0.92	1.00	0.85	1.05	0.96	1.85	1.1	1.09
Tensile strength (MPa) [95]											
-Gum	28	7	18	10.5	4.5	2.2	28	0	18	14.5	2.8
-Crosslinked rubber	21	21	18	14	21	18	21	8.5	22	19.5	12.5
Shore A hardness [95]	30-95	40-95	40-95	40-75	20-95	40-90	40-90	20-80	60-95	45-95	40-90
Resilience [95]											
-RT	E <sup>9</sup>	G <sup>10</sup>	G	P <sup>11</sup>	F <sup>12</sup>	G	G	G	P	G	P
-HT	E	G	G	G	F	G	G	F	F	E	E
Tear resistance	E	F-G	G	G	F	F-G	G	F-G	G	F	F
Abrasion resistance [95]	E	G-E	E	F-G	E	G-E	E	F	G-E	E	F
Atmospheric aging resistance [95]	P	P	E	G-E	F	E	F	E	E	E	E
Oxidation resistance [95]	G	G	G	G-E	F	E	E	E	E	E	E
Heat resistance [95]	F-G	F-G	G	F-G	G	E	F-G	E	E	E	E
Low temperature flexibility [95]	E	G	F	F	F	G-E	F	E	F	F	P
Permeability [95]	F	F	G	E	E	G-E	G	F	G-E	G	G
Acid resistance [95]											
-Dilute	G	F	E	E	G	G-E	F	G	E	E	E
-Concentrated	F-G	F-G	G	E	F	G-E	P	P	E	E	P
Moisture resistance [95]	G-E	G-E	F	E	E	E	G	E	G-E	E	F
Hydrocarbon solvent resistance	P	P	F	P	G-E	P	G	F	E	F	G
Energy Density (MJ/m <sup>3</sup> )	0.006 [97]	0.026 [98]	-	-	0.084 [99]	-	0.09 [97, 100]	0.75 [101,102], 0.1	0.005 [97]	-	3.4 theoretical al [103], 0.022
Mechanical loss factor <sup>13</sup>	-	-	-	-	-	-	0.08 [97, 100]	0.05 [101-103]	-	-	<0.005 [103]

<sup>1</sup> Natural rubber; <sup>2</sup> Styrene butadiene rubber; <sup>3</sup> Ethylene propylene diene monomer rubber; <sup>4</sup> Polyurethane; <sup>5</sup> Silicones; <sup>6</sup> Fluorocarbon rubber; <sup>7</sup> chlorosulfonated polyethylene synthetic rubber; <sup>8</sup> Acrylic rubbers;

<sup>9</sup> Excellent; <sup>10</sup> Good; <sup>11</sup> Poor; <sup>12</sup> Fair

<sup>13</sup> At 80 Hz unless otherwise stated

**Table 15.** Dielectric and mechanical for elastomers with possible applications in wave energy transducers

Sample	Property, characteristic									
	Prestrain x%, y%	Actuation Pressure (MPa)	Thickness Strain (%)	Area strain (%)	Maximum Strain, % [96]	Young's Modulus (MPa)	Breakdown electric field (MV/m)	Dielectric constant*	Dielectric loss factor*	
Silicone (Nusil CF19-2186)[101,102]										
	Prestrain x%, y%	Actuation Pressure (MPa)	Thickness Strain (%)	Area strain (%)	Maximum Strain, % [96]	Young's Modulus (MPa)	Breakdown electric field (MV/m)	Dielectric constant*	Dielectric loss factor*	
Silicone (Dow Coming HS3)[101,103]	45,45	3	39	64	-	1	350	2.8**	6.3**	
Polyurethane (Deerfield PT6100S) [97,100]	68,68	0.3	48	93	-	0.1	110	2.8**	79**	
Fluorosilicone (dow corning 730) [97]	Nominal	1.6	11	-	100	17	160	7**	21**	
Fluoroelastomer (Lauren L143HC) [97]	Nominal	0.39	28	-	-	0.5	80	6.9**	48**	
Isoprene natural rubber latex [97]	Nominal	0.11	8	-	-	2.5	32	12.7**	15**	
Acrylic (3M VHB 4910) [101,103]	Nominal	0.11	11	-	-	0.85	67	2.7**	21**	
Acrylic (3M VHB 4910) [101,103]	300,300	7.2	61	158	380	3	410	4.8**	90**	
Acrylic (3M VHB 4905) [98]	15,15	0.13	29	40	380	-	55	4.8**	-	
SEB75 [98]	Nominal	0	11	12.4	380	2.3	34	4.2**	20.9**	
ACN rubber [99]	Nominal	-	16	19	-	12	29-40	2.1**	29**	
0050 SBR [96]	60,60	0.3	20	-	-	4	50	14**	-	
0078NRSBR [96]	Nominal	-	-	-	341	2.68		1262.9	1200000	
0132NBRSSBR(1)[96]	Nominal	-	-	-	690	2.01		4.51	0.28	
0132NBRSSBR [96]	Nominal	-	-	-	324	1.19		870.83	22719	
0142NBR [96]	Nominal	-	-	-	457	1.53		12.93	1.57	
0213EPDM [96]	Nominal	-	-	-	300	2.87		1633.7	14987	
0256CRSBR [96]	Nominal	-	-	-	320	1.58		7636	55887	
0266BUTYL [96]	Nominal	-	-	-	311.4	2.14		3392.7	77548	
94110067NR [96]	Nominal	-	-	-	601	1.44		27266	400000	
94110087NRSBR [96]	Nominal	-	-	-	622	1.31		3.28	0.06	
94110284PDMS [96]	Nominal	-	-	-	317	1.38		4.4	0.3	
9411292PDMS [96]	Nominal	-	-	-	200	0.82		3.31	0.025	
NO CODE [96]	Nominal	-	-	-	321	1.50		3.22	0.0087	
3M VHB 4910 [96]	Nominal	-	-	-	250	1.37		11610	178820	
5% BaTiO <sub>3</sub> (commercial) Siloxane composite (AB II MB5)[96]	Nominal	-	-	-				3.27	0.0025	
					961	0.06				
5% BaTiO <sub>3</sub> (commercial) Siloxane composite (AB IV MB5)[96]	Nominal	-	-	-	249	0.16		3.85	0.035	
BaTiO <sub>3</sub> (nanorods) Siloxane composite [96]	Nominal	-	-	-	850	0.038		4.53	4.47	
BaTiO <sub>3</sub> (cubic) Siloxane composite [96]	Nominal	-	-	-	898	0.015		9.52	1.3	
TiO <sub>2</sub> Siloxane composite [96]	Nominal	-	-	-	902	0.018		5.36	0.52	
Lead zirconate Siloxane composite [96]	Nominal	-	-	-	635	0.72		5	0.1	
Mn complex Siloxane composite M <sub>1</sub> L 15% R2 [96]	Nominal	-	-	-	800	0.023		4.4	1.99	
Fe complex Siloxane composite M <sub>2</sub> L 15% R2 [96]	Nominal	-	-	-	-	-		4.75	0.5	
Cr complex Siloxane composite M <sub>3</sub> L 15% R1 [96]	Nominal	-	-	-	-	-		4.31	0.066	
	Nominal	-	-	-	-	-		6	0.54	

\*At 1 Hz

\*\*At 1 kHz